

ResearchOnline@JCU

This file is part of the following reference:

Grabau, Peter John (2016) *The simulation of vibrations experienced by patients during helicopter winching and retrieval*. PhD thesis, James Cook University.

Access to this file is available from:

<http://researchonline.jcu.edu.au/44642/>

The author has certified to JCU that they have made a reasonable effort to gain permission and acknowledge the owner of any third party copyright material included in this document. If you believe that this is not the case, please contact

*ResearchOnline@jcu.edu.au and quote
<http://researchonline.jcu.edu.au/44642/>*

The Simulation of Vibrations Experienced by Patients During Helicopter Winching and Retrieval

Thesis submitted by

Peter John Grabau (BEng(Elect), MEngSc, James Cook University, Australia)

in April 2016

For the degree of Doctor of Philosophy

in the College of Science, Technology and Engineering

James Cook University

Supervisor: A/Prof. Mohan Jacob

DECLARATION

I declare that this thesis is my own work and has not been submitted in any form for another degree or diploma at any university or institute of tertiary education. Information derived from the published and unpublished work of others has been acknowledged in the text, and a list of references is given.

Peter Grabau

April, 2016

STATEMENT OF ACCESS TO THIS THESIS

I, the undersigned, the author of this work, understand that James Cook University will make this work available for use within the University Library, and via the Australian Digital Thesis Network, for use elsewhere.

I understand that as an unpublished work, a thesis has significant protection under the Copyright Act. I do not wish to place any restriction on access to this thesis. However, any use of its content must be acknowledged and could potentially be restricted by future patents.

Peter Grabau

April, 2016

DEDICATION

To my family, Karen and Emily

ACKNOWLEDGEMENTS

I would like to express my sincere appreciation and thanks to my supervisor, A/Prof Mohan Jacob for his unending kind support, guidance, faith and encouragement throughout this thesis.

Thanks are also extended to my supervisory committee for their support and guidance.

Special thanks to Dr Denise Blake of The Townsville Hospital who had the original idea for the project and has been its main driving force. I have appreciated the camaraderie, lengthy conversations, helpful discussions, medical expertise and your never ending patience, encouragement, support and faith in this project. You have been a great source of friendship as well as good advice and collaboration.

I would like to acknowledge the financial and in-kind support from the following organisations:- Queensland Emergency Medicine Research Foundation, Divers Alert Network, The Townsville Hospital Private Practice Research and Education Trust Fund and Emergency Management Queensland – Townsville.

Finally, thanks to my family and friends for their love, support and encouragement. To my dog Emily, who slept at my feet for hundreds of hours, kept me company in the wee hours and reminded me to take breaks by expecting me to respond to her squeaking toys. But most of all thanks to my loving, enthusiastic, encouraging and patient wife Karen whose support throughout this PhD is so appreciated.

ABSTRACT

Due to the potential for Decompression Illness (DCI) to cause permanent or fatal injuries patients experiencing significant DCI symptoms while SCUBA diving on offshore reefs often require urgent helicopter aeromedical transfer to a specialist hyperbaric treatment facility. During these transfers patients are placed supine in a rescue litter (winch basket) for winching up to the helicopter and remain supine in the litter for the duration of the flight. The litter is secured directly to the cabin floor exposing patients to the high level of vibrations generated by the helicopter.

The risks associated with exposing patients to the high levels of vibration experienced during helicopter retrieval are not understood and consequently there is no existing policy or recommendation for the safe transport of patients with respect to the levels of vibration experienced during helicopter transport. This is despite research showing that the human body is vulnerable to the range of vibration frequencies commonly found in helicopters. A number of researchers have highlighted the potential risks and recommended studying the effects in clinical laboratory trials however this has not transpired due to the unavailability of a suitable vibration simulator capable of reproducing the vibrations experienced by a patient during actual retrieval.

Helicopter vibrations are characterised as three-dimensional, tonal, time-varying and broad spectrum with a high root-mean-squared (Armstrong) average level and a high crest factor making them difficult to generate artificially. Consequently recommended practice for vibration testing of helicopter instrumentation is to use real pre-recorded vibration data to drive the simulator however this data is not publicly available and will need to be recorded as part of the development of a simulator. The ideal simulator for use in clinical trials studying the effects of helicopter vibrations on retrieval patients would therefore accommodate a test subject supine in a rescue litter and reproduce pre-recorded real vibrations.

This thesis presents the results of research into the feasibility of creating a helicopter patient retrieval vibration simulation system which both records real patient vibration data during actual helicopter winching and retrieval and reproduces the vibration experience in a laboratory vibration simulator that can be located adjacent to a hyperbaric chamber. The research showed that the system was feasible and resulted in two operational systems. The first records tri-axial vibrations at the head, waist and feet of a patient supine in a rescue litter during winching and retrieval and the second is a vibration simulator which reproduces vertical axis vibrations for a patient supine in a rescue litter. The system is initially being applied to clinical trials studying the effects of transport induced vibrations on persons suffering from Decompression Illness (DCI). There are four main contributions from this thesis:

Firstly, the development of a vibration measurement system which attaches to the underside of a helicopter rescue litter and records real patient vibration data during all flight modes including winching. The system is non-invasive allowing the rescue litter to be safely moved into the cabin at the top of a winching operation. Vibrations are sensed using three tri-axial Micro Electro Mechanical Systems (MEMS) accelerometer sensors mounted in a protective void under the rescue litter. The sensors are aligned with the lateral, longitudinal and vertical axes and situated under the patients head, waist and feet. Simultaneous sampling of the nine vibration channels allows for comparison of the vibrations at the head, waist & feet and reconstruction of the vibrations in three dimensions. The system has been tested in a Bell 412 rescue helicopter and the recorded vibrations have been verified against manufacturer's data and vibration levels published in the literature.

Secondly, is the use of low-cost Micro Electro Mechanical Systems (MEMS) accelerometers as vibration sensors. MEMS accelerometers offer the advantages of being low cost, low power and low profile however their use as vibration sensors is not established as they require individual calibration by the user and some researchers have reported non-ideal frequency response characteristics. Their low profile makes them ideal for this application as it allows the sensors to be safely mounted in the protective void under the rescue litter making the system less vulnerable to damage during movement of the litter. The thesis presents the detailed development of the MEMS based sensors including the procedure that was used for their calibration.

Thirdly, is an algorithm which allows high speed continuous streaming of data to an SD card from a low-power 8-bit microcontroller by means of a serial interface. The algorithm uses three techniques to improve the data streaming rate. It begins at initialisation by erasing sufficient space on the SD card to store all the data for the test and then creating a single contiguous test file in the file allocation table linked list. During recording data is then written in whole segments to the next physical SD card memory segment without reference to the file allocation table. The algorithm is a critical part of the vibration measurement system enabling non-volatile storage of the measured data.

Finally, the design and development of a vibration simulator capable of supporting a subject lying supine in a rescue litter and reproducing the real vibrations recorded by the vibration measurement system. Powerful electrodynamic shakers provide the vibratory force ensuring high fidelity of reproduction. The simulator will allow clinical trials into the effects of vibrations on patients during helicopter winching and retrieval.

CONTENTS

Declaration	I
Statement of Access to this Thesis.....	II
Dedication	III
Acknowledgements	IV
Abstract	V
Contents	VII
List of Figures	XI
List of Tables	XIV
Chapter 1 : Introduction	1
1.0 Motivation and Aim.....	1
1.1 Research Objectives	3
1.2 Publications	5
1.3 Thesis Organisation	5
Chapter 2 : Background and Literature Review.....	7
2.0 Introduction	7
2.1 Decompression Illness (DCI) in Scuba Divers	8
2.2 Helicopter Transportation of DCI Patients	9
2.3 Effects of Vibration on the Human Body	11
2.4 Recommendations and Standards for Patient Transfer.....	12
2.5 Vibration Levels During Helicopter Aeromedical Retrieval.....	13
2.6 Characteristics of Helicopter Vibrations.....	16
2.7 Clinical Study	17
2.7.1 Clinical Study Methodology	18
2.8 Current Practice in Vibration Testing and Simulation.....	18
2.9 Helicopter Patient Vibration Data Measurement.....	23

2.10	Conclusions	24
Chapter 3 : The Vibration Measurement System		27
3.0	Introduction	27
3.1	Design Considerations	28
3.1.1	Operational Requirements	28
3.1.2	Operating Environment	29
3.1.3	Sensor Mounting	30
3.1.4	Vibration Sensors	31
3.1.5	Anti-aliasing Filter	33
3.1.6	Simultaneous Sampling of all Vibration Signals.....	34
3.1.7	Choice of Microcontroller	34
3.1.8	Data Storage	35
3.2	System Hardware.....	36
3.2.1	System Architecture	36
3.2.2	Sensor Boards.....	39
3.2.3	Controller Unit	40
3.2.4	Controller Unit to Sensor Board Communications.....	41
3.2.5	System Power	42
3.3	System Software	43
3.3.1	Software Overview.....	43
3.3.2	csv File Format.....	44
3.3.3	SD Card Operation	45
3.3.3.1	SD Card Initialisation	47
3.3.4	Sampling Control Software	51
3.3.5	Background Software	53
3.3.6	SD Card Algorithm	55
3.3.7	File Conversion (hex to csv) Software	56
3.3.8	Vibration Analysis Software	60

3.4	Summary and Conclusions	61
Chapter 4 : Vibration Measurement System Verification		63
4.0	Introduction	63
4.1	Criteria for Success.....	65
4.2	Methodology.....	66
4.2.1	System Calibration	66
4.2.1.1	Determination of Sensor Board Static Sensitivity	67
4.2.1.2	Determination of Sensor Board Frequency Response	68
4.2.1.2.1	Input Signal Generation.....	69
4.2.1.2.2	Collection and Presentation of Results	69
4.2.2	Collection of Flight Data.....	70
4.3	Results	71
4.3.1	System Calibration – Results	71
4.3.2	Flight Testing	75
4.3.2.1	Flight Test 1 – 28 th March 2011	76
4.3.2.2	Flight Test 2 – 6 th April 2011	89
4.3.2.3	Flight Tests 3 and 4 – 24 th April 2011	95
4.4	Summary and Conclusions	102
Chapter 5 : The Vibration Simulator.....		103
5.0	Introduction	103
5.1	Operational Specification	104
5.2	Simulator Design	107
5.3	Time Waveform Replication	115
5.3.1	Recording of Flight Data.....	115
5.3.2	Processing of Flight Data Ready for Simulation.....	116
5.3.3	Determination of the Shaker System FRF	116
5.3.3.1	Excitation Signal for FRF Estimation.....	119
5.3.4	Drive Signal Generation.....	120

5.3.4.1	Implementation	123
5.4	Summary and Conclusion.....	124
Chapter 6 : Conclusions and Future Work.....		126
6.0	Introduction	126
6.1	Vibration Measurement System	127
6.2	Vibration Simulator	127
6.3	Future Work.....	128
Appendix A : Example Flight Record.....		130
Bibliography.....		134

LIST OF FIGURES

- Figure 1.0 Medevac 11A rescue litter and 70kg mannequin
- Figure 1.1 Patient supine and secured in a Medevac 11A rescue litter
- Figure 2.0 Emergency Management Queensland (EMQ) Bell 412
- Figure 2.1 Position of rescue litter during flight
- Figure 2.2 Approximate rescue litter (winch basket) location during flight
- Figure 2.3 Patient secured on a backboard
- Figure 2.4 Kong model 870.00 stretcher
- Figure 3.1 An empty rescue litter in its normal flight position
- Figure 3.2 Shows the cavity beneath the litter created by the 19mm tubular frame
- Figure 3.3 Bruel & Kjaer 4321 Triaxial Piezoelectric Charge Accelerometer (left) and 4 channel Charge Conditioning Amplifier (right).
- Figure 3.4 The Vibration Measurement System
- Figure 3.5 Vibration Measurement System sensors mounted in their normal operational position underneath the rescue litter
- Figure 3.6 Sensor Board block diagram
- Figure 3.7 Controller board block diagram
- Figure 3.8 Showing the line driver/receiver setup for communications between the Controller Unit and Sensor Boards
- Figure 3.9 Example showing four records from a csv vibration data file suitable for importation into Excel
- Figure 3.10 SD Card Initialisation Flowchart
- Figure 3.11 Shows one cycle of the vibration signal sampling control waveforms
- Figure 3.12 Controller Background Software Flowchart
- Figure 3.13 Example showing four records (rows) from a quasi csv vibration data file as recorded on the SD Card
- Figure 3.14 File Conversion Software Flowchart
- Figure 3.15 Example of file conversion program results
- Figure 4.1 Showing the test setup for calibration of the Sensor Boards

- Figure 4.2 Block diagram of the test setup for static calibration of the Sensor Boards
- Figure 4.3 Block diagram of the test setup for calibration of the Sensor Boards
- Figure 4.4 Bode plot of frequency response of sensor #1
- Figure 4.5 Bode plot of frequency response of sensor #2
- Figure 4.6 Bode plot of frequency response of sensor #3
- Figure 4.7 Showing the rescue litter and mannequin positioned in the helicopter
- Figure 4.8 0.3 sec (600 samples) of vibration data for all channels for 60 ft winch hover
- Figure 4.9 0.3 sec (600 samples) of vibration data for all channels for 60 ft landing hover
- Figure 4.10 Vertical axis frequency plots for the head, waist and feet during winch hover and landing hover
- Figure 4.11 Vertical and Lateral axis frequency domain plots for the same 15 second period of 60 feet winch hover
- Figure 4.12 Example of short-term variations in vibration signals
- Figure 4.13 Example of short-term variations in vibration signals and the effect of averaging on the frequency plots
- Figure 4.14 Comparison of vertical axis frequency components recorded during winch hover for a 70kg Mannequin and 72.5kg human
- Figure 4.15 Comparison of vertical axis frequency components recorded during approach for a 70kg Mannequin and 72.5kg human
- Figure 4.16 The effects of turbulence on helicopter vibrations
- Figure 4.17 Showing the effect that a small change in atmospheric conditions can have on the helicopter vibration spectrum.
- Figure 4.18 Sensors mounted on the helicopter floor for flights 3 and 4
- Figure 4.19 Comparison of vertical axis vibrations recorded in winch hover for three different sensor configurations
- Figure 4.20 Comparison of longitudinal axis vibrations recorded in winch hover for three different sensor configurations
- Figure 4.21 Comparison of lateral axis vibrations recorded in winch hover for three different sensor configurations
- Figure 4.22 Torn and raised floor matting under feet sensor
- Figure 4.23 Feet sensor mounted on torn floor matting
- Figure 5.1 Dongling ESS-050 500 Nt shaker and PA1200 amplifier

- Figure 5.2 Spring based vibration isolating mount
- Figure 5.3 An example of the vibration isolating mount installed in the table
- Figure 5.4 Side elevation schematic drawing of the vibration simulator
- Figure 5.5 The vibration simulator
- Figure 5.6 Block diagram of vibration simulator computer control and communications
- Figure 5.7 Message Structure used for PC-to-MCU communications
- Figure 5.8 The Time Waveform Replication strategy
- Figure 5.9 Typical Electrodynamic Shaker Frequency Response
- Figure 5.10 The overlap-add process
- Figure 5.11 Signal flow for drive signal generation for the two shaker systems

LIST OF TABLES

Table 2.0	Vehicular vibration frequencies and the areas of human physiology that they affect
Table 2.1	How different levels of Whole Body Vibration (WBV) experienced by humans during vehicular transport are perceived
Table 2.2	Levels of helicopter vibrations reported in the literature
Table 2.3	Bell 412 Vibration Sources and Frequencies
Table 3.1	Showing the functionality of the Vibration Measurement System Controller unit and Sensor Boards
Table 3.2	SD Card Commands
Table 4.1	Frequency response data for the Z-axis of sensor 2 with a high level input of 600 mV _{P-P}
Table 4.2	Sensitivity results of each of the three sensors boards vertical axes
Table 4.3	Summary of field testing flights which verified the correct operation of the vibration measurement system
Table 4.4	RMS and Peak accelerations (mg) and Crest Factors for the nine axes of vibrations during different flight modes of the flight of 28 th March 2011
Table 4.5	Comparison of vertical vibration levels
Table 5.0	Maximum peak/rms vibration levels and crest factors recorded during flights
Table 5.1	Specifications for the ESS-050 Electrodynamic Shaker
Table A.1	Flight Record for the second flight of 6 th April 2011

CHAPTER 1

INTRODUCTION

1.0 MOTIVATION AND AIM

In cases of trauma or serious illness it is critical to transport patients to specialist care as quickly as possible which often necessitates retrieval by helicopter for transfer directly to the hospital. Initial access to these patients is often difficult as they may be on small boats or in ravines necessitating their being winched into the helicopter in a rescue litter (winch basket), such as the Medevac 11A (Figures 1.0, 1.1). In these cases patients remain in the rescue litter for the duration of the retrieval flight which is typically up to two hours. During flight the rescue litter is secured directly to the hard cabin floor exposing the patient to high levels of vibration from the helicopter frame (Figure 2.1).

The risks associated with exposing patients to the high levels of vibration experienced during helicopter retrieval are not understood and consequently there is no existing policy or recommendation for the safe transport of patients with respect to the levels of vibration experienced during helicopter transport. Researchers such as Stephenson (2009) and Silbergleit (1991) have alluded to the potential dangers of such exposure and recommended that clinical studies be conducted to quantify the risks however this has not transpired due to the unavailability of a suitable vibration simulator capable of reproducing the vibration environment experienced by a patient during actual retrieval.

This thesis is *motivated* by the need to quantify the risks associated with exposing seriously ill patients to the high levels of vibrations experienced during helicopter winching and retrieval. The risks can only be quantified by clinical laboratory trials which require a suitable vibration simulator capable of accommodating and vibrating test subjects as they would be during actual winching and retrieval.

The *aim* of this thesis is to investigate the feasibility of creating a helicopter patient retrieval vibration simulation system to be used in clinical trials to quantify the risks associated with exposing seriously ill patients to the high levels of vibrations experienced during helicopter winching and retrieval. The vibration simulation system is required to reproduce, under controlled laboratory conditions, the vibrations experienced by patients supine in a rescue litter (Figures 1.0, 1.1) during helicopter aeromedical winching and retrieval. This simulator will initially be used in a clinical study assessing the hypothesis that *vibrations generated by rotary wing aircraft increase the quantity of nitrogen bubbles in the blood stream leading to more severe symptoms of*

Decompression Illness (DCI) in SCUBA¹ divers who have developed initial symptoms of DCI and are being medivaced to specialist care. This study will involve simulating dives and helicopter retrievals by first compressing subjects in a hyperbaric chamber during a routine hyperbaric treatment following a current T14 (241.3 kPa) dive table and then vibrating a selection of subjects using the vibration simulation system to simulate a helicopter retrieval. The level of nitrogen bubbles in the blood stream will be assessed using Doppler ultrasound following the treatment and again after the simulated retrieval or an equivalent period to determine if the retrieval has increased the quantity of nitrogen bubbles in the blood stream. If the hypothesis is proved correct, further trials will be conducted using the simulator to determine acceptable levels of vibration and assess vibration minimisation strategies.



Figure 1.0: Medevac 11A rescue litter and 70kg patient (mannequin) in winching configuration. The head cover is used to protect the patient's head during winching. One of the four triangular winch harness attachment clips can be seen next to the head protector. Both the head protector and winch harness are removed once the litter is inside the helicopter cabin. The litter frame is titanium to save weight and there is a hard plastic mesh inner liner. Note that here a wooden table top is shown under the litter.

¹ *Self Contained Underwater Breathing Apparatus*



Figure 1.1: Patient supine and secured in a Medevac 11A rescue litter. The patient is secured in the litter with four quick release restraints and the patient and litter are secured to the helicopter floor with two additional restraints (not shown). The grey metallic box fastened under the blue quick release strap is the control unit for the vibration measurement system (Chapter 3).

1.1 RESEARCH OBJECTIVES

The project has investigated the feasibility of developing a simulator for reproducing, under controlled laboratory conditions, vibrations experienced by patients supine in a rescue litter (Figure 1.0) during helicopter aeromedical winching and retrieval. This was achieved by investigating the following research questions:

1. *Is it feasible to record the vibrations experienced by patients lying supine in a rescue litter during helicopter winching and retrieval?*

and

2. *Is it feasible to simulate the vibrations experienced by patients lying supine in a rescue litter during helicopter winching and retrieval?*

These questions have both been answered experimentally, the first by successfully developing the Vibration Measurement System (Chapter 3 and 4) and the second by successfully developing the Vibration Simulator (Chapter 5).

This project has made the following contributions in the area of patient transportation:

1. *A non-invasive system for recording vibrations experienced by patients during helicopter transportation in a rescue litter.* The system is unique in that it provides synchronised sampling and storage of high bandwidth tri-axial vibrations at the head, waist and feet of a patient lying supine in a rescue litter during all flight modes that are encountered during helicopter patient retrieval. The system operates reliably in a physically demanding environment which has high levels of mechanical stress, vibrations and electrical noise and limited physical space for locating the sensors as they cannot protrude from the rescue litter.
2. *A vibration simulator for reproducing the vibrations experienced by patients during helicopter transportation in a rescue litter.* The simulator is unique in its ability to reproduce high bandwidth vertical axis vibrations as experienced by a patient lying supine in a rescue litter during helicopter winching and retrieval.
3. *A unique algorithm for high speed data streaming to a Secure Digital (SD) card mass storage device.* This algorithm makes it feasible to stream high speed data to an SD card using a low power 8 bit microcontroller (MCU) and is an enabling element in the design of the vibration recording system.
4. *The use of low-cost Micro Electro Mechanical Systems (MEMS) accelerometers as vibration sensors.* MEMS accelerometers offer the advantages of being low cost, low power and low profile however their use as vibration sensors is not established as they require individual calibration by the user and some researchers have reported non-ideal frequency response characteristics. Their low profile makes them ideal for this application as it allows the sensors to be safely mounted in the protective void under the rescue litter making the system less vulnerable to damage during movement of the litter. The thesis presents the detailed development of the MEMS based sensors including the procedure for their calibration.

1.2 PUBLICATIONS

This work will be published in the following papers:

Grabau, P., Blake, D., and Jacob, M. “*The Measurement of Vibrations Experienced by Recumbent Patients During Helicopter Aeromedical Retrieval*” IEEE Transactions on Information Technology in Biomedicine

Grabau, P., Blake, D., and Jacob, M. “*The simulation of vibrations experienced by DCI patients during helicopter aeromedical retrieval*” The Journal of Sound and Vibration.

1.3 THESIS ORGANISATION

Chapter 1 commences by providing background on the main issue which this thesis will help to answer, that is, the possibility that during the helicopter aeromedical retrieval of patients suffering from DCI, helicopter vibrations may cause excess nitrogen bubbles to be dislodged from the blood vessel walls and enter into the blood stream possibly worsening the patient’s condition. It then explains the current practise for helicopter aeromedical retrieval of DCI patients to give an appreciation of the operational environment and the stresses to which the patient is subjected. This is followed by an outline of the testing procedure that is proposed for the clinical trials which, in turn, identifies the need for the vibration simulator that is investigated in this thesis. The basis of a practical vibration simulator is then outlined including the need for real vibration data being available to drive the simulator. The chapter concludes with the two research questions that are investigated followed by the contributions that the thesis makes.

Chapter 2 explains the origins of the project and summarises the relevant information that has been found in the literature. It begins with an introduction to DCI and why it is thought that the condition is worsened by exposure to vibrations. The operation procedures and environment of the helicopter are explained with an emphasis on the levels of vibration to which the patient is exposed. Relevant standards and recommendations for the safe transport of DCI patients with regard to vibration levels are discussed along with the levels of patient vibrations reported in the literature. A brief summary of the methodology proposed for the clinical study is presented to give an appreciation of the need for the vibration simulator. This is followed by a review of industry vibration testing and simulation along with applicable methods for measuring field vibrations. The chapter concludes by presenting the conclusions reached as a result of the work presented in the chapter.

Chapter 3 presents the architecture and design of the vibration measurement system. A specification is developed by considering the operational environment, flight modes and

helicopter vibration characteristics. Using the specification a MEMS vibration sensor is selected and the detailed hardware and software design described. Use of a MEMS sensor is novel and the process leading up to its choice is described in detail. An algorithm for streaming high-speed data to an SD via a serial connection is also presented.

Chapter 4 describes the verification and calibration of the vibration measurement system. The use of MEMS accelerometers as vibration sensors is not an established procedure and therefore a thorough calibration and verification of the complete measurement system is undertaken to prove their suitability. The process involves laboratory calibration and detailed analysis of recorded flight data.

Chapter 5 presents the design and development of the vibration simulator. The operational specification is developed and from this a vibration actuator is selected and the rest of the table designed. Algorithms for system identification and control of the simulator are identified.

Chapter 6 gives a summary of the complete thesis and offers suggestions for future work.

CHAPTER 2

BACKGROUND AND LITERATURE REVIEW

2.0 INTRODUCTION

This chapter explains the origins of this project and summarises the relevant information that has been found in the literature.

Section 2.1 is a brief introduction to the etiology of Decompression Illness occurring in SCUBA divers. It explains the mechanism by which nitrogen bubbles form within the blood stream and how this can translate to serious illness. It is shown that Decompression Illness is surprisingly common, most frequently occurring in remote inaccessible locations necessitating urgent patient helicopter transfer to specially equipped medical facilities.

Section 2.2 describes the operational procedures and environment of the helicopter during winching and retrieval of a patient suffering from symptoms of Decompression Illness. It emphasises the level of vibrations to which the patient is exposed due to the requirement for them to remain in the rescue litter for the duration of the retrieval.

Section 2.3 identifies a number of articles linking vibration exposure and its effects on the human body to establish that the body is vulnerable to vibrations of different types. It also reviews a number of papers which have alluded to a possible connection between vibration exposure and the level of bubbles in the blood stream of Decompression Illness patients.

Section 2.4 reports on standards and recommendations for the safe transport of Decompression Illness patients with regard to vibration levels.

Section 2.5 reviews the literature with regard to the levels of vibration experienced by patients during helicopter aeromedical retrieval.

Section 2.6 discusses the unique characteristics of helicopter vibrations and the levels of vibrations reported in the literature.

Section 2.7 presents a summary of the methodology proposed for the clinical study to give an appreciation of the need for the vibration simulator and its operational requirements.

Section 2.8 is a review of vibration testing and simulation. It includes the types of simulators that are available, the areas of research and development in which they are employed, the different input signals and the controllers used to ensure the correct levels of vibration in tests.

Section 2.9 investigates options for sensing the vibrations experienced by patients during helicopter aeromedical winching and retrieval.

Section 2.10 provides the conclusions reached as a result of the work presented in this chapter.

2.1 DECOMPRESSION ILLNESS (DCI) IN SCUBA DIVERS

Decompression Illness symptoms most commonly present following SCUBA diving. SCUBA divers breathe dry filtered compressed air containing nitrogen at the surrounding ambient pressure. The air is absorbed into the blood stream via the lungs and distributed to body tissue by the arterial blood flow. As a diver ascends at the end of a dive the ambient pressure decreases and the blood may become supersaturated causing nitrogen bubbles to form in the tissue walls and blood stream. Some bubbles will become attached to the vein and artery walls while others will travel in the blood stream and either be extracted by the lungs, reabsorbed into the blood or travel towards the body extremities along the decreasing diameter arteries eventually causing a blockage. These blocking bubbles are considered to be one of the key factors in the etiology of Decompression Illness (DCI) (Hedge 2015). DCI is a serious life threatening condition which in severe cases can result in permanent paralysis or death.

DCI is surprisingly common. Data published for 2004 shows that in that year there were thirteen deaths related to breathing compressed air in Australia (Walker 2009) while eighty nine deaths were reported by Divers Alert Network America (DAN) in Canada and the United States (Pollock 2007) however it is difficult to know how many divers get injured as there is no mandatory reporting system in place. The Townsville Hospital Hyperbaric Medicine Unit was the second busiest chamber in Australia for treating DCI in 2009. Twenty three divers were treated with symptoms ranging from mild joint aches to leg paralysis with urinary retention to unconsciousness.

If a SCUBA diver has symptoms of DCI it is usually impractical, due to time and distance, for the dive boat to transport the diver to shore therefore helicopter retrieval is the preferred alternative. This form of aeromedical retrieval commonly requires the diver to be winched from the dive boat as there are relatively few landing areas on the reef. Further, the Townsville Hospital Hyperbaric Medicine Unit has the only operating public chamber in North Queensland and numerous patients are relocated there by aeromedical transfer from other centres.

This clinical study (Section 2.7) will investigate the hypothesis that the vibrations to which a DCI patient is exposed during helicopter winching and transport in a rescue litter may increase the

severity of the illness by dislodging bubbles that are attached to the vein and artery walls before they can be reabsorbed into the blood stream.

2.2 HELICOPTER TRANSPORTATION OF DCI PATIENTS

Understanding the operational procedures and environment of the helicopter during winching and retrieval of a DCI patient explains the high level of vibrations experienced by the patient and provides the basis for appreciating the criteria used in the design of the vibration simulation system.

Helicopters provide the fastest means of retrieval for a patient suffering DCI on a dive boat in remote regions of the Great Barrier Reef. The Emergency Management Queensland Bell 412 (Figure 2.0) based in Townsville is representative of the type of helicopter used for these operations. As helicopters are unable to land on dive boats the patient must be winched aboard for the retrieval flight. When the helicopter arrives at the dive boat it establishes hover at approximately 100 feet then the rescue litter (Figures 1.0, 1.1) and a crew member are lowered to the boat deck. The crew member stabilises the patient and places them supine in the litter. The litter/patient with crew member hanging beside are then winched up to the hovering helicopter. During winching the patient is exposed to the full rotor downwash resulting in severe buffeting and vibration. Upon reaching the helicopter the litter with supine patient is man handled inside the cabin and secured to the floor immediately behind the pilots seats (Figures 2.1, 2.2) where they stay for the duration of the flight as per recommended practice for the transport of DCI patients (Stephenson 2009). From this position there is no view of outside the helicopter and even experienced crew members become disorientated increasing their level of anxiety. There is very little space in the helicopter which makes it difficult for medical personnel to attend to the patient if required. Also the helicopter does not carry a more comfortable stretcher for the patient as winching is not permitted when carrying this type of stretcher due to the severe restrictions it places on movement inside the cabin. The helicopter floor is hard vinyl matting on a plywood over metal frame base and the rescue litter is a tubular titanium frame with a hard plastic mesh liner. No vibration isolation is provided under the litter as it would be a trip hazard and therefore the considerable vibrations of the helicopter floor are transmitted directly to the patient.



Figure 2.0: Emergency Management Queensland (EMQ) Bell 412 is typical of the rescue helicopters used for retrieving DCI patients from the Great Barrier Reef to The Townsville Hospital. Note the winch above the sliding door in line with the main rotor vertical shaft. The sliding door can be identified by the double large square windows.



Figure 2.1: Position of rescue litter during flight. The sliding door is shown open as it would be during winching and landing but it is closed in other flight modes. The hinged door in front of the sliding door is not opened in flight. The rescue litter is positioned on the helicopter floor up against the rear of the pilot/co-pilot seat. To the left of the litter can be seen the right most of four crew/medical officer seats. There is just enough room between the crew seats and the litter for the crew/medical officer feet.

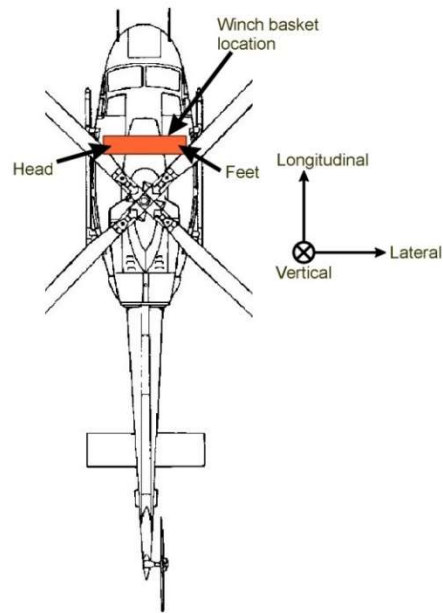


Figure 2.2: Approximate rescue litter (winch basket) location during flight.

2.3 EFFECTS OF VIBRATION ON THE HUMAN BODY

It is well known that exposure to vibrations similar to those produced by helicopters can have a marked impact on the human body. For example, vibration is known to increase metabolic rate (secondary to increased muscle activity), and increase alveolar ventilation (Scott 2006). Lythgo (2009) showed that vibration of greater than 30 Hertz increases blood cell velocity by 27% and Otsuki (2008) demonstrated a generalized vasodilation, which is thought to be due to nitric oxide released as a result of “tribonucleation” – the formation of micronuclei of gas in crevices created by shearing forces within the endothelium.

A number of researchers have expressed reservations about exposing DCI patients to helicopter vibrations as it is suspected that these vibrations may increase bubble generation and dislodgement of bubbles from the walls of blood vessels although currently there is no definitive evidence of this. In a retrospective review Bennett (1995) found no difference in diver outcome looking at mode of transfer but the diver numbers were small and the majority of divers were not retrieved via a helicopter. Bennett (1998) outlined retrieval options and factors to consider when choosing the most appropriate method of transporting DCI patients. He raised the issue of vibration possibly adversely effecting bubble generation, evolution or distribution. Stephenson (2009) identifies vibration as the principle physical stressor in flight with the potential to increase the level of bubbles precipitating out of solution through tribonucleation. He recommends that

vibrations should be minimized for DCI patients and that the patients should be kept supine during transport however patients in remote locations with significant DCI symptoms require urgent transportation to a recompression chamber and their movement priority will justify transportation in suboptimal aircraft. In a recently published article, Germonpré (2009) reported pre-dive vibration at 35-40 Hz *reduced* bubble formation, presumably by dislodging pre-existing micronuclei from the crevices. He argues that low frequency vibration post-dive would also dislodge bubbles and thus increase the risk of venous gas emboli.

Despite these theoretical assertions, the question of whether or not vibration in a rotary wing aircraft causes increased bubbles to flow in the bloodstream of DCI patients has not been empirically answered. If helicopter transport does make DCI worse, the need for alternative ways of transporting patients will be proven. Options could include different transport modes, or modifying helicopters and helicopter stretchers to reduce vibration.

2.4 RECOMMENDATIONS AND STANDARDS FOR PATIENT TRANSFER

Currently there is no existing policy or recommendation for the safe transport of patients with respect to the levels of vibration experienced in helicopter or any other form of transport. ISO 2631 *Mechanical vibration and shock - Evaluation of human exposure to whole-body vibration* is the only standard that makes reference to vibrations experienced during vehicular travel but it is targeted towards long term exposure such as that experienced by long distance drivers or machinery operators. The standard refers to long-term Whole Body Vibration (WBV) exposure and there is no evidence linking this to short term exposure of injured subjects. It does however provide an indication of the range of vibration frequencies that affect the human body (Table 2.0) and the level of discomfort that vehicular vibrations of different amplitudes generate (Table 2.1). Whilst this is not directly relevant to DCI bubble formation it does need to be considered from the point of view of patient stress and discomfort during retrieval flights which can last up to two hours.

Table 2.0: Vehicular vibration frequencies and the areas of human physiology that they affect (ISO 2631).

Physiology	Frequency Range
Health	0.5 Hz to 80 Hz
Comfort and perception	0.5 Hz to 80 Hz
Motion sickness	0.1 Hz to 0.5 Hz

Table 2.1: How different levels of Whole Body Vibration (WBV) experienced by humans during vehicular transport are perceived (ISO 2631).

Whole Body Vibration Level (ms^{-2})	Whole Body Vibration (mg)	Perception
Less than 0.315 ms^{-2}	Less than 32.1 mg	not uncomfortable
0.315 ms^{-2} to 0.63 ms^{-2}	32.1 mg to 64.2 mg	a little uncomfortable
0.5 ms^{-2} to 1 ms^{-2}	51 mg to 101.9 mg	fairly uncomfortable
0.8 ms^{-2} to 1.3 ms^{-2}	81.5 mg to 132.5 mg	uncomfortable
1.25 ms^{-2} to 2.5 ms^{-2}	127.4 to 254.8 mg	very uncomfortable
Greater than 2 ms^{-2}	Greater than 203.9 mg	extremely uncomfortable

2.5 VIBRATION LEVELS DURING HELICOPTER AEROMEDICAL RETRIEVAL

There have been a number of studies investigating the levels of vibrations experienced by patients during helicopter aeromedical retrieval. For example Silbergleit (1991) measured and analysed the vibrations experienced by a spinal injury patient immobilized on a backboard (Figure 2.3) during helicopter transport. They mounted a tri-axial accelerometer on the backboard adjacent to the subject's head and reported peak vibration levels of 830 mg and RMS levels of 190 mg along the three axes. They note that their study needs to be followed by clinical trials to determine the significance of their results (Table 2.2). Alberti (2006) measured the whole body vibrations experienced during simulated helicopter mountain rescue of a patient in a Kong model 870.00 stretcher (Figure 2.4). Eight channels of acceleration data were recorded, including tri-axial measurements from a seat-pad placed under the subject's pelvis, in accordance with ISO 2631. The reported mean unweighted whole-body-vibration level was 1.02ms^{-2} (104 mg) which is classed as *uncomfortable* by ISO 2631 (Table 2.1). The frequency response function (FRF) of the rescue litter was determined experimentally by supporting one end on a rigid mount and exciting the other with an electrodynamic shaker. The FRF was shown to be a typical 2nd order low-pass characteristic with a narrow resonant peak at 4Hz which is attributed to the compliance of the belt matting supporting the patient. The FRF shows that with this type of stretcher the patient will effectively be isolated from the helicopter floor vibrations.

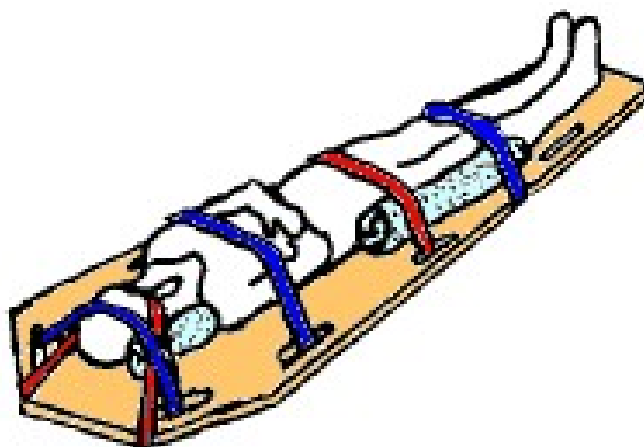


Figure 2.3: Patient secured on a backboard. A backboard is a stiff board normally used for transporting spinal injury patients.

Table 2.2: Levels of helicopter vibrations reported in the literature. Crest factor is the ratio of peak-to-rms vibration levels and is used for determining the level of shock (impact) in vibrations. Crest Factor does not necessarily indicate the severity of vibrations. The r.m.s. method of assessing vibration has been shown by several laboratories to underestimate the effects for vibrations with substantial peaks, i.e. high Crest Factor (ISO 2631).

Author	Kottapalli (2000)	Silbergleit (1991)	Alberti (2006)	Bouchut (2011)
RMS level	382 mg (3.75 ms ⁻²)	190 mg (1.86 ms ⁻²)	104 mg (1.02 ms ⁻²)	102 mg (1 ms ⁻²)
ISO 2631 Perception	Extremely uncomfortable	Very uncomfortable	Uncomfortable	Uncomfortable
Peak level	700 – 800 mg (6.87 – 7.85 ms ⁻²)	830 mg (8.142 ms ⁻²)		
Crest Factor	1.8 – 2.09	4.38		



Figure 2.4: Kong model 870.00 stretcher. These stretchers are designed for mountain rescue and have attachments at each end which allow them to be placed on the shoulders of rescue personnel. They are not suitable for helicopter winching.

The relevance of ISO 2631 to this work is questioned as it recommends safe vibration levels for long-term Whole Body Vibrations (WBV) exposure and there is no evidence linking this to short-term vibration exposure of injured subjects. The standard does help by providing indications of the vibration levels that could be expected and the levels of discomfort which patients would be experiencing.

Bouchut *et al.* (Bouchut 2011) compared the physical stressors experienced by neonates during transport by helicopter and ground ambulance. For the comparison measurements of noise, whole body vibrations, rate of turn, acceleration and pitch were taken as the five most representative dynamic harshness indicators. The results showed that a helicopter produces a higher-level but more stable (lower relative dispersion) whole body dynamic exposure than an ambulance, with a mean noise level of 86 ± 1 dBA versus 67 ± 3 dBA, mean whole body vibration of 1 ± 0.1 ms⁻² (102 ± 10.2 mg) versus 0.4 ± 0.2 ms⁻² (41 ± 20 mg), and acceleration of 1 ± 0.05 ms⁻² (102 ± 5 mg) versus 0.4 ± 0.1 ms⁻² (41 ± 10.2 mg). For the helicopter the mean whole body vibration level of 1 ± 0.1 ms⁻² (102 ± 10.2 mg) is experienced for 20% of the total duration and the peak whole body vibration level is 2.5 ms⁻² (255 mg). ISO 2631 describes this level of whole body vibration

as *uncomfortable*. A ground ambulance has many more dynamic effects in terms of braking, shock, and impulsive noise than a helicopter (1 impulse per 2 minutes vs. 1 per 11 minutes).

2.6 CHARACTERISTICS OF HELICOPTER VIBRATIONS

Most helicopter vibrations are generated by the rotors (main and tail), engine and transmission all of which are mechanically linked and kept at constant frequencies by the engine governor. The vibration spectrum is therefore characterized as containing a range of strong, predictable tonal components, generally in the 10-250Hz range, in addition to broad-band noise (Wu 2003). For example Table 2.3 shows the frequencies of the vehicle generated vibration sources for the Bell 412 helicopter as used in this study. Each helicopter model has a unique vibration spectrum due to its construction however whilst the frequency components of a particular model are constant their amplitudes vary continuously depending on a range of variables such as the measurement position in the helicopter, the vehicle configuration (its take off weight etc), flight mode (e.g., take-off, hover, cruise, approach and landing) and atmospheric. For this reason manufacturers do not publish vibration amplitude data. Typical floor vertical axis vibration levels reported in the literature show an average of 382 mg-rms with a peak value of 700-800 mg and are most severe during approach and landing (Kottapalli 2000, Wu 2003) (Table 2.2).

Table 2.3: Bell 412 Vibration Sources and Frequencies. Note that the vibration frequency components (tones) are fixed due to the engine governor and that the vibration levels are not reported as they vary constantly with flight mode. The right hand column of alphabetical characters are used to identify frequency components in the frequency domain plots shown in the analysis and appendices. (Courtesy Bell Helicopters).

BHT-412-MM-2



Table 18-1. Excitation Frequencies and Sources

VIBRATION SOURCE	APPROX RPM	APPROX HZ	
1/Rev Main Rotor	324	5.40	A
2/Rev Main Rotor	648	10.80	B
4/Rev Main Rotor	1,296	21.60	C
1/Rev Tail Rotor	1,662	27.70	D
6/Rev Main Rotor	1,944	32.40	E
8/Rev Main Rotor	2,592	43.20	F
2/Rev Tail Rotor	3,324	55.30	G
1/Rev Lower Hydraulic Pump	4,300	71.70	H
1/Rev Tail Rotor Driveshaft	4,302	71.70	I
1/Rev Transmission Input Shaft	6,600	110.00	J
1/Rev Upper Hydraulic Pump	6,600	110.00	K
4/Rev Tail Rotor	6,648	110.60	L
Oil Cooler	8,200	136.00	M
Rotor Brake	8,300	138.00	N

2.7 CLINICAL STUDY

This section presents a summary of the methodology proposed for the clinical study to give an appreciation of the need for the vibration simulator and its operational requirements.

The motivation for this thesis is the desire to conduct a clinical study evaluating the hypotheses that vibration generated by a helicopter increases bubble generation in SCUBA divers. The study will quantify some of the risks associated with transporting seriously ill DCI patients in helicopters. In spite of a number of researchers warning of the dangers of exposing DCI patients to helicopter vibrations and recommending that clinical studies be conducted to quantify the risks there is no evidence of any such study being conducted. For a study of this type a minimum sample size of fifty subjects ought to be tested in the initial study. This makes it impractical to

use actual dives and helicopter retrievals due to the safety risk, high operational costs of helicopters and the inability to ensure identical conditions for each subject making the analysis of results extremely difficult. The study will therefore be conducted using simulated dives and helicopter retrievals by first compressing subjects in a hyperbaric chamber to a routine dive table and then vibrating a selection of subjects on a helicopter vibration simulator. A review showed that commercial vibration simulators (tables) are quite commonly used for structural and reliability testing in the construction, automotive and aerospace industries however their high price excluded them from consideration for this study. As no suitable simulator was available the research presented here was undertaken to investigate the feasibility of creating a helicopter patient retrieval vibration simulation system.

2.7.1 CLINICAL STUDY METHODOLOGY

It is anticipated that the initial clinical study will involve multiple simulated dives and retrievals for a minimum of fifty subjects over a period of time. The testing will be conducted in the hyperbaric department of The Townsville Hospital with the vibration simulator located adjacent to the department's hyperbaric chamber. Subjects will be compressed in the chamber following a current T14 (241.3 kPa) dive table and their level of bubbles assessed using Doppler Ultrasound at 20, 40 and 60 minutes after hyperbaric exposure. Following the 60 minute assessment, subjects will be randomised to either a "vibrate" or "still" arm of the study. Subjects assigned to the "vibrate" arm will be placed on the vibration simulator for a simulated retrieval flight. During the simulated flight their bubble level will be assessed at 1, 5, 10 and 20 minute marks and then at 20 minute intervals to see if they are producing bubbles or if there is an increase in the number of bubbles initially found.

Subjects assigned to the "still" arm will be asked to lay still in a supine position on a hospital stretcher, again with re-assessment conducted at 1, 5, 10 and 20 minutes. Whichever arm the subject is in, they will be continually re-assessed until peak bubble detection and decline or for a maximum of 120 minutes.

2.8 CURRENT PRACTICE IN VIBRATION TESTING AND SIMULATION

Vibration testing and simulation is a mature investigative tool which is applied in the fields of seismic, structural dynamics and reliability investigations (Randall 1977). Seismic testing is an integral part of the design process for civil projects in earthquake prone areas and investigates their structural integrity when exposed to seismic events. Structural dynamics testing investigates vibration modes and responses of mechanical structures including aircraft and terrestrial vehicles when they are subjected to typical real world input forces such as engine vibrations, turbulence or shocks. Reliability investigations aim to improve the reliability of electrical and mechanical

assemblies used in vehicles etc. by identifying components which may be susceptible to shock or vibration damage. This section reviews current industry practice and research in vibration simulation and testing that is relevant to the vibration simulator developed in of this thesis. The review presents contributions from the three fields of vibration investigation and for each discusses input vibration test signals, modelling and control of the simulators used for testing.

A major area of study in the civil and architectural field is the response of structures such as bridges, highways or buildings to earthquake or seismic ground motions (Chen 2015). These are non-rigid high order structures which if excited at their resonant frequencies or at sufficiently high amplitudes by a seismic event can suffer cumulative damage such as cracking leading in extreme cases to catastrophic failure (Li 2014). Therefore in earthquake prone areas buildings are designed with resonant frequencies outside those exhibited by earthquakes and with internal vibration damping mechanisms. As part of the process designs are verified in laboratory trials where instrumented test specimens, generally scale models of full size (termed Substructure testing), are mounted on low friction moving tables (shaker tables) and subjected to a range of vibrations to determine the building dynamic characteristics including resonant frequencies and failure criteria (Cunha 2006, Alonso 2010, Uchiyama 2011, Severn 2012, Li 2014). Testing encompasses mounting or connecting a device under test (DUT) to either a servo-hydraulic or electrodynamic shaker actuation device and subjecting it to a range of appropriate vibration signals usually in the horizontal plane however six-axis platforms which can be driven in the horizontal and vertical axes as well as rotating about these axes are becoming more common although they are expensive (Alonso 2010, Severn 2012). Accelerometers and displacement measuring transducers are mounted in critical locations on the DUT to provide feedback of its acceleration and displacement response.

For structural testing, sinusoids and Field Data Replication (FDR) are the most appropriate test signals (Van Baren 2007, Luan 2014). Sine sweeps covering the range of seismic frequencies yield the structure's frequency response highlighting any resonances and adequately simulate the damage growth (Goud 2009). However the application of a single sinusoidal frequency may excite responses at harmonic frequencies as well as the fundamental requiring the inclusion of expensive narrow band tracking filters to isolate the target fundamental response (Keller 2002, Goud 2009). FDR signals take the form of power spectral density (PSD) or time domain waveform replication (Gomes 2008, Luan 2014). PSD signals are random vibrations whose frequency spectrum is shaped using an acceleration PSD and overall signal intensity using a root-mean-squared (RMS) averaged acceleration level. The shaker feedback controller then generates random vibrations to match the specification as well as forcing a shaped random amplitude response with a Gaussian normal distribution (Van Baren 2007). Time domain waveform replication signals for seismic testing are recorded seismic waves which allow testing with typical

real-life conditions. Seismic waves vary with geographic location and so data bases of recorded waves are available for standardisation of tests. A criticism of FDR time domain testing is that the technique only reproduces a single field measurement and does not introduce sufficient variability into the test however this is the most common type of testing signal as it is repetitious and allows comparison of results (Van Baren 2007).

Vibration is a major cause of failure in aerospace and automotive mechanical and electrical systems and therefore products undergo intensive vibration reliability testing as part of the development and production cycles in an effort to identify failure issues as early as possible in the life of the product (Anderson 1967, Anderson 1967, Van Baren 2007). These products differ from the previous civil structures as they are generally smaller, rigid and time invariant which means that they have less effect on the operation of the vibration actuator making control more straight forward. The controlled variable for these tests is typically acceleration and feedback is provided by accelerometers mounted on the DUT. Test signals are mostly of the field data replication type in the form of PSD or time domain waveform replication. However research has shown that many product faults are not being detected during PSD vibration testing. This is thought to be due to the Gaussian amplitude distribution restricting the test signals ability to reproduce the peak accelerations which occur in actual use of the product. For example, with a Gaussian distribution the vibration amplitude will exceed three times the RMS level only 0.27% of the time whereas recorded field data exceeds this level at six times this rate. The difference is significant as most fatigue damage is caused by vibrations in the range of two to four times the RMS level. Van Baren (2007) proposes adding a Kurtosis control parameter to the PSD and RMS specification which would increase the amount of time that the random vibrations are running at higher levels to that experienced in actual use. Birdsong (2001) however favours the direct use of time-domain FDR testing using recorded data. He discusses important issues such as data verification, compensation techniques and the effects of DC and velocity offset before presenting an example application of reliability testing of a jeep using his proprietary software. Lepine (2013) presents a similar technique in his study of vibration induced fatigue in bicycle riders.

All vibration simulators require some form of feedback controller to accurately produce a vibration signal matching a specification. There are two main reasons for this, firstly vibration simulators use some form of high bandwidth vibration actuator, such as an electrodynamic shaker to vibrate the DUT. Electrodynamic shakers however produce a force proportional to an input voltage signal and by Newton's second law of motion the acceleration generated is proportional to the mass of the DUT (Lang 1997). Therefore if any system parameters such as the DUT mass are changed or the DUT is non-rigid the simulator will no longer be generating the correct accelerations. The second reason is that the electrodynamic shakers are powered by a variable gain amplifier which must be set to zero at power up and then manually set to the desired power

level making it highly unlikely that the power level can be set consistently. Feedback controllers can be purchased from the shaker manufacturer however they are expensive and their algorithms are proprietary. In an effort to reduce costs and have greater control over the system performance a number of researchers have investigated shaker control algorithms particularly for seismic testing of non-rigid structures.

Shaker table performance standards and assessment methods are used to allow comparisons of control strategies (Chen 2015). Assessment methods can be broadly divided into time-domain and frequency-domain. Time-domain analysis is applied to time-domain waveform replication signals where it compares the time histories of reference and achieved accelerations and because of its simplicity the most common index of time-domain tracking performance is the normalised RMS error between the time histories of the two accelerations. Due to the time delay imposed by the need to have sufficient samples care must be exercised when calculating the RMS error to ensure the true time-shift correction is applied. Frequency-domain performance assessment is the most widely adopted as it provides a more precise signal specification. Signals are specified by their Power spectral density (PSD) shape and RMS level as described previously.

The operating principal of an electrodynamic shaker is based on the electromagnetic force produced by the interaction of two magnetic fields. For a large shaker both magnetic fields are generated by electromagnets. The field coil is attached to the shaker base and generates a static magnetic field. The armature coil is attached to the moving iron core (table) and generates a variable magnetic field proportional to the voltage applied to the power amplifier. The iron core is also used to support small devices under test or for transmitting the generated vibratory force to a device under test. A number of first principles models of electrodynamic shakers can be found in the literature. For example; Lang (2001) presents a detailed state-space model of a shaker based on the cross-coupled dynamics of the mechanical and electrical parts. The mechanical interaction between the shaker body, coil and table with the device under test is represented as spring-mass-damper systems with an applied force proportional to the current in the electrical system. The electrical system is modelled similarly to a dc motor with an applied voltage generating a current flowing through the coil resistance and inductance and opposed by a back emf generated by the movement of the magnet in the coil. They also present a method for deriving a simplified shaker bode type frequency response plot and show the effect of including the mass of a device under test. Uchiyama (2003, 2011) presents a single degree of freedom state-space shaker model derived by approximating the shaker mechanical dynamics to a single spring-mass-damper system.

The main challenges in controlling electrodynamic shaker systems are their nonlinear frequency response, the difficulty of achieving predictable accelerations in the DUT due to the manual shaker power amplifier gain control, time varying shaker characteristics due to internal heating

and the effects of non-rigid loads. The lowest cost and most common control algorithm is the conventional controller which overcomes these challenges by using a simple iterative control algorithm that does not require a system model and assumes any variation in the shaker system characteristics will be relatively small and slowly varying. The control variable is the shaker table acceleration and the error function is the difference, in the frequency domain, between the acceleration PSD of the device under test (the measured PSD) and that of a reference or standard PSD. This controller uses a hybrid closed/open loop control strategy where at start-up an iterative algorithm adjusts the input PSD level of each frequency band until the measured PSD matches the reference or standard. The system then operates open loop for the remainder of the test. Depending on whether the shape of the reference PSD is smooth or piece wise continuous the PSDs are divided into frequency bands which have a width of an octave, third octave or that of the acceleration FFT bins. At each iteration the ratio of the PSD of corresponding bands in the measured and reference curves are calculated and the input PSD band level weighted accordingly. The time domain input signal is then calculated from the updated input PSD using an inverse FFT transformation (Van Baren 2007, Steinwolf 2008, Martino 2012). The RMS signal level, being the square root of the area under the PSD curve, is also used as an additional measure of the system performance. Gomes (2007, 2008) presents a good illustration of a low cost iterative controller using a PC sound card to generate and read the vibration signals, an electrodynamic shaker as the system vibration actuator and a MEMS accelerometer as the vibration sensor. The example given is for random vibration testing with a standard automotive reference PSD curve. The iteration algorithm is as described above with the input random time domain signal being generated as a multisine signal with random phase angles. At start up the controller assumes that the system frequency response is linear and sets the initial input PSD equal to the reference. Results show RMS level errors of 0.11% after ten iterations of a frequency tone of 500Hz and 0.65% for a standard PSD curve after fifteen iterations.

Iterative techniques take some time to settle to the correct PSD levels which makes them unsuitable for controlling short time tests such as seismic events and may result in accumulated damage to the test specimen prior to the correct excitation levels being achieved. To overcome this Uchiyama (2005) proposes the use of a robust acceleration controller designed using μ -synthesis. The controller shows good performance for both static and transient response however it does require a detailed model of the system and its performance is degraded at low frequencies below 3 Hz. In an effort to improve the controller performance at low frequencies Uchiyama (2006) presents a similar scheme with a cascade combination of robust acceleration and displacement control. A displacement transducer provides low frequency displacement feedback where accelerations are below the noise level of the accelerometer. The system shows improvement in both RMS and peak errors.

Goud (2009) presents a method for lowering the cost of sine sweep vibration tests by eliminating the need for expensive narrow band tracking filters. The controller operates in a similar fashion to Gomes (2008) in that the shaker drive is generated from a random signal whose PSD is iteratively modified until the measured PSD of the DUT matches that of a defined reference which in this case would be the current amplitude and frequency of the sweep. The shaker drive signal is filtered by an adaptive finite impulse response (FIR) filter to minimise the level of noise and results in a reduction of the number of iterations required to achieve the desired response. The method achieved good results in simulations but there are no reports of it being implemented on an actual system. No details are provided of the adaptive filter or iteration algorithm.

Because of the existence of disturbances and non-linear factors in shaking tables, the system transfer functions will change during the process of tests. To overcome this Luan (2014) describes two different controllers for the control of a seismic shaking table being used in Power Spectral Density (PSD) and time domain waveform replication tests. Both controllers use a Model Reference Adaptive Inverse Control (MRAIC) algorithm for controlling the shaker (Plett 1998, Widrow 2014). Strong robustness is achieved by adding a Filtered-X LMS adaptive filter disturbance elimination circuit separating system disturbances from the command signal. The MRAIC algorithm can achieve effective control of shaking tables by the accurate identification of the system impedance function. The system iteratively adapts the controller transfer function so that the shaker output frequency spectrum converges to a desired or reference model spectrum. The time domain waveform replication controller achieved a replication accuracy of 95.7% when tested with a typical El-Centro seismic wave which is an 18 second wave with a peak acceleration of 0.4g.

2.9 HELICOPTER PATIENT VIBRATION DATA MEASUREMENT

For the type of simulation required in the clinical study some form of Field Data Replication (FDR) signal, either random or pre-recorded time-domain, would be required to drive the simulator (Section 2.8). Irrespective of which type is selected there is a need for recorded field data to establish the vibration Power Spectral Density curve shape and to be used for a pre-recorded time-domain input signal. Neither this data nor a suitable recording system were available necessitating a major investigation into the feasibility of recording it as part of the project. The main unknown was the availability of a suitable vibration sensor. This section investigates options for sensing the vibrations experienced by patients during helicopter aeromedical winching and retrieval.

The choice of sensor for vibration measurement is between the traditional piezoelectric accelerometer and the recently introduced Micro-Electro Mechanical Systems (MEMS) accelerometer. The traditional piezoelectric accelerometer is designed for vibration measurement

and offers high reliability, rugged construction, high sensitivity, low noise and is calibrated by the manufacturer however they require a heavy charge amplifier which would be difficult to accommodate in a rescue litter. The MEMS accelerometer is designed for use in low cost consumer devices measuring device status such as tilt or freefall and as such does not require calibration by the manufacturer, however it is not necessarily accurate or linear. Recently a number of researchers (Kok 2005, Thanagasundram 2006, Albarbar 2008, Albarbar 2009) have conducted studies into using low cost miniature MEMS accelerometers for vibration measurement in machine condition monitoring. Thanagasundram *et al* reported that an Analog Devices ADXL105 MEMS accelerometer compared favourably with a Bruel and Kjaer (B&K) 4370V piezoelectric type when used for spectral analysis. Albarbar *et al* used sinusoidal, random and impulsive signals to compare the performance of an (unnamed) piezoelectric accelerometer against three (unnamed) MEMS accelerometers. Their results showed that even with sinusoidal excitation the sensitivity could be nonlinear with the level of input and concluded that MEMS sensors could be suitable for condition monitoring but the results were variable and individual types needed to be assessed to determine their suitability. Badri (2010) presents a method for correcting MEMS accelerometer data in the time domain. First a frequency response function (FRF) which is the ratio of the responses of the MEMS to the reference accelerometer is determined experimentally. A filter, with the inverse response, called the characteristic function (CF) is synthesized as the inverse of the FRF. The CF frequency response is smoothed using curve fitting and then the filter coefficients are determined using the discrete filter least squares fit to the filter transfer function $H(\omega)$. There could be problems for real-time implementation due to the filter delay which is proportional to the number of filter coefficients.

2.10 CONCLUSIONS

Decompression Illness is a serious life-threatening condition which is surprisingly common among SCUBA divers along the Australian coast. The condition is caused by nitrogen bubbles coming out of solution in the blood stream and blocking the arterial flow to the body extremities. However, not all bubbles travel in the blood stream immediately, instead a significant proportion attach themselves to the artery walls from which they would normally be reabsorbed back into the blood stream or tissue. Patients showing symptoms are nearly always on small boats in remote inaccessible areas and require urgent helicopter transport to specialist facilities. Operational requirements and recommendations dictate that patients are winched and transported supine in a rescue litter resulting in their full exposure to the high level of vibrations of the helicopter floor. This point is confirmed by reported vibration levels which are at the high end for comfort and health.

It is *suspected* that these vibrations are being absorbed by the patient's body and dislodging the bubbles which are attached to the artery walls, increasing the level of bubbles in their arterial flow and hence the severity of the illness. This hypothesis needs to be tested in a clinical trial which will expose fifty subjects to simulated dives in a hyperbaric chamber and retrieval flights using a vibration simulator. Whilst vibration simulators are available none suitable were found and therefore this research project was created to investigate the feasibility of developing a custom simulator.

A successful simulator design will require identification or development of a suitable actuator with its associated controller, an appropriate input drive signal and the mechanical and electronic components of the simulator. The most suitable type of actuator is an electrodynamic shaker and a comprehensive range of shakers with their accompanying power amplifiers are available from manufacturers. Electrodynamic shakers are specified by a range of parameters including the maximum force generated, stroke length, bandwidth and the mass that they can support, all of which will need to be quantified as part of the design process. The key to quantifying these parameters is found in the identification and analysis of the input drive signal that will be used for the study.

The input drive signal will be a Field Data Replication type, either a random signal specified by its Power Spectral Density shape, RMS level and amplitude distribution or an acquired time-domain vibration signal measured during an actual winching and retrieval flight. Neither of these are available and as the specification for the random signal would be developed from an analysis of typical acquired time-domain data anyway, the acquisition of typical time-domain data is to be the first priority for the project.

The process of acquiring time-domain vibration data begins by identifying a suitable vibration sensor. Vibrations are measured with accelerometers of which there are two relevant types, the traditional piezo-electric accelerometer and the more recent Micro Electro-Mechanical System devices. Helicopter vibrations reported in the literature show RMS levels of 102 mg to 382 mg with peak levels of around 800 mg and helicopter manufacturer's data shows that a bandwidth of 150 Hz would be sufficient. Both types of accelerometer are suitable however the advantage of the MEMS type is its small size, low profile, low power requirements and it does not require a large, heavy charge amplifier although their characteristics and performance such as frequency response will require further investigation to verify their suitability.

The most suitable type of controller for the simulator electrodynamic shaker is an iterative controller which overcomes the non-linear frequency response of the shaker and the power amplifier gain setting by adjusting the Power Spectral Density of the shaker input signal so that the PSD of its output matches a standard. The iterative controller is the simplest to implement and

gives quite satisfactory performance although it does take a number of iterations to settle but this is not expected to be an issue in this scenario. No affordable commercial controller could be found therefore a major part of the second phase of the project will be the development of a suitable controller.

CHAPTER 3

THE VIBRATION MEASUREMENT SYSTEM

3.0 INTRODUCTION

This chapter presents the vibration measurement system that was developed for recording the vibrations experienced by a patient during helicopter winching and retrieval. This work is the initial stage in answering the first of the research questions posed in this thesis “*Is it feasible to record the vibrations experienced by patients lying supine in a rescue litter during helicopter winching and retrieval?*”. The following chapter (Chapter 4) on *Vibration Measurement System Verification* completes the answer to this question by proving the validity of the recorded data.

The recorded vibrations will become the “*real vibration data*” or “*Time Waveform Replication (TWR) data*” used to drive the vibration simulator presented in Chapter 5. The simulator will play back the recorded vibrations to simulate a helicopter retrieval flight and so the measurement system must be capable of recording all flight modes and flight sequences that would be encountered in a typical retrieval. An extensive search failed to find any real vibration data or any existing system capable of recording the real vibration data and therefore the decision was taken to investigate and design the vibration measurement system presented in this chapter.

In operation the vibration measurement system records a complete retrieval flight starting with winching a patient from the deck of a small boat. To simulate this the system is mounted to a rescue litter with a mannequin as shown in Figures 1.1, 3.2, 3.5 and the litter is placed on a low bench in a field. A formatted SD card is inserted in the Controller SD card slot and fresh batteries installed. The system is powered on and goes through its initialisation sequence after which it is ready to commence recording vibrations. Once recording commences vibrations are recorded continuously during winching, hover and flight through to landing. To allow the recorded vibrations to be matched to the flight a manual record of flight mode and aircraft parameters is kept at 15 second intervals (Table A.1). After flight the SD card data file is transferred to a PC where it is converted into multiple 15 second csv files for data analysis in Excel.

The chapter is organised as follows:

Section 3.1 describes the development of an operational requirement for the system and an investigation of appropriate sensors and other electronics.

Section 3.2 presents the design and development of the system hardware

Section 3.3 present the system software.

Section 3.4 is the summary and conclusion for the chapter.

3.1 DESIGN CONSIDERATIONS

This section provides details of the major system components and the reasons behind their choice. This in-part provides the basis for the operational specification of the Vibration Measurement System.

3.1.1 OPERATIONAL REQUIREMENTS

The following operational requirements for the Vibration Measurement System were developed using the vibration levels reported in the literature (Sections 2.5, 2.6) and a study, by the author, of the operational environment in the helicopter:

- **Reliability:** The Bell 412 helicopter costs around \$4000 per hour to operate. As funding for the project is limited the vibration measurement system has to perform to requirements 100% of the time.
- **Non-invasive:** The measurement system must be attached to the rescue litter in such a way that it can measure the vibrations experienced by the patient during winching and retrieval without impeding the normal safe operation of the helicopter and crew. This means that no part of the system may protrude from the rescue litter as this will form a catch hazard when the litter is moved into the helicopter at the end of the winching operation and a trip hazard during flight.
- **Cover all flight modes:** The measurement system must record continuously for the duration of a retrieval flight and include all flight modes in the correct sequence and duration. A typical retrieval flight would have winching, winch hover, climb, cruise, descent and landing flight modes and may last for up to two hours.
- **Portable:** The measurement system must be small enough to fit inside the rescue litter with a patient and not impede the normal operation of the retrieval. It must therefore be portable and completely self-contained.
- **Measure three axes (longitudinal, lateral and vertical) of vibration at the head waist and feet as recommended by ISO 2631. All nine channels to be sampled simultaneously:** ISO 2631 weights the axes with the vertical axis most important and therefore dominant. Cost constraints will limit the simulator to vertical axis vibrations only but collecting data from the three orthogonal axes will allow confirmation of the dominance of the vertical axis and examination of the vibration modes of the helicopter. Simultaneous sampling of the longitudinal, lateral and vertical axes will allow reconstruction of the three dimensional vibration signal if required.

- **Signal bandwidth of 200 Hz:** A signal bandwidth of 200 Hz will cover the range of frequencies that affect the human body and the major sources of helicopter vibrations (Table 2.3). To allow high resolution signal analysis the sampling frequency should be a minimum of seven times the required bandwidth. In this case the desired sampling frequency is set at 2 kHz.
- **Data storage requirement:** Data will be stored in a quasi csv format requiring 31 bytes to store each sample. This translates to over 450 MBytes for a two hour flight and a sustained storage rate of 62 kBytes per second.
- **Peak acceleration rate of 8 ms^{-2} (816 mg):** This is the peak level of vibration reported in the literature.
- **Resolution:** A resolution of 1% (8.16 mg) is deemed sufficient.

3.1.2 OPERATING ENVIRONMENT

Figure 3.1 shows an empty rescue litter in its flight position inside the helicopter. During retrieval the litter (with patient inside) enters the helicopter via the starboard sliding door (Figure 2.1) and must be manoeuvred into the position shown. To avoid the possibility of damage to the measurement system or safety issues for the crew no part of the measurement system can protrude beyond the litter. Notice that the litter is placed directly on the helicopter floor allowing the full vibrations of the floor to be transmitted directly to the patient.

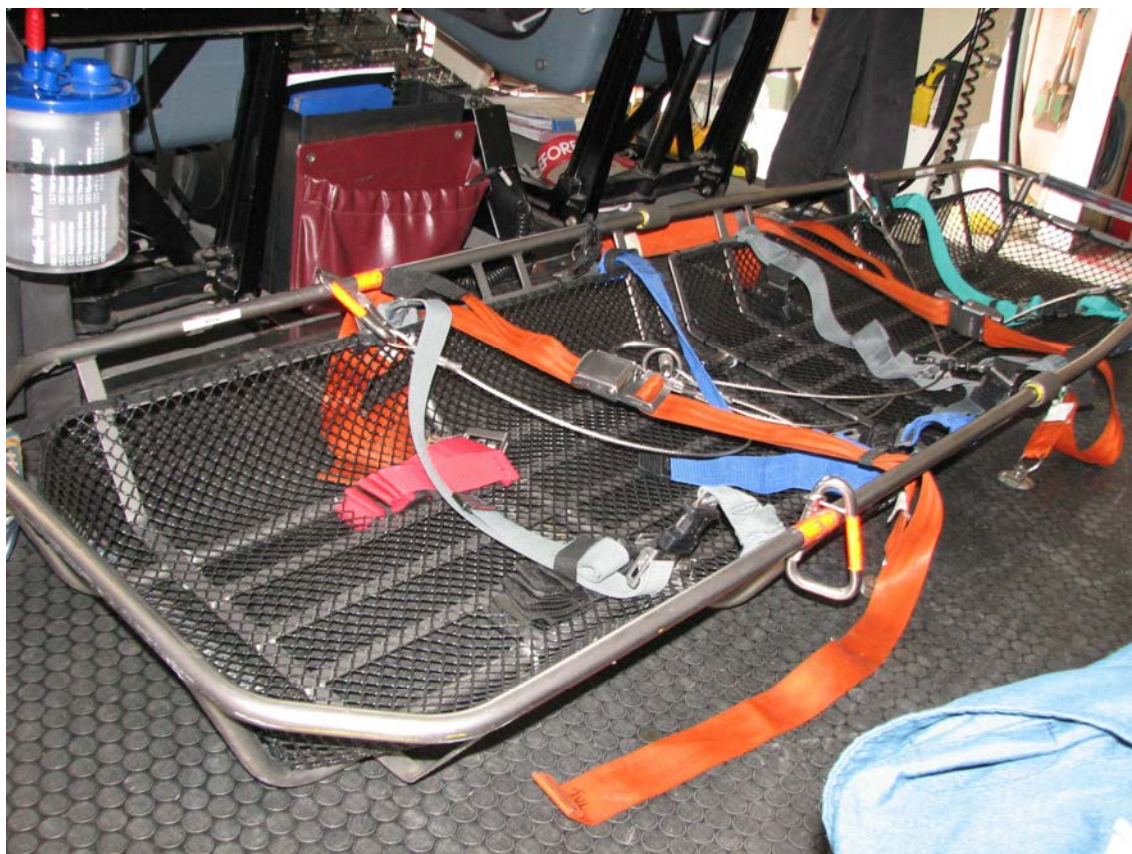


Figure 3.1: Shows an empty rescue litter in its normal flight position, in-between the pilots (upper left) and crew seats (bottom right). The patient's head would be positioned on the left with feet on the right. Past the feet can be seen the open hinged door which is not opened during winching (Figures 2.0, 2.1). The sliding door opening through which the rescue litter, with patient inside, is man-handled at the top of the winching operation is to the right and cannot be seen in this image. The winching harness (stainless cable) is removed during flight. The blue/grey quick release straps are used to secure the patient into the litter and the orange straps secure the litter to the helicopter floor. Notice that the litter is not rigidly attached to the floor allowing considerable movement in flight.

3.1.3 SENSOR MOUNTING

The vibration sensors need to be mounted so that they give a true representation of the level of vibrations experienced by the patient. Ideally they would therefore be in-between the inside of the litter and the patient where the patient makes contact with the litter, unfortunately this would be quite uncomfortable for the patient. There is however a low (19mm) cavity underneath the litter created by the tubular frame (Figure 3.2) which is an ideal sensor location as the sensors measure the same vibrations as experienced by the patient and the frame provides a degree of

protection for the sensors. The frame is however quite flexible and any sensor mounting technique will need to allow for this.



Figure 3.2: Shows the cavity beneath the litter created by the 19mm tubular frame. Note that in this image the litter is inverted. Due to its lightweight construction the litter frame suffers considerable flexing during handling particularly when held from the ends as it is when the litter is being manoeuvred into the helicopter.

3.1.4 VIBRATION SENSORS

The traditional vibration measurement sensor is the piezoelectric accelerometer an example of which is the Bruel & Kjaer (B & K) 4321 Tri-axial Piezoelectric Charge Accelerometer (Figure 3.3) which has three orthogonally mounted accelerometers aligned with its longitudinal, lateral and vertical axes. These accelerometers are designed for industrial machine condition monitoring and as such are rugged, reliable and environmentally sealed. They feature high sensitivity, low noise, high bandwidth and are calibrated by the manufacturer but their frequency response does not extend down to dc and they are therefore unable to measure the gravity vector. They are however relatively large (the B & K 4321 is 35 x 35 x 17mm) and expensive and require a large charge amplifier (Figure 3.3) to provide power and signal conditioning for the sensor. For use in this scenario three accelerometers and charge amplifiers would be required and they do not have the facility to be synchronised or to set the sampling rate. For these reasons piezoelectric accelerometer were not suitable for this project.

The sensor chosen for measuring the vibrations is the Freescale MMA7260 Micro Electromechanical System (MEMS) tri-axial accelerometer. There is some discussion in the literature on the suitability of MEMS accelerometers for measuring machinery vibrations (Section 2.9) however testing conducted as part of this thesis has validated this choice (Chapter 4). A summary of the relevant features of this device follow:

- **3-axis acceleration measurement:** This will allow measurement of vibrations along the longitudinal, lateral and vertical axes.
- **Sensitivity:** 800 mV/g gives it a measurement range of $\pm 1500 \text{ mg}$ (14.7 ms^{-2}) which is well above the required peak acceleration of 816 mg.
- **Low noise level of 4.7 mV rms:** This is 0.14% of full scale and 0.72% of the required peak acceleration and gives a Signal-to-Noise Ratio (SNR) of over 40dB which is more than adequate to ensure quality of measurements.
- **Theoretical resolution 0.73 mg (7.18 mms⁻²):** When sampled with a 12 bit analog-to-digital converter (ADC).
- **Bandwidth dc-to-150 Hz:** This is less than the desired 200 Hz but still sufficient to include the major frequency tones expected to be generated by the helicopter. As the bandwidth extends down to dc these accelerometers are able to measure the gravity vector.
- **Power supply 3.3 Vdc:** This is compatible with the power requirements of the rest of the measurement system electronics.
- **Analog outputs – suitable for simultaneous sampling:** Simultaneous sampling of the nine vibration channels and sampling at 2 kHz requires sensors with analog outputs which can be connected to external microcontroller controlled Sample/Hold (S/H) and ADC circuits.
- **Low – power, cost, profile (25 x 25 x 4 mm):** The sensor is designed for low power portable applications and consumes less than 500 μA . The profile height (4 mm) is for the sensor mounted on an evaluation board and makes it suitable for mounting in the cavity underneath the rescue litter.
- **Frequency response:** The frequency response is not specified by the manufacturer and so the device will require calibration.

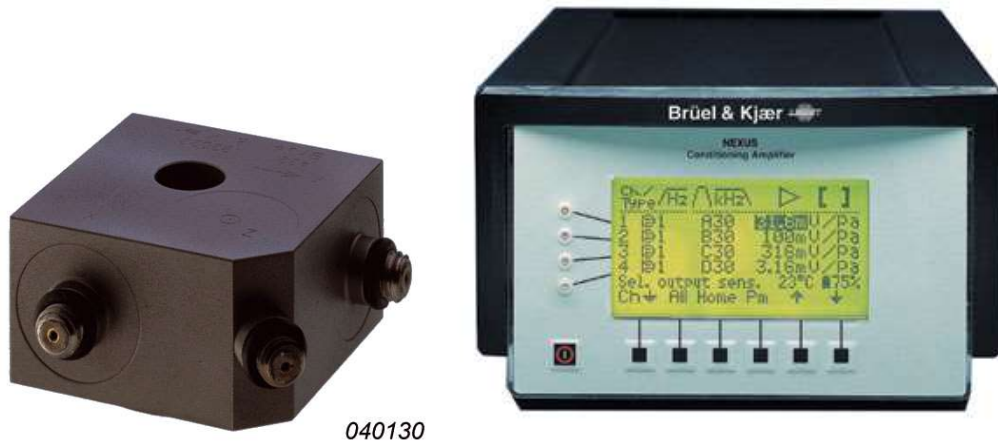


Figure 3.3: Bruel & Kjaer 4321 Triaxial Piezoelectric Charge Accelerometer (left) and 4 channel Charge Conditioning Amplifier (right).

3.1.5 ANTI-ALIASING FILTER

The system requires an anti-aliasing filter on each of the accelerometer analog outputs to limit its bandwidth before being sampled. The main considerations in the choice of the anti-aliasing filter is a flat response in the pass-band, linear phase response, rapid transition from pass-band to stop-band and sufficient stop-band attenuation to prevent aliasing of the higher frequency components of the signal. The MAX7424 is a 5th order Butterworth switched capacitor filter with a maximally flat pass-band response, a typical stop-band attenuation of -70 dB and a clock-tuneable corner frequency from 1 Hz to 45 kHz.

In this application the required stop-band attenuation is set by the theoretical resolution that can be achieved by the system sampling of the analog signal (0.73 mg). The requirement is that the maximum level of input signal must be attenuated sufficiently to make it less than the resolution at the sampling frequency. In this case the maximum signal is 816 mg and -70 dB attenuation of this signal level would reduce it to 0.258 mg while a 5th order filter with a corner frequency of 150 Hz will achieve -70 dB attenuation at 752 Hz making both specifications well within the requirement.

The filter also requires a square wave clock signal of 15 kHz to set the corner frequency at 150 Hz. This is supplied directly from a clock module in the controlling microcontroller. Note that here unity-gain analog buffers are included on the input and output of each filter to provide signal isolation for each stage (Figure 3.6).

3.1.6 SIMULTANEOUS SAMPLING OF ALL VIBRATION SIGNALS

A requirement for the vibration measurement system is that all nine channels of vibration data are sampled simultaneously at 2 kHz. Whilst microcontrollers feature multiple analog-to-digital converter (ADC) inputs they usually have a maximum of two ADCs which are connected to multiple inputs via a software controlled analog switch and therefore cannot sample multiple inputs simultaneously. The solution is to place a Sample/Hold (S/H) unit, such as the SMP04, in each analog input circuit before the microcontroller ADC input (Figure 3.6). The S/H units have a “*Sample*” input which allows the S/H to capture and hold the analog input at any instant. Synchronous sampling is achieved by pulsing all the “*Sample*” inputs using a single buffered digital input/output (DIO) pin on the controller MCU.

Care must be taken with this design to ensure that at its maximum rate of change the input signal will not change by more than the system resolution (0.73 mg) in the width of the S/H pulse. Here the absolute maximum rate of change of an input signal with a maximum input level of 800 mg and a maximum frequency of 150 Hz and would be 0.754 mg/ μ Sec. Note that the maximum rate of change of the input is proportional to both the signal amplitude and frequency and as all the vibration tones will be lower in both amplitude and frequency then the maximum levels quoted above then, provided the “*Sample*” pulse is kept to around 1 μ sec the S/H will have no effect on the signal quality.

3.1.7 CHOICE OF MICROCONTROLLER

The microcontroller (MCU) chosen is a Freescale MC9S08JM60CLD which is a low-power 8-bit MCU in a 44 pin LQFP package. Note that this device is low-power in terms of power consumption but high-power in terms of performance for an 8-bit MCU. The relevant features of the MC9S08JM60CLD are:

- **High performance 8-bit MCU:** At the time of this project the MC9S08 family of MCUs were one of the most powerful 8-bit MCUs available and they included a rich array of on chip peripherals including USB, ADC and timer ports.
- **Low power 3.3 VDC operation:** The MC9S08 family are designed for use in battery powered portable devices and can operate with a power supply voltage from 2.7 to 5.5 Vdc with typical power supply current of 22 mA at maximum clock speed. This is important as the MCU needs to operate at its maximum speed for this project.
- **8 channel 12 bit ADC:** The MC9S08JM60CLD has two analog-to-digital converters (ADC) each of which can be connected to one of four analog input pins under software

control. The ADCs can operate in 8, 10 or 12 bit mode and can complete a conversion in 48 μ Sec.

- **Memory capacity:** 4kB RAM, 60 kB Flash. Both the RAM and flash memory are sufficient for this system.
- **44 pin LQFP package:** The 44 pin LQFP package is suitable for use in small production runs and hand soldered prototype boards.
- **Sophisticated software development support:** Freescale provides the licence free Codewarrior Integrated Development Environment (IDE) which includes the Processor Expert (PE) rapid development suite of software. This is a sophisticated professional IDE that is well suited to developing this type of system.

3.1.8 DATA STORAGE

The system requires over 400 MBytes of data storage for a two hour flight which is provided using a 2 GByte non-volatile flash memory Secure Digital Standard Capacity (SDSC) card. SD cards are cheap and reliable and used extensively in portable devices such as digital cameras. Relevant features of the SDSC card are:

- **Small size:** SDSC cards are 32 x 24 x 2.1 mm which makes them small enough to be fitted on a printed circuit board (PCB). They can be made removable using a standard SD card PCB socket.
- **Large mass storage capability:** SD cards come in a variety of storage capacities and operating speeds. The 2 GB SDSC card is a relatively low capacity variant but it can be partitioned into 1 GB partitions and each formatted to FAT16 standard.
- **Flash memory:** SD cards use non-volatile NAND Flash memory which is addressed as sequential 512 bytes blocks. This means that all read/write/erase operations are carried out on full blocks. When erased NAND Flash memory is in a logic “1” state and a write operation performs a bit-wise logical AND between the current contents and the new data, consequently SD cards are unsuitable for use as Random Access Memory (Thanagasundram 2006). In normal operation to write a single byte to an SD card the block in which the next available byte exists is read, the whole block is erased and rewritten with the original data plus the additional byte, therefore a simple write operation involves four separate operations and can take a considerable amount of time over a serial connection.
- **Low voltage operation:** SD cards are low power devices that operate at 3.3 Vdc which is compatible with the other electronic components in the vibration measurement system.

- **Simple interfacing:** SD cards offer both licensed high speed parallel and unlicensed low speed Serial Peripheral Interface (SPI) interfacing options. The SPI option is used exclusively in microcontroller based applications as there are no license fees associated with its use and most microcontrollers have an SPI port as part of their peripheral suite.
- **Requires a FAT16 file operating system:** The SD card appears as a hard disk mass storage device to the microcontroller and so the microcontroller will require a file operating system as part of its software to allow it to create, open, close, read and write files on the SD card. The operating system must match the structure that has been implemented on the SD card when it has been formatted. Due to its simplicity and lower memory requirements most 8-bit microcontrollers use a FAT16 operating system so called due to the 16-bit entries in the File Allocation Table (FAT) which is a linked list of the 512 byte blocks that make up a file. SD cards however come formatted for a FAT32 operating system and must be reformatted to FAT16 before they can be used. The card host is required to have software to enable standard file operations such as File Create, File Open, File Close, File Write, File Read etc.

3.2 SYSTEM HARDWARE

3.2.1 SYSTEM ARCHITECTURE

The Vibration Measurement System architecture reflects the operational environment of the helicopter, the physical construction of the rescue litter and the need for high quality measurements to be taken synchronously at the head, waist and feet of the patient during all flight modes. A distributed architecture (Figure 3.4, 3.5 and Table 3.1) is employed consisting of a central Controller Unit with a master microcontroller (MCU), user interface, SD card and system power and three Sensor Boards each with a tri-axial accelerometer, signal conditioning circuitry and analog-to-digital (ADC) converter provided by an MCU. The three Sensor Boards are connected to the controller unit by shielded multi-wire cable which supplies power, sampling synchronisation clock and bidirectional digital serial communications between the central controller and Sensor Boards. This distributed architecture minimises the noise level of the system by having the shortest possible analog signal path lengths, shielding long cables and utilising digital communications between the controller and remote Sensor Boards.

Inside the cabin of the helicopter is an electrically noisy environment with a large number of high power instruments, motors, radio frequency (RF) communications equipment and rotating machinery all with the potential to induce noise on the analog signals coming from the vibration sensors. The distributed architecture with the ADC on the Sensor Board adjacent to the sensor

gives the shortest possible analog signal paths minimising the potential for noise pickup before sampling. Positioning the sensors under the head, waist and feet of the patient means that they will be physically separated, from the controller, by up to one meter and must be connected by cables as a wireless connection has the potential to cause interference with the helicopter on-board systems. Long cables however act as antennas and have the potential to capture surrounding electrical noise as well as radiate broadband interference generated by the high switching speeds of the digital signals used for communicating along the cables. To minimise these effects the cable between the controller and Sensor Boards is shielded with the shield earthed at the controller.

Digital serial communications in the form of a Serial Peripheral Interface (SPI) bus is used for communications between the controller and Sensor Boards. To ensure reliability of communications all signals on the SPI bus and the Sample signal are driven by high power line drivers and terminated by Schmidt trigger input receivers. The line drivers minimise the drop in signal level and signal rounding over the length of the cable while the Schmidt trigger receivers further reduce signal rounding and eliminate any noise in the received digital signal.

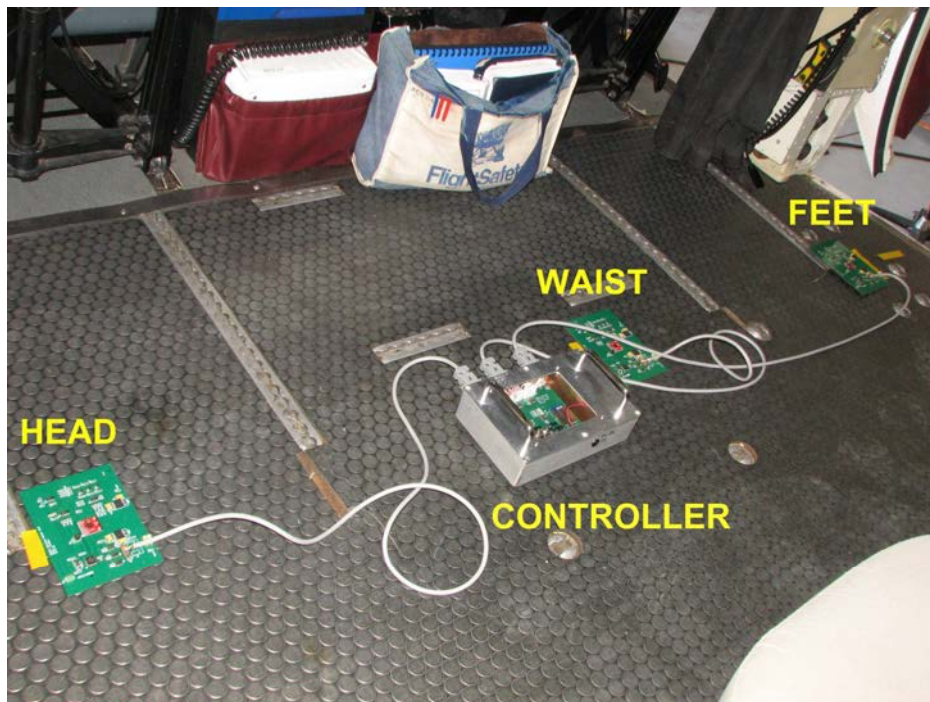


Figure 3.4: The Vibration Measurement System. Image shows the Controller unit (CONTROLLER) in its metal enclosure and the three Sensor Boards (HEAD, WAIST and FEET) connected by their shielded cables. In this instance the sensors are mounted on the helicopter floor to record the vibrations of the floor itself.

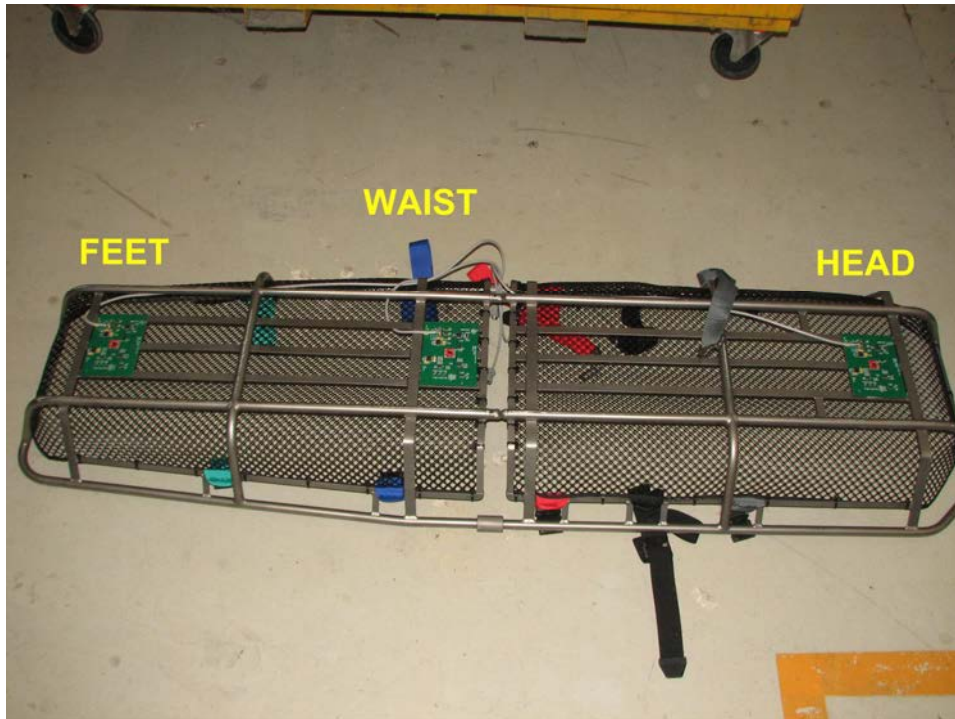


Figure 3.5: Vibration Measurement System sensors mounted in their normal operational position underneath the rescue litter. Note that the sensor circuit boards are sized to fit across the three flat longitudinal stringers maximising their mechanical support and contact with the patient.

Table 3.1: Showing the functionality of the Vibration Measurement System Controller unit and Sensor Boards.

System Component Functionality	
<p>Controller:</p> <ul style="list-style-type: none"> • MC9S08JM60 MCU <ul style="list-style-type: none"> ○ Sampling timing control ○ User interface ○ SPI comms (master) ○ Sample record formatting ○ SD card file operation • Power • SD card 	<p>3 x Sensor Boards:</p> <ul style="list-style-type: none"> • MMA7260 tri-axial accelerometer • Signal conditioning • Sample/Hold circuits • MC9S08JM60 <ul style="list-style-type: none"> ○ Signal sampling ○ SPI comms (slave) ○ Anti-aliasing filter clock

3.2.2 SENSOR BOARDS

The Sensor Boards (Figures 3.5, 3.6 and Table 3.1) are designed to accommodate a vibration sensor positioned so as to provide contact with the patient, signal conditioning circuitry, Sample/Hold circuitry to allow sampling synchronisation and a microcontroller (MCU) to control the operation of the Sensor Board, provide signal sampling with an analog-to-digital converter (ADC), temporary storage of samples in random access memory and communications with the system controller using a Serial Peripheral Interface (SPI) port.

The vibration sensors printed circuit boards (PCB) are sized so that they can be attached to the three longitudinal stringers of the rescue litter (Figure 3.5). This provides protection for them in the cavity underneath the litter but also ensures direct contact with the patient guaranteeing that the sensors measure the same vibrations as experienced by the patient (Figure 3.2). The longitudinal stringers however flex considerably when the litter (with patient inside) is lifted by the ends, for example when it is being man handled into the helicopter at the top of a winching, and care must be exercised to ensure that the board is properly supported when attached to the stringers and that all solder joints are of high quality with sufficient solder to give good mechanical adhesion for the board components.

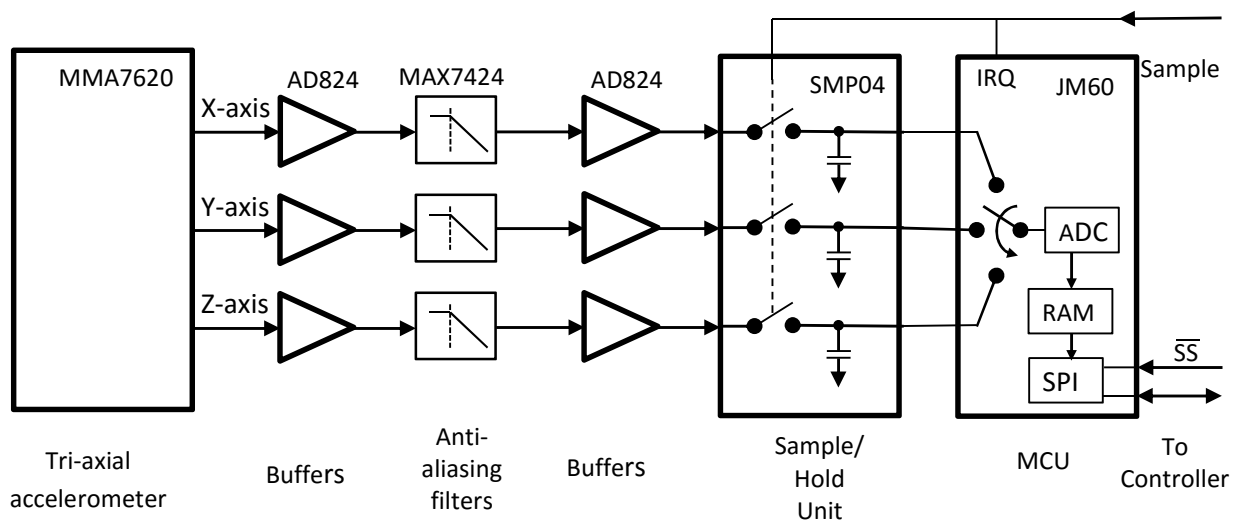


Figure 3.6: Sensor Board block diagram. Analog vibration signals originate in the tri-axial accelerometer and flow from left to right. Note that each Sensor Board has three vibration channels.

The system controller initiates synchronous sampling of all the vibration channels by pulsing the Sample signal low. When the Sample signal is low the Sample/Hold (S/H) is in sample mode and acquires the input signal level making the output equal to the input. The rising (trailing) edge of the Sample pulse places the S/H in hold mode keeping its output constant and also generates an interrupt request on the Sensor Board MCU. The MCU services the interrupt request by sampling the three input analog signals sequentially with its ADC and saving the results in temporary RAM storage. The MCU then prepares to send the results over the SPI bus when prompted by the controller. After initiating the sampling process the controller waits sufficient time for the Sensor Boards to complete their sampling and then reads the results from the three Sensor Boards consecutively.

Power is supplied to the Sensor Boards from the controller at +9–10 Vdc. The +9–10 Vdc is used directly to power the SMP04 Sample/Hold unit as well as being filtered and regulated to provide separate +3.3 Vdc analog and digital power for the other componentry on the board. To minimise digital switching noise propagation into the analog signals via their power supplies the Sensor Boards utilise separate analog and digital 3.3 Vdc power supplies with physically separated ground planes.

3.2.3 CONTROLLER UNIT

The controller unit (Figure 3.4, 3.7, Table 3.1) controls the sampling process by initiating sampling on the Sensor Boards, reading the sample results from the Sensor Boards and storing them in a quasi csv format on the SD card. In addition the controller holds the system power source (6 x AA drycell batteries) and provides a simple user interface allowing the operator to initiate the sampling process. The controller unit and power source are housed in a diecast metal box that is placed in the rescue litter with the patient during flight (Figure 1.1).

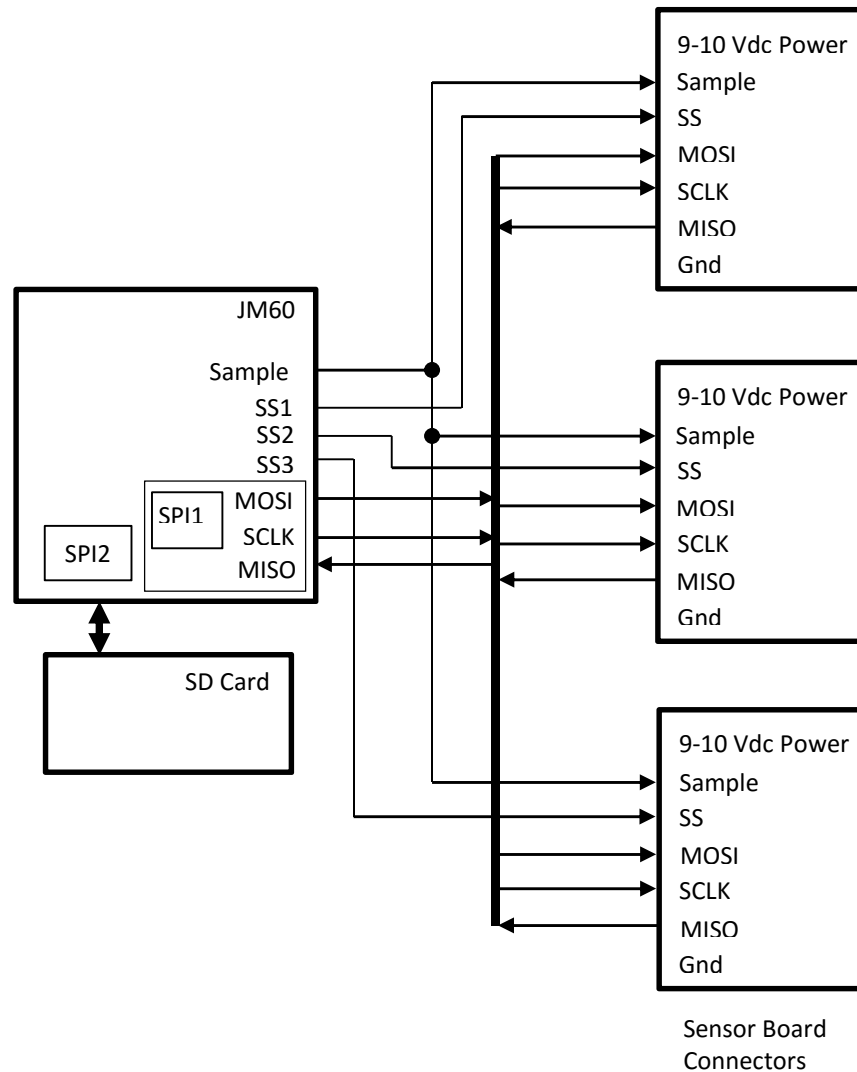


Figure 3.7: Controller board block diagram showing the SPI communications between the MC9S08JM60 (JM60) microcontroller, the SD card (SPI2) and Sensor Boards (SPI1) as well as the Sensor Board control signals Sample and Slave Select (SS1, SS2, SS3). The bus drivers and receivers for the Sensor Board communications are not shown.

3.2.4 CONTROLLER UNIT TO SENSOR BOARDS COMMUNICATIONS

The Vibration Measurement System uses a buffered SPI bus between the Controller Unit and the Sensor Boards to ensure reliable high speed communications. The buffering is shown in Figure 3.8. SPI signals MOSI, SCLK, SS, MISO and the Sample signal are transmitted on the bus with tri-state bus drivers and received into Schmidt-triggered line receivers. The tri-state bus drivers serve two purposes; firstly they provide sufficient drive capability to transmit high speed digital signals over the length of the bus and secondly their tri-state capability is required for multiplexed

bus signals such as MISO where only one of the three Sensor Boards can be transmitting on the bus at any one time. The Schmidt-triggered receivers overcome any signal rounding introduced due to the capacitance of the bus or signal noise picked up by the bus to ensure that a clean high transition speed signal is passed onto the receiving components.

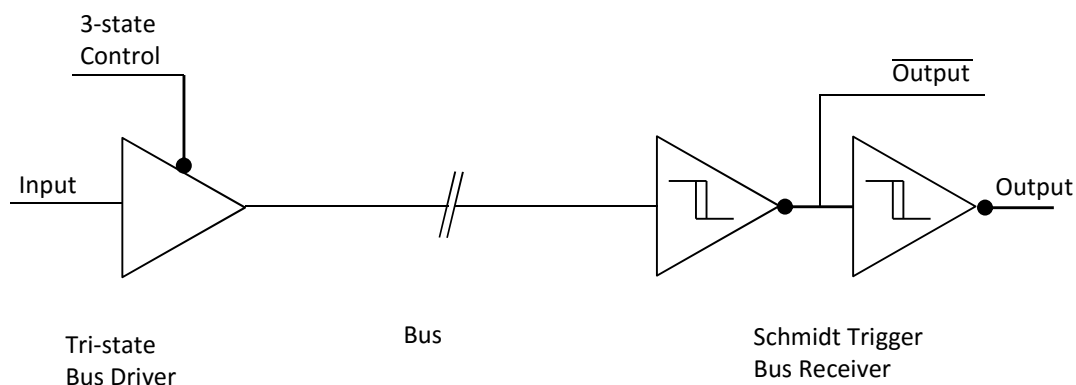


Figure 3.8: Showing the line driver/receiver setup for communications between the Controller Unit and Sensor Boards.

3.2.5 SYSTEM POWER

For normal operation power for the system (+9-10 Vdc) is supplied by six AA drycell batteries located in the Controller unit enclosure however there is also provision for the connection of an external +9Vdc power source for use during system development. In the controller an LD1085 voltage regulator converts this power to +3.3 Vdc to operate the controller electronics which are digital only. The +9-10 Vdc power is also distributed to the three Sensor Boards to provide power to the SMP04 Sample/Hold unit directly as it requires a power supply greater than +6 Vdc. The +9-10 Vdc is also converted to two separate analog and digital +3.3 Vdc supplies by individual regulators.

Providing a separate analog +3.3 Vdc power supply on the Sensor Boards impedes the propagation of digital switching noise into the analog signals and helps in minimising the overall system noise level. The analog +3.3 Vdc power supply also provides a reference voltage for the microcontroller analog-to-digital converter and the vibration sensor both of which are ratiometric. The LD1085 voltage regulator is used as it provides a stable low-noise reference voltage with high noise rejection and low temperature coefficient.

3.3 SYSTEM SOFTWARE

This section provides an introduction to the software of the Vibration Measurement System which comprises the controller and Sensor Boards operating programs that record the patient vibrations during flight and the post-flight file conversion and data analysis software. Software forms a major part of the system as it is wholly computer based both in the Embedded Microcontrollers of the flight data measurement system and the file conversion, verification and analysis done on a Personal Computer. Although software and hardware are discussed separately it should be noted that in this type of design software and hardware work together, complementing each other and an appreciation and understanding of both is required to fully comprehend the value of the system concept and to undertake its design. This section should therefore be read in conjunction with the section on System Hardware (Section 3.2).

The system uses a variety of software for the different tasks performed ranging from the *hard real-time*² embedded C software in the Controller and Sensor Boards to C++ for the file conversion and Excel for the data analysis and presentation. Each of these tasks is explained separately in the following sections as well as background information on relevant topics such as .csv files and SD Card operational commands.

At the time of designing the system, the controller and Sensor Board MC9S08JM60 microcontrollers (MCU) were among the most high-performance low-power 8-bit MCUs available however they experienced performance issues when attempting to achieve the sampling times and SD card data write rates required in this design. Realizing the required sustained SD card data write speed was a significant issue and required a detailed understanding of the SD Card theory and operating software as well as the development of a novel algorithm for writing large data files to the SD card at high speed (Section 3.3.3).

The presentation of the system software commences with a general overview explaining the function of each of the parts and their interaction.

3.3.1 SOFTWARE OVERVIEW

The system software is divided into two major parts; firstly that which runs in the controller and Sensor Boards during flight, recording the vibration data on the SD card (Section 3.3.2 – 3.3.5) and secondly the post flight analysis software which converts the flight data into 15 second csv files and performs the data analyses (Section 3.3.7, 3.3.8).

² A time critical real-time system

The controller software is the heart of the vibration measurement system providing the user interface, sampling timing, Sensor Board communications and SD card operation (Table 3.1) whilst the Sensor Board software is responsible for sampling the analog-to-digital converters, generation of the anti-aliasing filter clocks and communications with the controller. The embedded MCUs at the heart of the Controller and Sensor Boards use a hard real-time operating system (RTOS) which ensures timely response to their real-time software tasks such as periodic signal sampling as well as background processes such as writing to the SD card. A RTOS allows prioritisation and scheduling of software tasks into three levels with hardware interrupts having the highest priority followed by real-time tasks and then background tasks. All tasks can be further prioritised within these levels by either setting their priority level in hardware or scheduling the order in which they are serviced with the real-time scheduler. Software for the embedded systems is written in C using the Freescale Codewarrior Integrated Development Environment.

The purpose of the post-flight data analysis is two-fold. Firstly the file conversion software converts the SD card data file into a form suitable for data analysis (.csv) and use as the real vibration data to drive the vibration simulator. The file conversion software is written in Microsoft Visual C++ and runs on a PC. Secondly the data is analysed to verify that it is a true representation of patient vibration data and so provide an answer to the first research question *Is it feasible to record the vibrations experienced by patients lying supine in a rescue litter during helicopter winching and retrieval?* The analysis results also provide a clear picture of the patient vibration characteristics which will be used in the design of the vibration simulator. The data analysis is performed in Microsoft excel.

3.3.2 csv FILE FORMAT

This section provides background on the Comma Separated Value (csv) file format as applied in this project. The vibration measurement system uses a modified csv format to store up to two hours of recorded vibration data in a single large file on the SD card. The post-flight file conversion software (Section 3.3.7) subsequently converts this into sequential 15 second segments which are then converted to correct csv format and saved in individual csv files. The csv format is used because it is ASCII³ text based allowing viewing with a text editor program and csv files can be imported directly into Microsoft Excel where the vibration data analysis is performed.

³ American Standard Code for Information Interchange is a character encoding scheme which encodes 128 specified characters into 7-bit binary integers

A csv file (Figure 3.9) is a delimited text file for storing tabular data. Each row is termed a record and is made up of multiple fields (columns) each holding a single data entry which can be numeric or text. Fields are separated by a delimiter which in this case is a comma and records are terminated by a line terminator such as a carriage return /linefeed (CR/LF) character pair. Each record (row) contains the same number of fields in the same order. ASCII encoding is used for all file entries and numeric values are in decimal notation, therefore one byte of storage is required for each character or numeric digit.

```
08870,01907,01941,03064,01796,01955,03106,01955,01838,03083CRLF
08871,01908,01941,03059,01794,01955,03103,01957,01843,03095CRLF
08872,01909,01943,03054,01793,01957,03102,01961,01846,03106CRLF
08873,01910,01947,03045,01793,01956,03102,01967,01843,03115CRLF
```

Figure 3.9: Example showing four records from a csv vibration data file suitable for importation into Excel. The records are shown as they would appear in a text editor such as Notepad. Each record has ten fields delimited by commas. The CRLF line terminator at the end of each record would be two bytes 0x0D and 0x0A (using hexadecimal notation). The left field of each record is the sample number and the other fields are the vibration levels from the nine vibration channels. Note that the sample number and vibration level are 16-bit binary numbers and therefore require five decimal digits to represent them.

Vibration data stored on the SD card by the vibration measurement system during flight is in a quasi csv format where the numeric fields are in 16 bit hexadecimal format as there is insufficient time available between samples for the MCU to perform the hexadecimal-to-decimal-to-ascii conversion.

3.3.3 SD CARD OPERATION

A Standard Capacity Secure Digital card (SDSC) (Section 3.1.8) provides the mass storage for the vibration measurement system allowing it to store the flight vibration data. SDSC cards are commonly used for mass storage in embedded applications due to their large capacity, low power requirements and Serial Peripheral Interface (SPI) serial communications capability. Consequently, most MCU manufacturers and a number of third parties offer software suites that provide basic functionality for their devices to operate SD cards. However these suites are directed more towards the standard file create/read/modify operations where write speed is not an issue

and they are not suitable for real-time systems requiring sustained high-speed data rates writing to files. For this application a custom algorithm was developed to enable the 8-bit MCU to write the vibration data to the SD card at the required speed (Section 3.3.6). This section presents the custom algorithm along with an introduction to SD card operation.

All operations on an SD card are performed with 6 byte commands as defined in the SD card specification. Table 3.2 gives a summary of the commands used to operate the SD card in the vibration measurement system.

Prior to use an SDSC card must be correctly formatted to the FAT16 standard using software available from the SD card association (usb.org). Formatting sets up the card Volume Structure including the Master Boot Record, Partition Table, Partition Boot Sector, File Allocation Table (FAT) and Root Directory (MEI 2000).

Table 3.2: SD Card Commands. This is a listing of the SD card commands that are used to initialise and operate the card in the vibration measurement system. Those commands whose command index begins with A such as ACMD41 are termed application specific commands and they must be preceded by a CMD55 to tell the card that the next command is an application specific command.

Command Index	Abbreviation	Command Description
CMD0	GO_IDLE_STATE	Reset the SD memory card.
CMD8	SEND_IF_COND	Sends SD Memory Card interface condition that includes host supply voltage information and asks the card if it can operate at the host supply voltage.
CMD9	SEND_CSD	Read the card-specific data register (CSD).
CMD10	SEND_CID	Read the card identification register (CID).
CMD13	SEND_STATUS	Read the card status register
CMD16	SET_BLOCKLEN	Set block length (SDSC only)
CMD17	READ_SINGLE_BLOCK	Read a single block
CMD18	READ_MULTIPLE_BLOCK	Continuously read blocks until interrupted by a STOP_TRANSMISSION command
CMD24	WRITE_BLOCK	Write a single block
CMD25	WRITE_MULTIPLE_BLOCKS	Continuously write blocks
CMD27	PROGRAM_CSD	Write to the programmable bits of the CSD
CMD32	ERASE_WR_BLK_START_ADDR	Sets the address of the first block to be erased
CMD33	ERASE_WR_BLK_END_ADDR	Sets the address of the last block to be erased
CMD38	ERASE	Erases previously selected blocks
CMD55	APP_CMD	Informs the card that the next command is an application specific command
CMD58	READ_OCR	Read the Operation Conditions Register (OCR)
ACMD23	SET_WR_BLK_ERASE_COUNT	Set the number of blocks to be pre-erased before writing
ACMD41	SD_SEND_OP_COND	Sends Host Capacity Support (HCS) information [b30] and activates the card's initialisation process

3.3.3.1 SD CARD INITIALISATION

The SD Card initialisation process is described in detail in the SD Card File System Specification (MEI 2000). This section provides a summary of the procedure as implemented in this project. Figure 3.10 shows the initialisation sequence. It is assumed that the card has been formatted to FAT16 prior to use (Section 3.3.3). Card operational parameters that must be identified or set as part of the initialisation process are the communications mode, firmware version number,

operating voltage range, capacity, block length, file access variables and the data storage file “FILE.TXT”.

After power up the indicator LEDs are configured to provide user feedback on the system initialisation progress and the SD Card SPI port (SPI2) is configured to mode 0 with a baud rate of 375 kHz as the initial baud rate must be less than 400 kHz. The host then waits for 1 milli second to allow the SD Card power to stabilise before checking the Card Detect (CD) pin to confirm that a card is present. Eighty clock cycles are then sent with the Card Select not asserted (“1”). The SD Card powers up in SD communications mode and is transferred to SPI mode by issuing a GO_IDLE_STATE (CMD0) command. The card will switch to SPI mode and respond with the SPI mode R1 response token. The host then issues a SEND_IF_COND (CMD8) command to verify that the card is version 2 compliant. A valid response is an R7 token which includes the card version number and operating voltage range. A READ_OCR (CMD58) command is issued to read the card Operation Conditions Register (OCR) and verify that the card accepted voltage matches the host supply voltage. The card is initialised by continually sending SD_SEND_OP_COND (ACMD41) commands until the “in idle state” bit (b0) of the R1 response token clears to “0”. Note that each ACMD41 command must be preceded by a APP_CMD (CMD55) to tell the card that the next command is an application specific command. The OCR is read with a READ_OCR (CMD58) command and the Card Capacity Status (CCS) (b30) should be clear indicating a standard capacity (SDSC) card. The card block length is set to 512 bytes with a SET_BLOCKLEN (CMD16) command. The Card Specific Data register (CSD) is read with a SEND_CSD (CMD9) command and finally the SPI baud rate is set to high speed (4 MHz). The card is now initialised and ready for use.

The file system for recording the vibration data is set up next. The Master Boot Record is placed on the SD Card when it is formatted and defines the following parameters required for the operation of the card file system; the number of sectors per cluster, the number of bytes per sector, the sector number of the first sector of the File Allocation Table (FAT), the sector number of the first sector of the root directory and the sector number of the first sector of the data area. The MBR is read and a local variable is assigned to each of these parameters. Finally the data storage file “FILE.TXT” is created on the card. The File Allocation Table for “FILE.TXT” is modified to represent a 360,448 kByte file made up of sequential blocks and all the file blocks are erased. The system is now ready to record vibration data.

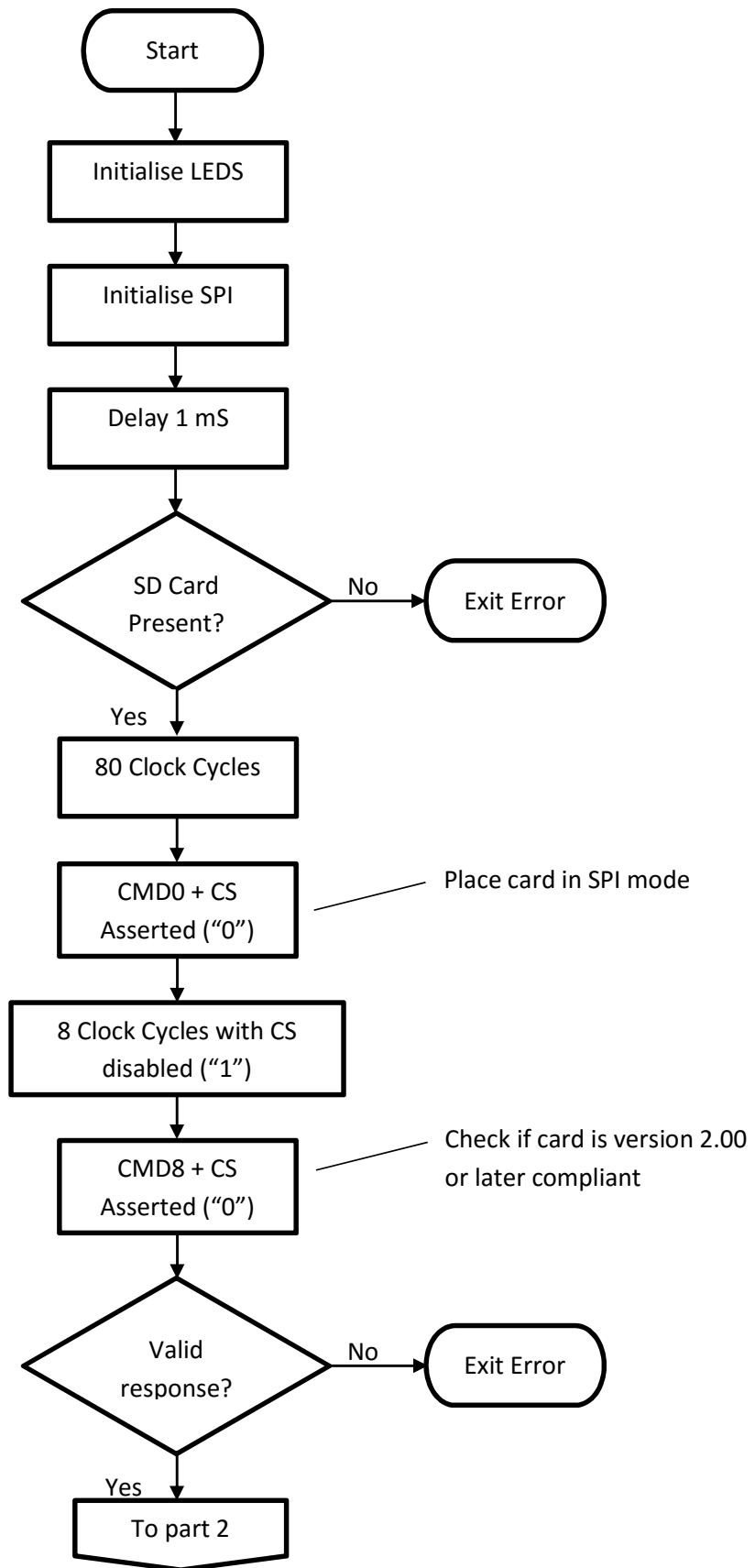


Figure 3.10: SD Card Initialisation Flowchart. Part 1/3

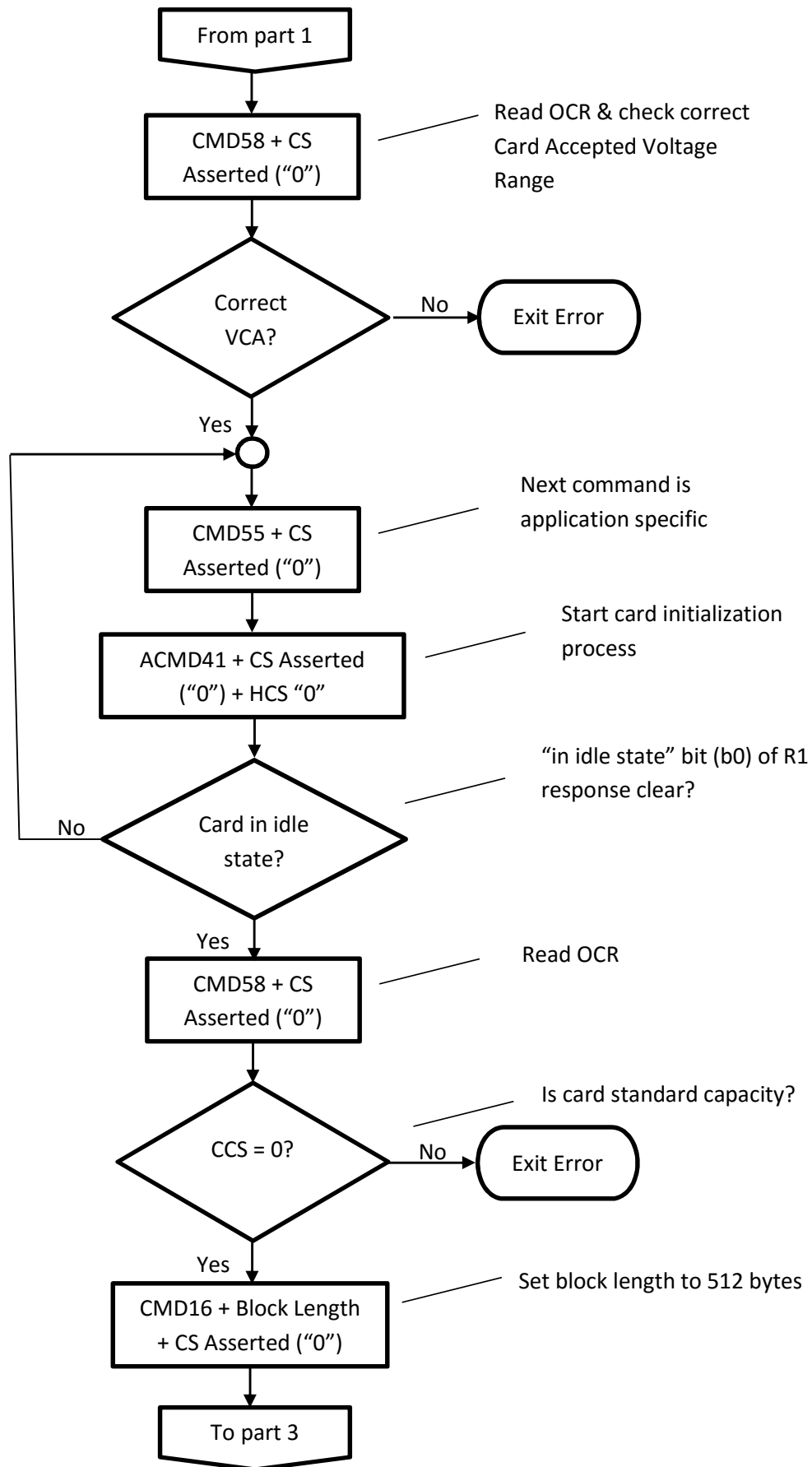


Figure 3.10: SD Card Initialisation Flowchart. Part 2/3

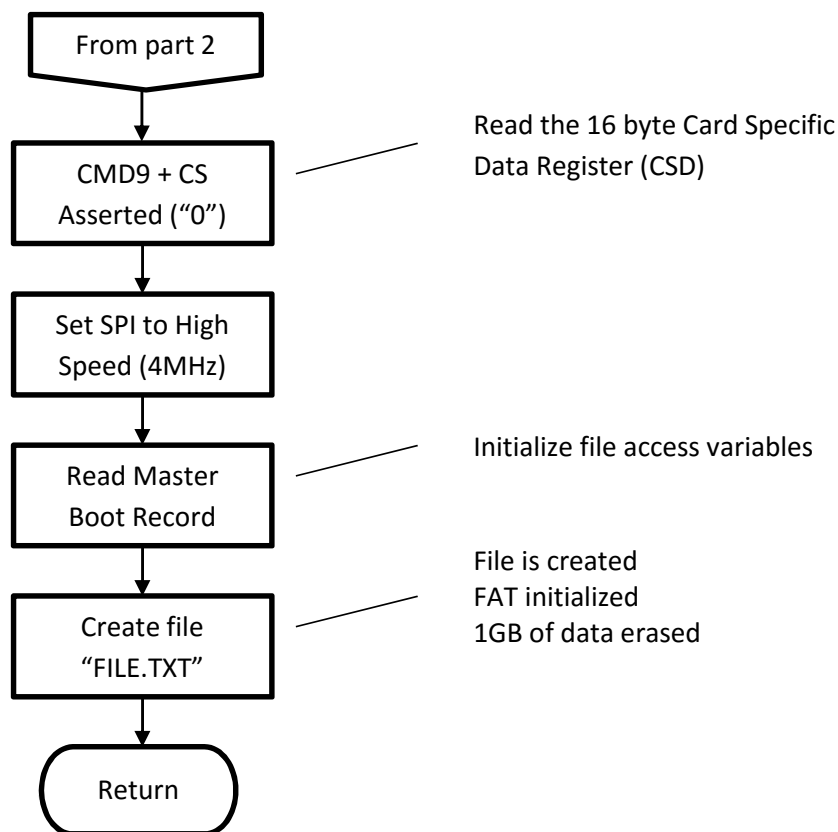


Figure 3.10: SD Card Initialisation Flowchart. Part 3/3

3.3.4 SAMPLING CONTROL SOFTWARE

The software for the Controller and Sensor Boards of the Vibration Measurement System uses a Real Time Operating System (RTOS) to prioritise and schedule the various tasks that must be performed. The sampling tasks are serviced by high priority hardware interrupts in order to maintain the correct sampling period (500 μ Sec). The sampling system is enabled during system initialisation and runs continuously however the sample data is not saved to the circular buffer and hence to the SD Card unless the system status is set to "SAMPLING" as explained in Section 3.3.5 Background Software.

One of the unique features of the vibration measurement system is its ability to synchronously sample nine channels of vibration data at a rate of 2 kHz which is made possible through the judicious design of system hardware and real time software. This section describes the mechanism for sampling the vibration channels and saving the sampled data on the SD Card.

The sampling control waveforms are shown in Figure 3.11. The sampling period of 500 μSec is set by a Pulse Width Modulated (PWM) signal generated by the Controller Timer 2 Channel 0 (TPM2CH0) and shown as the upper waveform in Figure 3.11. The PWM waveform is active (true) low with a duty cycle of 2% giving it a low pulse of 10 μSec at the start of each cycle. This waveform is buffered and sent to the three Sensor Boards where it connects to the Sample/Hold unit S/H input pins and the MCU Interrupt Request (IRQ) pin. The end of one sample cycle and the start of the next are marked “A” and coincide with the falling edge of the PWM waveform. The S/H units sample the vibration waveforms during the 10 μSec low pulse and hold their outputs constant, ready for sampling, after the rising edge. The pulse rising edge generates an IRQ interrupt request to the Sensor Board MCU. The IRQ Interrupt Service Routine samples the three vibration channels sequentially and places the results in a buffer ready for transfer to the Controller.

An overflow interrupt is also generated, in the Controller MCU, at the start of each cycle and its service routine initiates a 100 μSec “Sampling Delay Waveform” pulse on timer 1 channel 0 (TPM1CH0). This sampling delay provides sufficient time for the Sensor Boards to sample their three channels of vibration signals and prepare to transfer the results to the Controller. Following the 100 μSec delay the Controller sequentially reads the nine channels of vibration data, converts them to quasi csv format and places them in a circular buffer ready for writing to the SD Card.

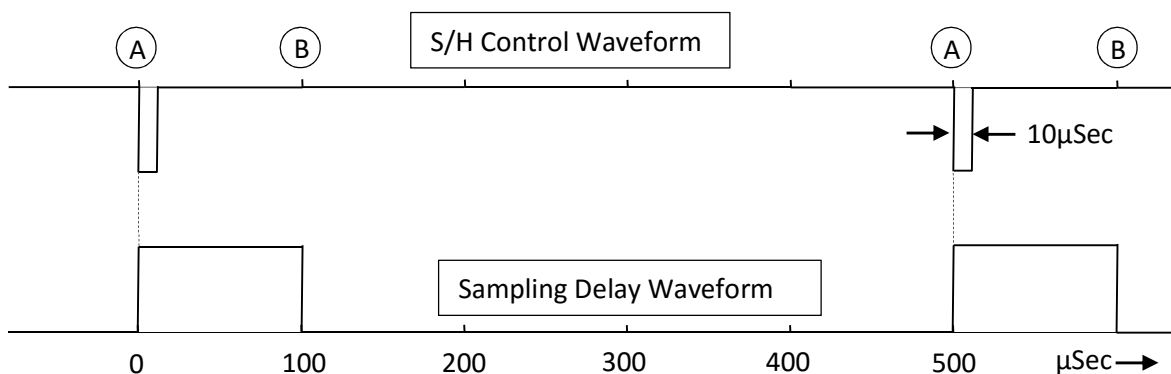


Figure 3.11: Shows one cycle of the vibration signal sampling control waveforms which provide for simultaneous sampling of the nine channels of vibration data. The upper waveform is a Pulse Width Modulated (PWM) signal generated by the Controller and sent to the three Sensor Boards to control their Sample/Hold units and initiate ADC sampling. The lower waveform is used by the Controller to provide a delay to allow the Sensor Boards to complete signal sampling before the Controller reads the sample results.

3.3.5 BACKGROUND SOFTWARE

The lowest priority software task is the background processing which make use of the free Central Processor Unit (CPU) resources available when the CPU is not servicing interrupts or the real-time queue. Background processing is ideal for non-time critical functions such as monitoring the user interface and writing data to the SD Card.

Figure 3.12 shows a flowchart for the background task in the Controller MCU. Following initialisation the Controller enters this infinite loop which has responsibility for monitoring the “Start” switch to initiate or terminate vibration sampling and writing full 512 byte blocks to the SD Card from the circular buffer.

The system status (“SAMPLING” or “NOT_SAMPLING”) is set by reading the Sampling switch. The sampling operation is instigated by the system initialisation routine and sampling occurs continuously from that point until power down however the results are only saved to the circular buffer and hence to the SD Card when the system status is “SAMPLING”. This means that the Sampling switch should be only set to Sampling once per flight to ensure the file “FILE.TXT” only contains the data from one recording session.

The circular buffer has a capacity of 2048 bytes which is half the total user Random Access Memory available on the MCU. The buffer is made as large as practicable to allow for the possible requirement to temporarily store multiple 512 byte data blocks due to other conflicting demands on the CPU such as servicing higher priority tasks. A number of different buffer configurations such a linear, dual linear and circular were investigated however experimentation showed that for equivalent size buffers the circular structure was found to be the most efficient way of storing data prior to writing it to the SD Card and the only structure able to cope with the real-time requirements.

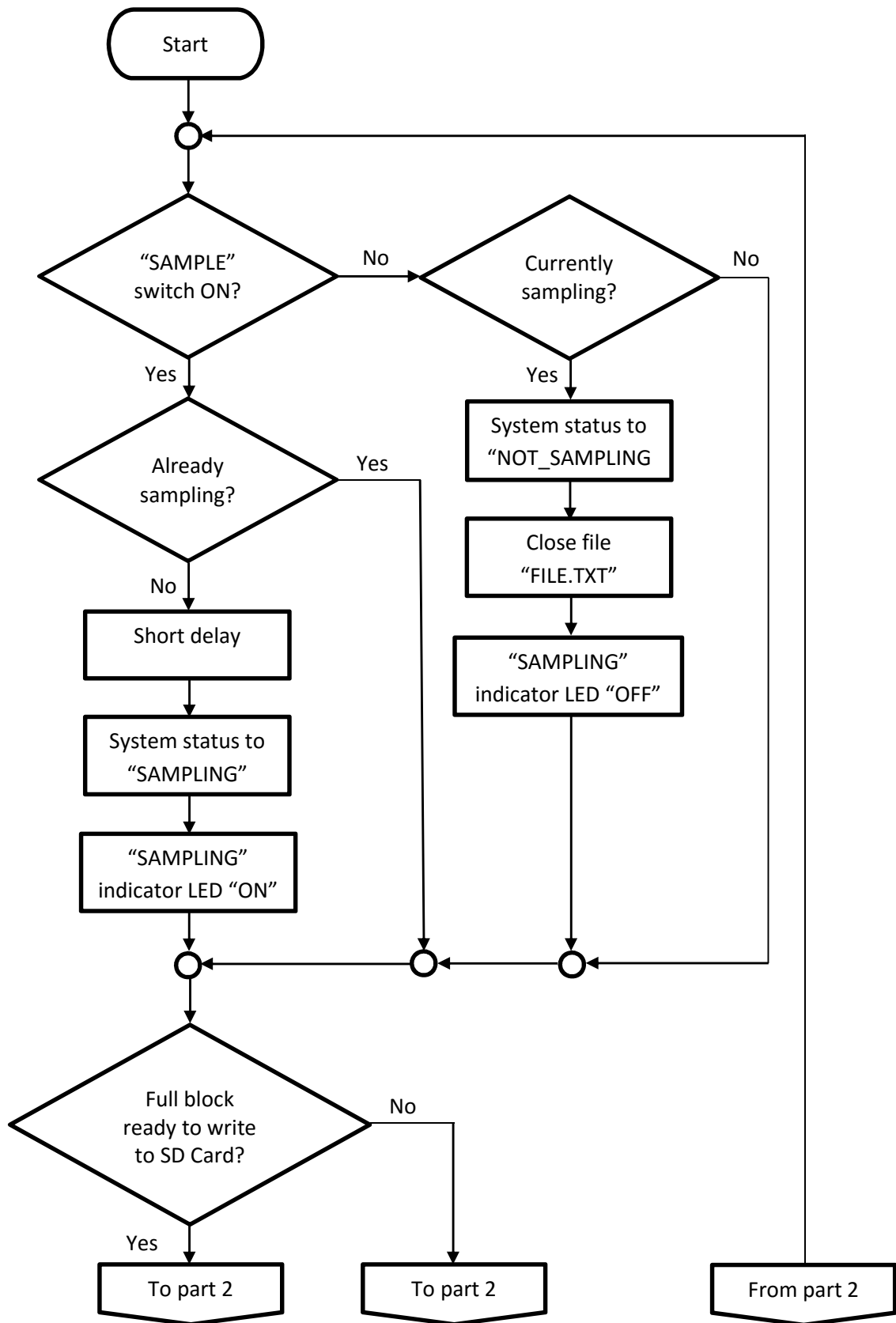


Figure 3.12: Controller Background Software Flowchart. Part 1/2

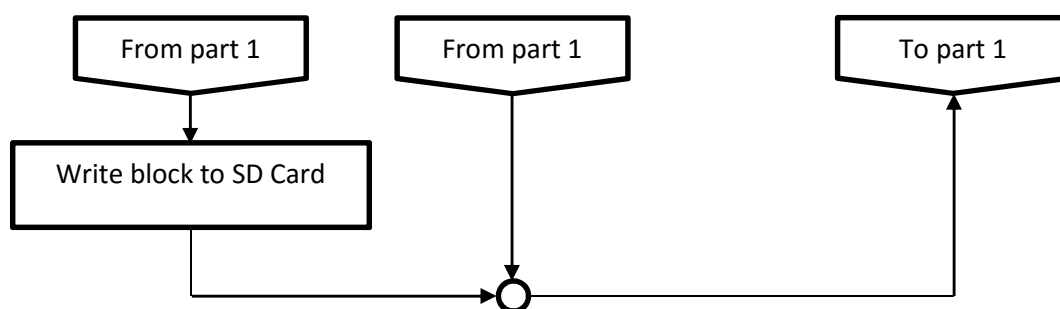


Figure 3.12: Controller Background Software Flowchart. Part 2/2

When data is written to an SD Card under normal conditions the operating system assumes that the first byte of data will be written to the next available storage location on the card which will probably be part way into a memory block (or sector). As the SD Card read, write and erase commands only operate on complete blocks the operating system first reads the block containing the next available location, erases the complete block, concatenates the new data to the existing block contents and writes the total back to the SD Card block. If the total is now greater than the block size (512 bytes) the procedure is repeated for the next and subsequent blocks. The procedure is the same irrespective of whether the next available location was at the start of a block or not and consequently it is quite slow when used in this manner. Whilst this procedure is necessary for a standard operating system which must be able to read and write small amounts of data it is not suitable for writing large amounts of data at a sustained rate of 62 kBytes per second. Therefore as part of the project a new algorithm for writing to the SD Card was developed.

3.3.6 SD CARD ALGORITHM

This algorithm was developed after gaining a detailed understanding of the existing operating system software for writing to the SD Card as the new algorithm was to be integrated into the existing system. The algorithm is in two sections and assumes that the SD Card is formatted to FAT16 standard and there are no existing files on the card:

The first section executes as part of the system initialisation (Section 3.3.3.1). The file "FILE.TXT" is created on the SD Card with a File Allocation Table (FAT) reflecting a file size of 360,448 kByte (11,000 clusters) and this area of the SD Card data area is erased. This negates the need for erasing the data blocks when data is being written to the card.

The second section executes as part of the system background software (Section 3.3.5). When there is a full block of data in the circular buffer (512 bytes) the block is written to the next

available block location on the card with a single WRITE_BLOCK (CMD24) command. Having the card pre-erased and writing only full blocks saves the considerable time required for reading the current block, adding the new data to the existing block contents, erasing the block and then writing the block.

In summary, this algorithm maximises the SD card data streaming rate by:

- Erasing the whole file area during initialisation, and
- Creating one contiguous file in the FAT during initialisation
- Writing data a whole segment (block) at a time to the next physical segment

This eliminates the read/erase/write cycles, searches for the next available sector in the FAT and updating of the FAT linked list operations which occupy most of the time during standard SD card write operations.

3.3.7 FILE CONVERSION (hex-to-csv) SOFTWARE

This section describes the post flight file conversion process which generates the csv files that are used in the analysis phase to verify the validity of the recorded data and also to construct real vibration data files for driving the vibration simulator. The file conversion software is written in Visual C++ and runs on a PC.

Vibration data recorded by the vibration measurement system during flight is stored on the SD card in a single large file "FILE.TXT". This file is in a quasi csv format where the numeric fields use 4 digit, 16 bit hexadecimal words instead of the 5 digit ascii decimals required for true csv files (Figure 3.9, Figure 3.13). Hexadecimal is the default format used by the MCU to represent variables as it is the most efficient representation in terms of data storage and manipulation. The vibration data is stored in hexadecimal format as there is insufficient time available between samples for the MCU to perform the hexadecimal-to-decimal-to-ascii conversion required for the file to be a true csv file (Figure 3.9). Post flight this file must be converted to a proper csv format and split into multiple, smaller, more manageable files before analysis.

Before the recorded data can be analysed it is converted to proper csv format and split into separate 15 second files each of 30,000 records which are more manageable in Excel. During flight a hand written record of the helicopter status is maintained by the operator. The record is updated at 15 second intervals and includes information such as the flight mode (hovering, climbing, descending, etc), altitude, airspeed etc. During analysis the record is matched to the 15 second "TestFileenn.csv" files which are created during the file conversion process.

Prior to the file conversion process the file "FILE.TXT" is copied from the SD Card to a working folder on the PC hard drive. The conversion software starts by prompting the user for the source file ("FILE.TXT") location. The source file is then opened for reading and the first of the csv results files "TestFile1.csv" is created and opened for writing. The program then enters a loop which handles the conversion of a complete record (31 bytes). A record is read from the source file and its integrity is verified by checking that the Carriage Return / Line Feed line terminator (CRLF) and commas are present in the correct places. If the record is found to be not correct the conversion software attempts to recover by searching through the source file until it finds a CRLF byte pair or the End Of File marker (EOF). If a CRLF is located the software returns to the start of the record conversion loop.

```
0x1AB8,0x0145,0x05AD,0x0457,0x0139,0x0442,0x0543,0x0143,0x0458,0x046BCRLF
0x1AB9,0x0149,0x05AA,0x0452,0x013B,0x0444,0x0545,0x0147,0x0454,0x0469CRLF
0x1ABA,0x014B,0x05AB,0x0450,0x0140,0x0448,0x0548,0x0149,0x0452,0x0466CRLF
0x1ABB,0x0150,0x05A8,0x044D,0x0142,0x044A,0x054B,0x014B,0x0450,0x0464CRLF
```

Figure 3.13: Example showing four records (rows) from a quasi csv vibration data file as recorded on the SD Card. Each record is 31 bytes. The data fields are all 16 bit words and are shown in hexadecimal notation. Each record has ten fields delimited by commas (ascii 0x2C). The CRLF line terminator at the end of each record would be two bytes 0x0D and 0x0A. The left field of each record is the sample number and the other fields are the X, Y, Z axis vibration levels from the three tri-axial vibration sensors.

If the record is found to be correct its sample number is then checked. The sample number is the first field and should increment for each record. If the sample number is not correct it is assumed that records have been lost and the operator is notified. Note that the sample number is a 16 bit unsigned integer and the system interprets the 16 bit overflow as an incorrect record number and notifies the operator. This has not been corrected as it also serves to indicate the program progress to the operator. The record number and data fields are now converted from 16 bit hexadecimal numbers to five digit ascii decimal numbers and written to the current results file as a correct csv record. The number of records in the current results file is checked and if equal to 30,000 the file is closed and the next results file created and opened.

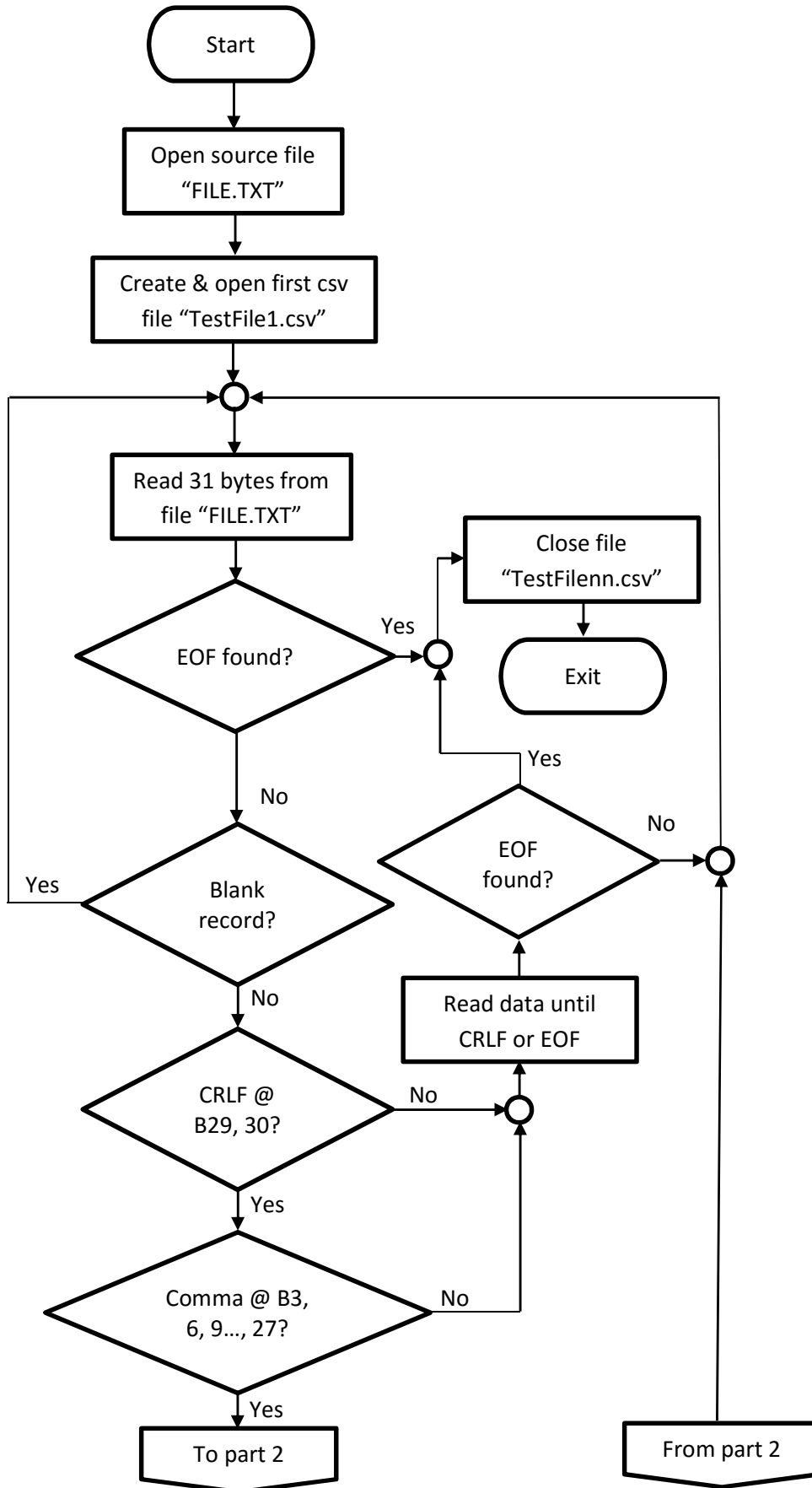


Figure 3.14: File Conversion Software Flowchart. Part 1/2

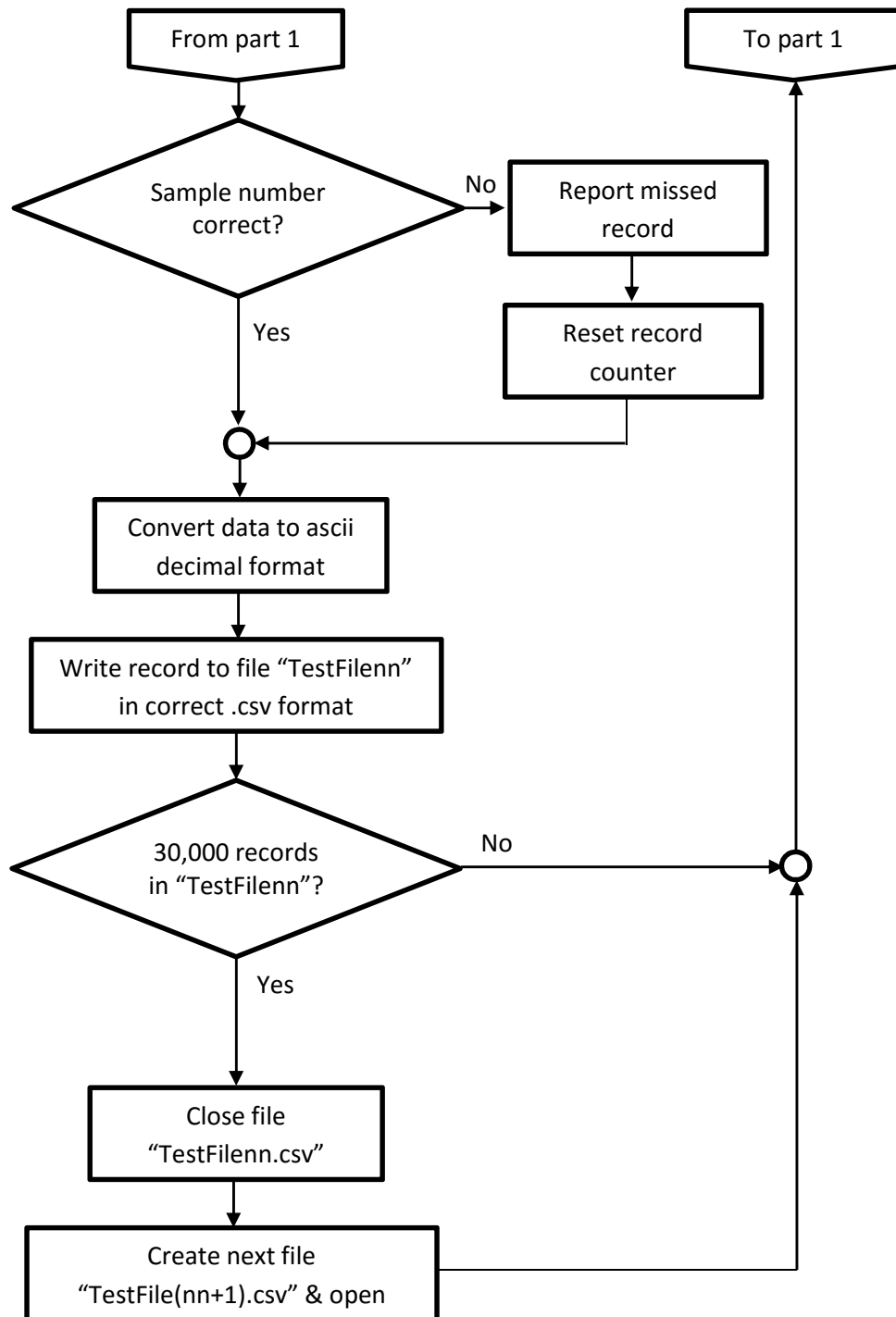


Figure 3.14: File Conversion Software Flowchart. Part 2/2

```
Source file :-  
C:\My Documents\Peter\Flight Test 240411-2\file.txt  
  
Conversion in progress  
  
64536  
130072  
195608  
261144  
326680  
347384  
392214  
457750  
523286  
588822  
654358  
719894  
785430  
850966  
916502  
982038  
1047574  
1113110  
1178646  
1244182  
1309718  
1311563  
Correct samples: 1320514  
Files created: 45  
Sample Incs > 1: 2  
Negative Sample Incs: 20  
  
Conversion complete
```

Figure 3.15: Example of file conversion program results. The values following the “Conversion in progress” message are the record count when the sample number did not increase by one. Note that most of these are spaced by 65,536 indicating they are due to the 16 bit sample number overflowing.

3.3.8 VIBRATION ANALYSIS SOFTWARE

Once the vibration data has been converted to 15 second csv files it is analysed to determine its spectral content and levels. The analysis has two goals; firstly to verify that the vibration data is in fact a true representative sample of the helicopter vibrations and secondly to determine the actual vibration levels which are required in the design of the vibration simulator. The analysis software is written in Visual Basic for Applications (VBA), also called Excel Macros. The reasons for using VBA are that it is readily available, possesses a rich suite of analysis and plotting tools, has the capability of automating all the necessary calculations and presentations and the author wanted to enhance his programming skill base in this area. VBA is an extremely powerful analysis and presentation tool with the ability to be integrated into all Microsoft Office products and access both spreadsheets and databases.

In the analysis procedure a 15 second csv file is opened in Excel which converts it to Excel format (.xls). The analysis macro then performs the following operations:

1. Nine new Excel worksheets are created and labelled for each of the vibration axes: “HeadLateral”, “HeadLongitudinal”, “HeadVertical”, “WaistLateral”, “WaistLongitudinal”, “WaistVertical”, “FeetLateral”, “FeetLongitudinal”, “FeetVertical”.
2. For each of the worksheets:
 - Twenty nine 1024 point Fast Fourier Transforms (FFT) are calculated with 0.5 second (1000 samples) spacing. This gives the FFT a bin spacing of approximately 1.95 Hz. The twenty nine FFTs cover the full 15 seconds of the file.
 - The FFT bins are averaged to provide an average bin level over the 15 second of the file.
 - The results are plotted for a frequency range 0 – 350 Hz. Appropriate labels and X and Y axis scales are added.
3. In the original worksheet, for each vibration axis the following calculations are made:
 - The RMS vibration level (m/s^2) over the 15 second period of the file
 - The peak vibration level (m/s^2) over the 15 second period of the file
 - The Crest Factor

3.4 SUMMARY AND CONCLUSIONS

The vibration measurement system has been successfully designed to meet the system requirements and its operation verified over a number of proving flights (Chapter 4). The system is unique in its ability to simultaneously sample and record nine channels of patient vibration data during winching and retrieval without interfering with the normal safe operation of the rescue helicopter. The design presented a number of challenges foremost of which was the need to devise an algorithm that would enable the MCU to write the vibration data to an SD card at the required sustained rate. Research showed that the available algorithms were unsuitable as they were intended for non-real-time applications where the time required to write data to the card was not an issue. Other challenges that were met include the non-invasive system implementation, simultaneous sampling of the nine channels of vibration data and low noise design.

The contributions from this chapter are:

- *A non-invasive system for recording vibrations experienced by patients during helicopter transportation in a rescue litter.* The system is unique in that it provides synchronised

sampling and storage of high bandwidth tri-axial vibrations at the head, waist and feet of a patient lying supine in a rescue litter during all flight modes that are encountered during helicopter patient retrieval. The system operates reliably in a physically demanding environment which has high levels of mechanical stress, vibrations and electrical noise and limited physical space for locating the sensors as they cannot protrude from the rescue litter.

- *A unique algorithm for high speed data streaming to a Secure Digital (SD) card mass storage device.* This algorithm makes it feasible to stream high speed data to an SD card using a low power 8 bit microcontroller (MCU) and is an enabling element in the design of the vibration recording system.
- *The use of low-cost Micro Electro Mechanical Systems (MEMS) accelerometers as vibration sensors.* MEMS accelerometers offer the advantages of being low cost, low power and low profile however their use as vibration sensors is not established as they require individual calibration by the user and some researchers have reported non-ideal frequency response characteristics. Their low profile makes them ideal for this application as it allows the sensors to be safely mounted in the protective void under the rescue litter making the system less vulnerable to damage during movement of the litter. The thesis presents the detailed development of the MEMS based sensors including the procedure for their calibration.

The successful completion of the vibration measurement system gives a partial affirmative answer to the research question “*Is it feasible to record the vibrations experienced by patients lying supine in a rescue litter during helicopter winching and retrieval?*”. The investigation is concluded in Chapter 4 which presents an analysis of the recorded vibrations to confirm the precise operation of the system.

CHAPTER 4

VIBRATION MEASUREMENT SYSTEM VERIFICATION

4.0 INTRODUCTION

This chapter presents the testing and analysis work that was conducted to verify the operation of the vibration measurement system. The results of the analysis are compared to the system performance specification (Chapters 2 and 3) to confirm that the answer to the first of the research questions posed in this thesis “*Is it feasible to record the vibrations experienced by patients lying supine in a rescue litter during helicopter winching and retrieval?*” is yes.

Two types of testing were employed, firstly the system was calibrated in a controlled laboratory environment and secondly field testing where real patient vibration data is collected during flight and analysed to show that it contains the correct frequency tones and amplitudes as reported in the literature and discussed in sections 2.4, to 2.6. The calibration involved measuring the frequency response of each of the Sensor Boards to determine the passband gain, bandwidth, linearity and high frequency roll-off. For this testing the Sensor Boards were mounted on an electrodynamic shaker which can generate high quality vibrations over the complete frequency range specified for this project (Figure 4.1, 4.2).

For the field testing the vibration measurement system was mounted to a rescue litter with a mannequin (Figures 1.1, 3.2, 3.4, 3.5) and used to collect vibration data from typical retrieval flights covering all flight modes. The data was then analysed to determine its spectral components and the results compared to levels published by the manufacturer and in the literature.

The chapter is organised as follows:

Section 4.1 outlines the criteria that the vibration measurement system must meet in order for it to be considered a success.

Section 4.2 presents the methodology that was employed in conducting the testing.

Section 4.3 presents the testing results and analysis.

Section 4.4 is the summary and conclusions for this chapter.

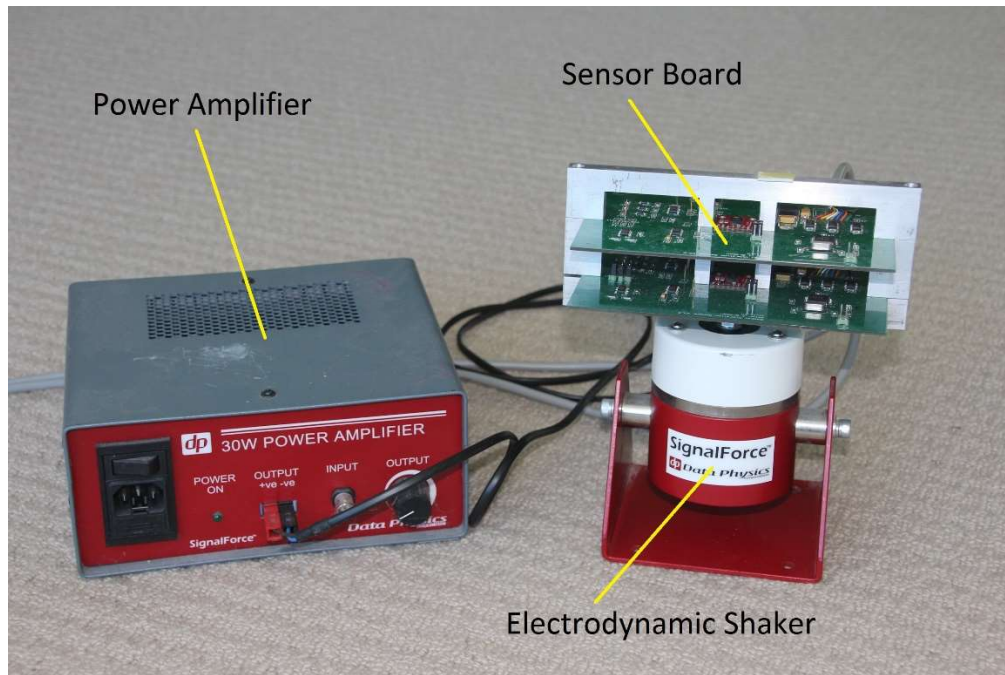


Figure 4.1: Showing the test setup for calibration of the Sensor Boards. In this case two Sensor Boards are mounted on a custom frame atop the electrodynamic shaker. The B & K 4375 reference accelerometer is not shown in this image but would be mounted on the top middle of the frame. Note that the Sensor Boards are rigidly supported at the ends and middle to ensure all the vibratory motion is transferred to the accelerometer without any flexing of the Sensor Board.

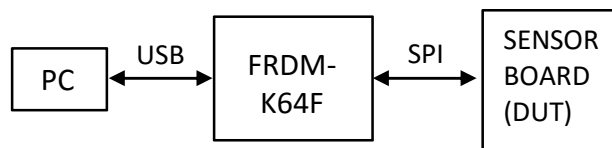


Figure 4.2: Block diagram of the test setup for static calibration of the Sensor Boards.

4.1 CRITERIA FOR SUCCESS

The Vibration Measurement System was designed and built to experimentally investigate the first research question posed in this project “*Is it feasible to record the vibrations experienced by patients lying supine in a rescue litter during helicopter winching and retrieval?*”. The system will be judged a success if its performance equals or exceeds the operational requirements as set out in Chapter 2 and 3. These requirements are summarised here along with their status prior to verification:

1. System bandwidth of 150 Hz. This will cover the frequency range of vibrations experienced in a helicopter (Table 2.3). The system bandwidth will be confirmed by measuring the frequency response during calibration.
2. Flat, linear response in the passband. A flat, linear passband response simplifies the calibration procedure to the determination of the accelerometer sensitivity (mV/g) which is used to calculate the measured vibration level. The passband response and proportionality constant (sensitivity) will be determined as part of the frequency response measurement.
3. Sampling frequency of 2 kHz. This will ensure a high fidelity sampled signal that is suitable for analysis and playback in the vibration simulator. The system has been designed to have a 2 kHz sampling rate.
4. Frequency transition rate of -100 dB per decade. This is necessary to prevent aliasing of high frequency signals. The 5th order anti-aliasing filter should provide the required transition rate but this will be confirmed as part of the frequency response measurement.
5. Peak vibration level of at least 830 mg (8.142 ms^{-2}). This is the level of vibrations reported in the literature. The sensor has a measurement range of $\pm 1500 \text{ mg}$ which will adequately cover this requirement.
6. Resolution of 1% (8.16 mg). The theoretical resolution with a 12-bit ADC is 0.73 mg (7.18 mms^{-2}) which adequately covers this requirement. Also the expected noise level is 5.9 mg with a power spectral density of 6.2 mg both of which are below the resolution level therefore the resolution should be achievable.
7. Non-invasive operation. This will be confirmed as part of the field trails.
8. Cover all flight modes. This will be confirmed as part of the field trails.
9. Portable. This will be confirmed as part of the field trails.
10. Measure 3 axes at the head, waist and feet. This will be confirmed as part of the field trails.
11. Record for two hours. This will be confirmed as part of the field trails.

4.2 METHODOLOGY

This section describes the experimental process that was employed to validate the vibration measurement system. It is divided into two sections, the first describing the laboratory calibration which determined the frequency responses of the three Sensor Boards (Section 4.2.1) and the second the flight testing and post flight analysis that verified correct operation of the system under actual flight conditions (Section 4.2.2).

4.2.1 SYSTEM CALIBRATION

Calibration is the process of determining parameters that force the output of an instrument to agree with a range of reference information. The literature describes MEMS accelerometer calibration techniques for three different applications, Inertial Measurement Units (IMU), angle of tilt and vibration measurement each of which exploits different characteristics of the MEMS accelerometer. IMUs are the sensor modules for Inertial Navigation Systems (INS) that are used in vehicle navigation to calculate vehicle velocity and position from measurements of acceleration and angular velocity. INS systems do not rely on any form of external measurement and are useful when other systems such as GPS are not operational, for example indoors. The calculation of position from measurements of acceleration relies on a double integration of the acceleration signal about its zero value and if the zero value is not known accurately position errors accumulate very rapidly. The accelerometer zero value, known as *zero offset*, can change due to internal and external physical factors such as temperature or power supply voltage. Calibration in this case refers to methods for estimating the zero offset at any time, see for example Amirsadri (2012).

Many MEMS accelerometers have the ability to measure dc acceleration as opposed to ac piezo accelerometers such as the Bruel & Kjaer BK 4375 which has a low frequency cut-off of 0.5 Hz. This ability allows a tri-axial MEMS accelerometer to simultaneously measure the gravity vector in three orthogonal directions and hence calculate the device's angle of tilt (Pedley 2013). Example applications include most smart phones and tablet devices. These devices generally use an accelerometer with a digital output such as the MMA8451 which is calibrated by the manufacturer, however the factory calibration can change as a result of the thermal stresses during soldering and alignment errors can be introduced during the device assembly. The original factory accelerometer calibration will be adequate for most consumer applications however improved accuracy can be obtained by calibration of the device after manufacture or by using a more sophisticated calibration model. The original factory calibration model uses six parameters representing sensitivity and zero offset on each of the three axes. The accelerometers are however capable of storing 12-parameter linear calibration models which correct for accelerometer package rotation on the circuit board and for cross-axis interference between the accelerometer

X, Y and Z-axes. For optimum accuracy a 15-parameter model which includes cubic nonlinearities in the accelerometer response can be employed (Pedley 2013). The determination of the calibration parameters is not a simple task and numerous authors, for example Kian (2011) and Artese (2008), have suggested simplified experimental techniques for their determination. This testing relies on having an accurate value for the gravity vector at the testing location, see for example data published by the Australian Government (Wellman 1985).

Measurement of the Sensor Board frequency response will calibrate the system by providing the following parameters: sensitivity, linearity, bandwidth, passband response and frequency transition rate. The frequency response is measured using the standard laboratory technique where the system output-to-input ratio is measured at a number of frequencies covering the required frequency range.

The calibrations performed in this work were a combination of dc static sensitivity and ac frequency response determination. The two methods were selected to complement each other in determining the Sensor Board sensitivity and hence provide a degree of confidence in the experimental results.

4.2.1.1 DETERMINATION OF SENSOR BOARD STATIC SENSITIVITY

Static sensitivity is the calibration technique recommended by the manufacturer for checking and improving the accuracy of an accelerometer after it has been mounted in a device (Pedley 2013). Static sensitivity refers to the accelerometer output when measuring the acceleration due to gravity. In this case the complete sensor system consisting of the accelerometer, buffer amplifiers and anti-aliasing filter is calibrated to determine the sensitivity of the complete system. The procedure for calibration of all three axes is identical to that described here for the Z-axis. A mounting is required that holds the device under test (DUT) such that the axis being tested can be positioned upwards and downwards vertically and small adjustments can be made about the vertical in both horizontal axes. Figure 4.2 shows a block diagram of the test setup. A C++ control program has been written to allow a PC to control the testing and present the result on a graphical user interface (Ifassiouen 2008). The PC communicates with a FRDM-K64F microcontroller board via a high speed USB connection. The FRDM-K64F has been programmed and connected to control the sampling of the DUT vibration channels mimicking the function of the controller in the vibration measurement system. The DUT is sampled at 2 kHz and the results transferred to the PC where they are filtered to remove noise and displayed in the GUI as raw analog-to-digital converter (ADC) values between 0 and 4096.

For testing, the DUT (in its mounting) is placed on a horizontal table with the Z-axis vertical and the DUT, FRDM-K64F and PC are powered up. The DUT is checked to be horizontal using a high quality bubble level. For reference a milli-volt meter is connected to a test point between the output of the second stage buffer amplifier and the analog-to-digital converter (ADC) input (Figure 3.6). The PC will continually update the ADC reading. The DUT angle of tilt about the horizontal axes is varied slowly until the ADC reading is a maximum/minimum and the result is recorded. The DUT is inverted and the test repeated. The difference between the two readings nominally represents 2 g of acceleration at the geographical location where the test is conducted. 1 g is listed as $9.7860973 \text{ ms}^{-2}$ at Townsville where the testing was done and the standard value for 1 g is 9.80665 ms^{-2} , a difference of 0.2% (Wellman 1985). The PC readings are recorded as ADC counts per g and using the voltmeter readings these can be converted to milli volts per g and the conversion factors recorded for later use. The results of the static sensitivity calibrations are presented in Section 4.3.1.

4.2.1.2 DETERMINATION OF SENSOR BOARD FREQUENCY RESPONSE

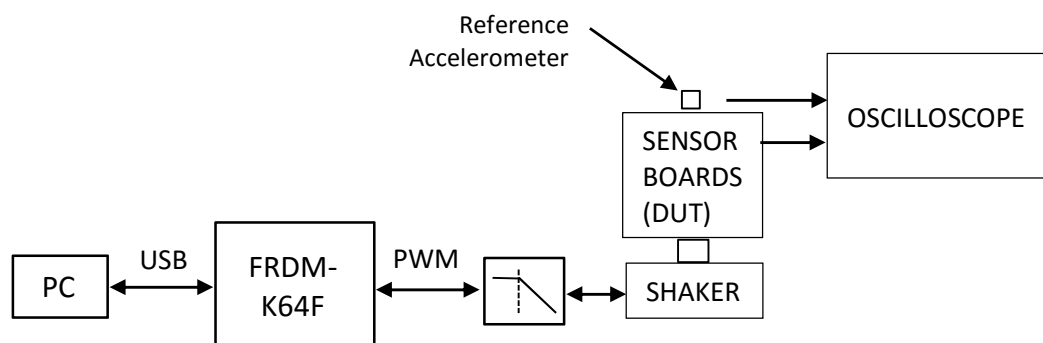


Figure 4.3: Block diagram of the test setup for frequency response calibration of the Sensor Boards.

Figures 4.1 and 4.3 show the experimental setup used to determine the sensor board frequency response. A high quality Bruel & Kjaer BK 4375 Piezoelectric Charge Accelerometer (Reference Accelerometer) is mounted with the Sensor Board under test on a Data Physics V4 T4 Electrodynamic Shaker (Shakernia, Ma et al.). The Shaker is a device for generating high-power, high-bandwidth mechanical vibrations and is commonly used in the aerospace and electronics industry for tasks such as determining a devices susceptibility to error or damage due to vibrations. The BK 4375 is calibrated by the manufacturer and is used here as an accurate reference. The BK 4375 is assumed to have a flat response over the complete frequency range of

interest. The oscilloscope is used to measure the amplitude of both the reference accelerometer and the Sensor Board responses. The Sensor Board response is measured at the output of the second buffer amplifier prior to the signal entering the analog-to-digital (ADC) converter and so provides a complete end-to-end calibration of the analog section of the vibration measurement system (Figure 3.6).

The experimental procedure is that measurements are taken at multiple points over the frequency range of interest. For each measurement the PC control screen is used to manually set the amplitude and frequency of the reference accelerometer and the amplitude and phase response of the sensor under test are then read from the oscilloscope. The results of the frequency response calibrations are presented in Section 4.3.1.

4.2.1.2.1 INPUT SIGNAL GENERATION

The sinusoidal tones used to drive the Electrodynamic Shaker are generated by the PC/FRDM-K64F/Low Pass Filter combination working as a Class-D (PWM) amplifier (Figure 4.3). The PC runs a custom C++ control program that generates the sinusoidal tones with amplitude and frequency as specified by the operator. The control program digitises the waveform levels using a sampling frequency of 2 kHz and transfers these to the FRDM-K64F (MCU) via the USB connection. The data is transferred as blocks with appropriate error checking to guarantee high quality signals. The MCU uses the data to modulate a 20 kHz Pulse Width Modulated (PWM) signal which is then low pass filtered to provide the sinusoidal input for the electrodynamic shaker. The modulation is limited to keep the input signal within the 1 V_{p-p} limit of the shaker power amplifier. The reference accelerometer signal is displayed on the oscilloscope and the operator makes adjustments using controls on the PC until the signal level is correct.

4.2.1.2.2 COLLECTION AND PRESENTATION OF RESULTS

The reference (input) and sensor under test (output) levels are manually read from the oscilloscope and recorded with the frequency in Excel spreadsheets (Table 4.1). Fourteen frequencies from 15 to 200 Hz and three reference levels of 200, 400 and 600 mV_{p-p} are used and the sensitivity in both mV/g and dB is calculated for each reading. Note that no responses are recorded at the lowest frequencies for the high level (600 mV_{p-p}) reference input as the shaker displacement required to generate these accelerations exceeds the physical stroke limits of the shaker. The sensitivities are then plotted for a graphical presentation of the results (Figures 4.4 – 4.6).

Table 4.1: Frequency response results for the Z-axis of sensor 2 (MMA7260) with a high level reference of 600 mV_{p-p} (1.94 g_{p-p}). The reference is the BK4375 piezo accelerometer.

Freq (Hz)	BK4375 (mV p-p)	BK4375 (g p-p)	MMA7260 (mV p-p)	MMA7260 sensitivity (mV/g)	MMA7260 sensitivity (dB)	Phase (deg)
15	600	1.94				
20	600	1.94				
25	600	1.94	1380	710.7	57.0	45
30	600	1.94	1400	721.0	57.2	53.7
40	600	1.94	1400	721.0	57.2	64.8
50	600	1.94	1400	721.0	57.2	90
60	600	1.94	1380	710.7	57.0	107
80	600	1.94	1260	648.9	56.2	144
100	600	1.94	1200	618.0	55.8	180
120	600	1.94	1040	535.6	54.6	218
140	600	1.94	840	432.6	52.7	270
160	600	1.94	540	278.1	48.9	320
180	600	1.94	300	154.5	43.8	360
200	600	1.94	165	85.0	38.6	381.6

4.2.2 COLLECTION OF FLIGHT DATA

The process of collecting flight data involves using the vibration measurement system mounted in the rescue litter with a mannequin and having it record during typical retrieval flights. The operation of the system has been described in detail in Chapter 3. Four typical flights have been conducted with different configurations to verify that the system was recording the correct information. These configurations were: standard configuration with the sensors mounted under the rescue litter and a mannequin in the litter; standard configuration but with a crew member in the litter instead of the mannequin; sensors mounted on the helicopter floor with no mannequin or litter; sensors mounted on the helicopter floor with mannequin in litter. The data was collected and processed as described in Chapter 3 and the results are presented in section 4.3.2.

4.3 RESULTS

The results of the verification are presented in two sections, firstly the laboratory calibration of the sensors and secondly the vibration data collected by the vibration measurement system during flight.

4.3.1 SYSTEM CALIBRATION – RESULTS

The system calibration was conducted in two parts, the determination of the sensor static sensitivity (section 4.2.1.1) and its frequency response (section 4.2.1.2). The results are presented in Figures 4.4 – 4.6 and Table 4.2.

The static sensitivity measurements are shown in Table 4.2 as *DC Input Level* and are well within the accelerometer manufactures quoted range of 800 ± 60 mV/g (Freescale Q4/2005). It should be noted that these measurements are for the full end-to-end vibration measurement system including the accelerometer channel, buffers, anti-aliasing filter, Sample/Hold circuit and analog-to-digital converter. Such close agreement with the accelerometer manufacturers published data gives a high level of confidence in these results.

The frequency response of the Sensor Boards was determined using the methodology of section 4.2.1.2. The frequency response measurement results for the vertical (Z) axis of each of the three Sensor Boards are presented in Figures 4.4 – 4.6 and their sensitivities, as calculated from the frequency responses, in Table 4.2. The testing involved determining the response of the Sensor Boards to three input levels (200, 400, 600 mV_{P-P}) over the frequency range 15 to 200 Hz. The input level at each frequency was set by adjusting the amplitude of the excitation sinusoidal voltage until the reference accelerometer (BK4375) output matched the desired level and the DUT output was recorded. The lower and upper frequency limits were dictated by the physical properties of the experimental system. In these tests the input acceleration was maintained constant at one of three levels 200, 400, 600 mV_{P-P}, however the amplitude of a sinusoidal acceleration waveform is proportional to $A\omega^2$ where A is the amplitude of the physical displacement (the peak distance the accelerometer moves) and ω is the frequency which means that to maintain the same level of acceleration, as the frequency is decreased, the displacement increases rapidly. In this case the frequency was decreased until the physical displacement limit of the electrodynamic shaker was reached at around 15 Hz. The upper frequency limit occurs when the Sensor Board output has been attenuated by the anti-aliasing filter to a level where it cannot be measured with the oscilloscope.

The frequency response results will be discussed with reference to the Criteria for Success (Section 4.1). The relevant items are: 1. System bandwidth of 150 Hz; 2. Flat, linear response in the passband; and 4. Frequency transition rate of -100 dB per decade. Analysis of Figures 4.4 – 4.6 show that these criteria have been met. The system bandwidth was established by noting the intersection of the low and high frequency asymptotes of the dB gain-vs-log frequency plot which occurs at the design frequency of 150 Hz. The flat passband response and the -100 dB/decade transition rate are also confirmed by examining the frequency response asymptotes. For each Sensor Board the frequency response to three levels of input, 200, 400, 600 mV_{p,p} (shown as series 1, 2, 3), were measured and plotted in order to evaluate the linearity of the passband response. As can be seen in the plots the responses are so closely aligned that they appear superimposed which confirms the linearity of the passband response.

The only issue identified by the system calibration can be seen in Table 4.2 where there is a large discrepancy between the dc and ac sensor sensitivity levels. The discrepancy is constant across the three sensors and the three input levels and appears to be a constant level shift of approximately 70 mV/g. The difference in methodology between the dc and ac measurements is the standard to which the sensor outputs were compared. For the dc measurements the standard is the gravity vector which is highly consistent and reliable provided care is taken to ensure the sensor is vertical. In addition the measured dc sensitivities agree closely with the manufacturers specifications. The ac measurements were referenced to a Bruel & Kjaer BK 4375 Piezoelectric Charge Accelerometer which is a high quality instrument however investigations revealed that the manufacturer recommends it be calibrated annually and there is no evidence that this has ever been done despite the instrument being at least ten years old (Kjær 2014). For this reason the dc sensitivities have been accepted as accurate and used in the system calculations.

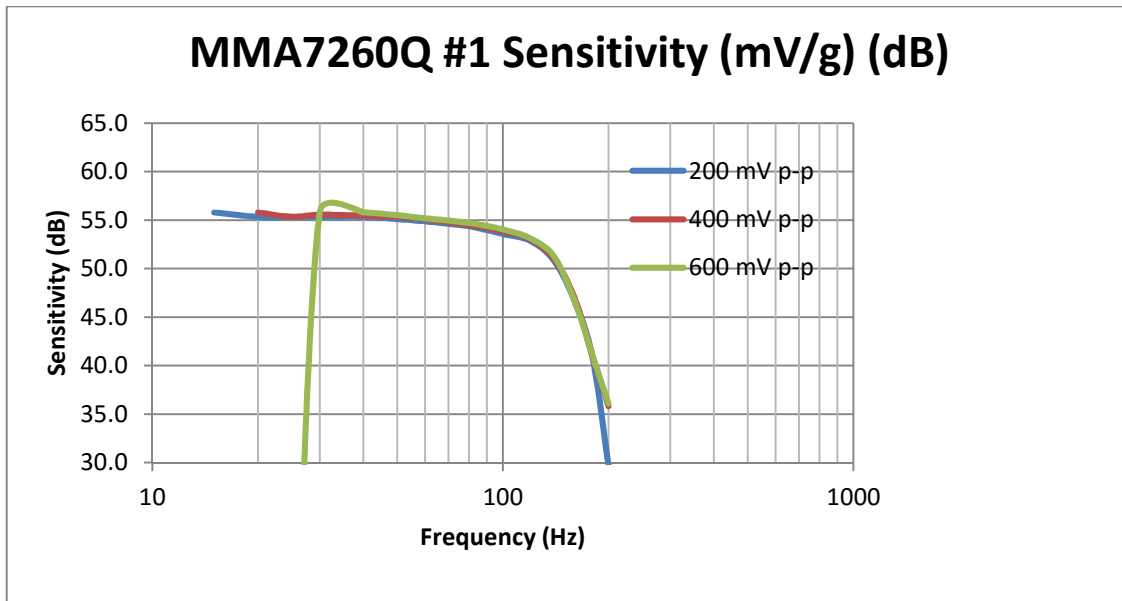


Figure 4.4: Bode plot of frequency response of Sensor Board #1 vertical axis with input levels of 200, 400 and 600 mV_{p-p}.

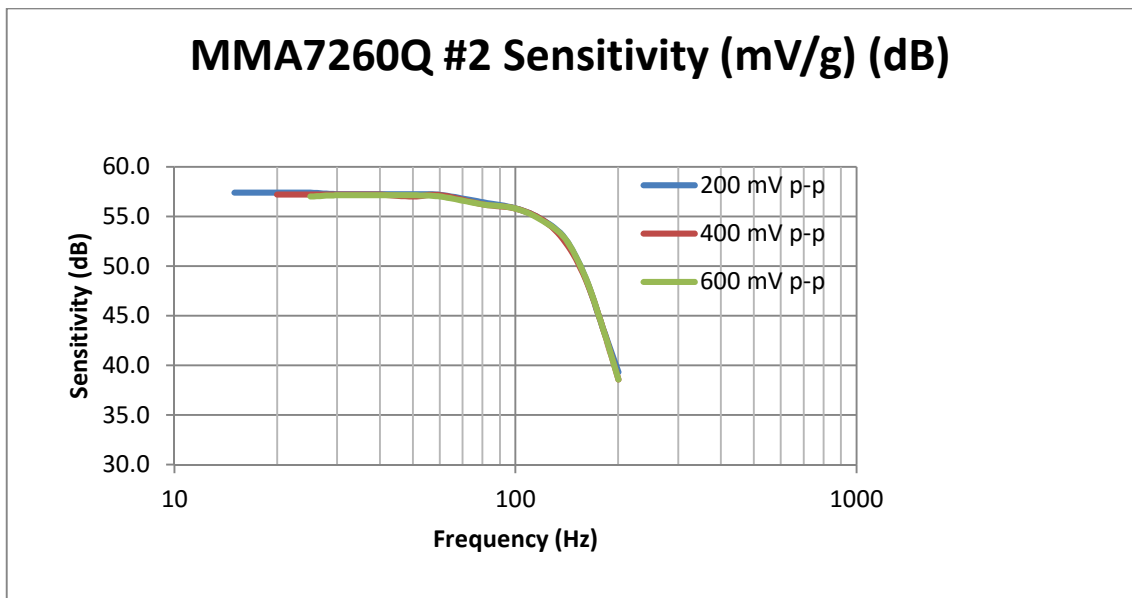


Figure 4.5: Bode plot of frequency response of Sensor Board #2 vertical axis with input levels of 200, 400 and 600 mV_{p-p}.

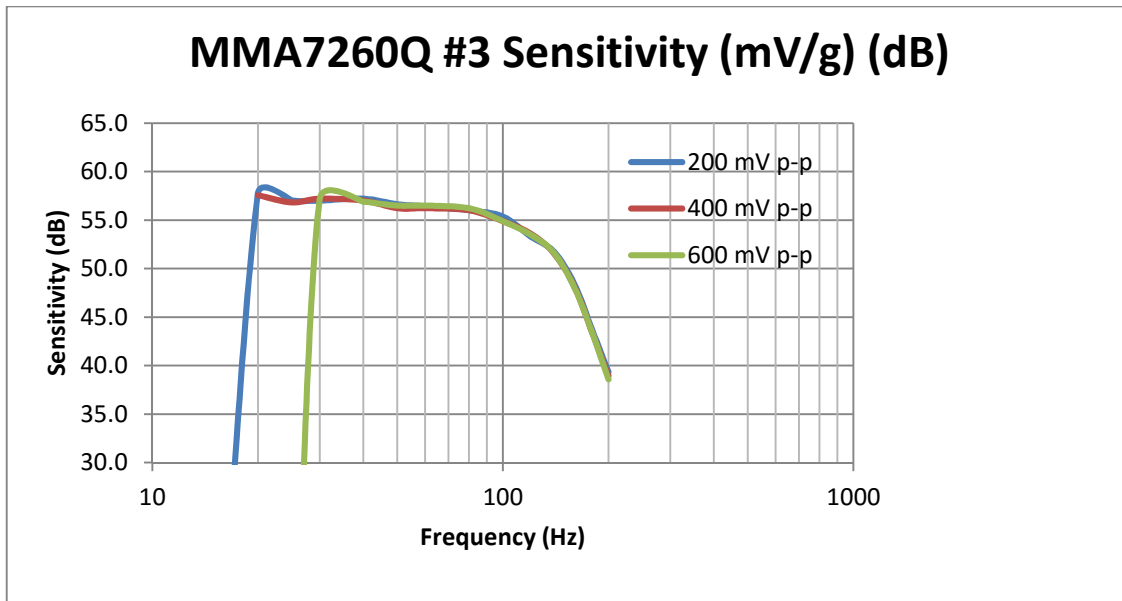


Figure 4.6: Bode plot of frequency response of Sensor Board #3 vertical axis with input levels of 200, 400 and 600 mV_{p-p}.

Table 4.2: Sensitivity results of each of the three Sensor Boards vertical axes.

Sensor Board Vertical Axis Sensitivity Levels (mV/g)			
	Sensor Board Number		
Input Level	1	2	3
DC	761 mV/g	799 mV/g	789 mV/g
200 mV _{p-p}	710.1 mV/g	736.7 mV/g	730.0 mV/g
400 mV _{p-p}	700.4 mV/g	726.2 mV/g	722.3 mV/g
600 mV _{p-p}	686.5 mV/g	717.6 mV/g	710.7 mV/g
Average of ac Levels	699.0 mV/g	726.8 mV/g	721.0 mV/g

4.3.2 FLIGHT TESTING

The flights provided real patient vibration data that was used to confirm correct operation of the vibration measurement system and provide real input data for the vibration simulator (Chapter 5). Four successful data collection flights were conducted with sufficient time allowed between each to permit the data to be analysed and interpreted. After correct operation was confirmed by the first flight subsequent flights were used to gain a more in-depth understanding of the complex vibrations that the rescue litter was experiencing. The data analysis resulted in a number of important conclusions:

1. The vibration measurement system was working correctly.
2. The helicopter floor was vibrating and flexing resulting in different vibrations being experienced at the head, waist and feet.
3. The helicopter floor vibrations were being directly coupled to the rescue litter and hence to the patient.
4. All the vibrations recorded were three dimensional circular motions as would be expected.

Table 4.3: Summary of field testing flights which verified the correct operation of the vibration measurement system.

Flight Test Summary			
Date	Duration	Purpose	Comment
28/03/2011	15 minutes	Initial proving flight	Sensors attached to Litter. Mannequin in Litter.
06/04/2011	20 minutes	Measure vibrations with human patient.	Sensors attached to Litter. 72.5kg human in Litter.
24/04/2011	20 minutes	Measure floor vibrations.	Sensors attached to floor.
24/04/2011	20 minutes	Measure floor vibrations with mannequin and litter.	Sensors attached to floor and mannequin/litter on floor.

Following each flight the data is retrieved from the SD card in the measurement system controller and broken up into a number of conveniently sized Excel files for processing and analysis. Each Excel file (called “TestFileenn.xlsx”) contains 15 seconds (30,000 samples) of data. The following data processing is then performed on each TestFile using Excel macros:

- For each sensor (Head, Waist and Feet) and each axis (Lateral, Longitudinal and Vertical) (Total of nine channels) 1024 point FFTs are performed each 1000 samples (0.5 seconds).
- The FFTs are then averaged to reduce noise and the resultant plotted as a 15 second frequency average. For example see Figures 4.12 to 4.14.
- For each channel the Average, RMS and Peak vibration levels and Crest Factor for the 15 second period are calculated. This data is collated in tabular form for each flight. For example see Table 4.4.
- For each channel, averages for each 0.5 second period are calculated along with the standard deviation of the averages.
- Other frequency and time domain plots as required.

The following sections will discuss each of the flights in detail focussing on the aim of each flight, the data collected, the analysis that was performed and the conclusions reached as a result of the analysis.

4.3.2.1 FLIGHT TEST 1 – 28th March 2011

The flight on 28th March 2011 was in a Bell 412 helicopter VH-ESB of Emergency Management Queensland and of approximately 15 minutes duration. It included typical decompression patient retrieval flight modes such as winch hover, climb, cruise, approach and landing but not actual winching. Vibration data was collected continuously from the three Sensor Boards attached to the base of the rescue litter (Figure 3.5). The weather was calm.

A 70kg rescue mannequin (buster) was restrained in the rescue litter (Figure 4.7) as standard for this type of patient retrieval. Note that while the mannequin and litter are securely restrained by quick release straps this restraint is not rigid and would allow considerable movement of the litter relative to the helicopter particularly at the level of vibration signals.

The aim of the flight was to verify correct operation of the vibration measurement system.



Figure 4.7: Showing the rescue litter and mannequin positioned in the helicopter. The litter is placed across the floor directly behind the pilots seats which are at the top of the picture. The mannequin is restrained in the litter with the red, blue and green belts and the litter is restrained in the helicopter by the yellow belts at each end.

Initial analysis was conducted to investigate if the vibration measurement system had correctly recorded the patient vibrations. An issue was identified with the formatting of the SD card data storage unit however the source of the problem was identified and the data successfully recovered from the card. The recorded .csv file was processed into 15 second Excel files (labelled “TestFilenn.xlsm”) and the line counter and line format checked to ensure there were no missing or damaged samples in the recorded data (Section 3.3.2). This showed that the recording and storage system was working correctly.

The next stage was to verify that the system was correctly measuring the actual patient vibrations. The vibrations were analysed to confirm correct system operation using the following performance criteria (Section 4.1):

- There is sufficient definition in the recorded vibrations.
- The system had a high signal-to-noise ratio.
- The bandwidth was 150 Hz.
- The correct frequency tones were present.
- The vibration levels were similar to those in the literature.

The flight data is first investigated to see if the tri-axial measurement system used to sense the vibrations shows sufficient definition in the recorded signals. The time domain plots, for example Figures 4.8 and 4.9, show 600 samples of nine channels of raw vibration data. The traces exhibit typical vibration characteristics for an air vehicle in calm stable flight in that they are all of similar overall width with no rapid deviations and the 1 g (993 counts) offset of the three vertical vibrations is clearly evident while the averages for the six horizontal signals are around the ADC mid-level (2048 counts) as expected for signals with little gravity component. Signal strengths are high with peak levels in the 240 – 700 mg range which translates to high definition with the 1.007 mg per count resolution of the ADC.

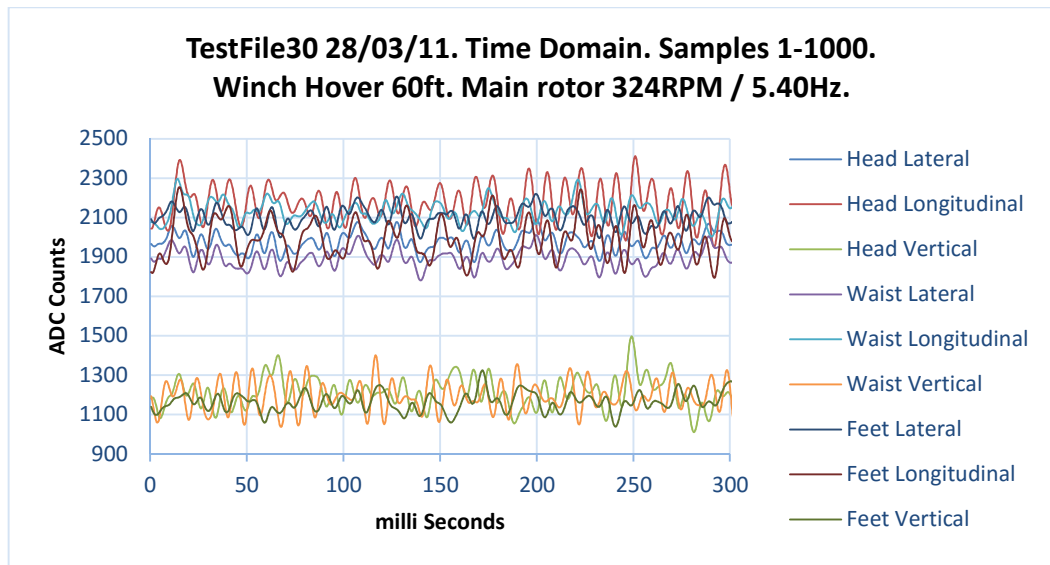


Figure 4.8: 0.3sec (600 samples) of vibration data for all channels for 60 ft winch hover.

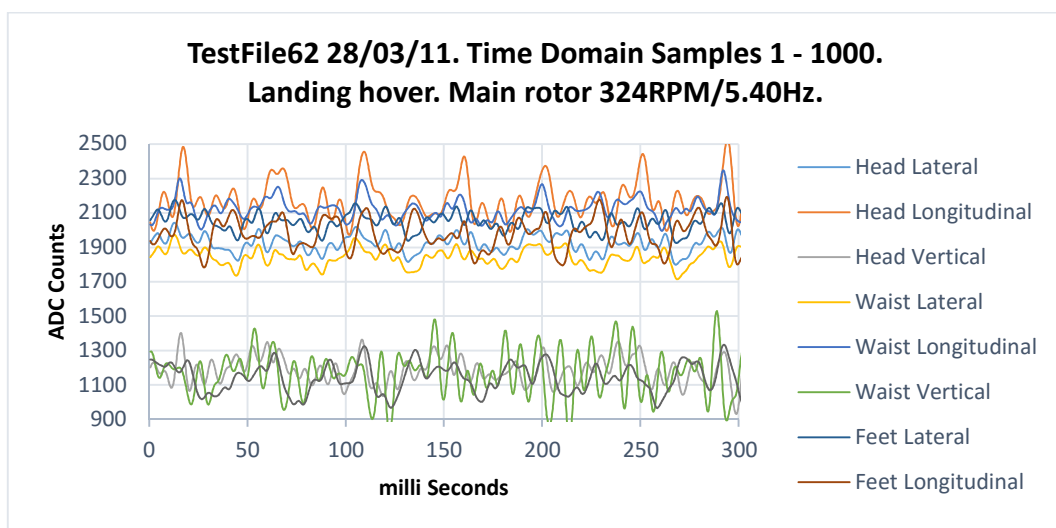


Figure 4.9: 0.3sec (600 samples) of vibration data for all channels for landing hover.

The accelerometer manufacturer quotes a noise level of 5.9mg giving a high signal-to-noise ratio of over 29dB. This can be seen in the time domain plots which show smooth traces for each channel indicating a low level of noise on the signal. In addition the corresponding frequency domain plots (vibration spectra), Figure 4.10, show narrow impulses (tones) at the relevant frequencies with low levels in between indicating high quality signals with a high signal-to-noise ratio.

The accelerometer frequency range (bandwidth) quoted by the manufacturer is 0 – 150Hz. In addition the Sensor Boards have high order anti-aliasing filters with a cut-off frequency of 150Hz (Section 3.2.2). This bandwidth is sufficient to measure the helicopter vibration frequencies up to the rotor brake (Table 2.3) and is adequate for the purposes of this study. The frequency domain plots (vibration spectra), for example Figure 4.10, show a range of high level vibrations below 150Hz but only low levels of signal above indicating that the system frequency response is performing as designed with the correct bandwidth.

Table 2.3 lists the sources and frequencies of the major vibration generating components of the helicopter which should appear as strong tonal impulses in a frequency domain plot of the recorded helicopter vibrations. Those frequencies, from the table, which are present in each of the frequency domain plots can be identified by the alphabetic characters listed in the right hand column of Table 2.3. Note that the table does not give an indication of the relative levels of these vibrations as they are expected to vary with the helicopter configuration and flight mode. Reference to the frequency domain plots, for example Figure 4.10, show a close correspondence between the frequencies listed in Table 2.3 and those of the frequency domain plots. This gives a high degree of confidence that the measurement system is working correctly.

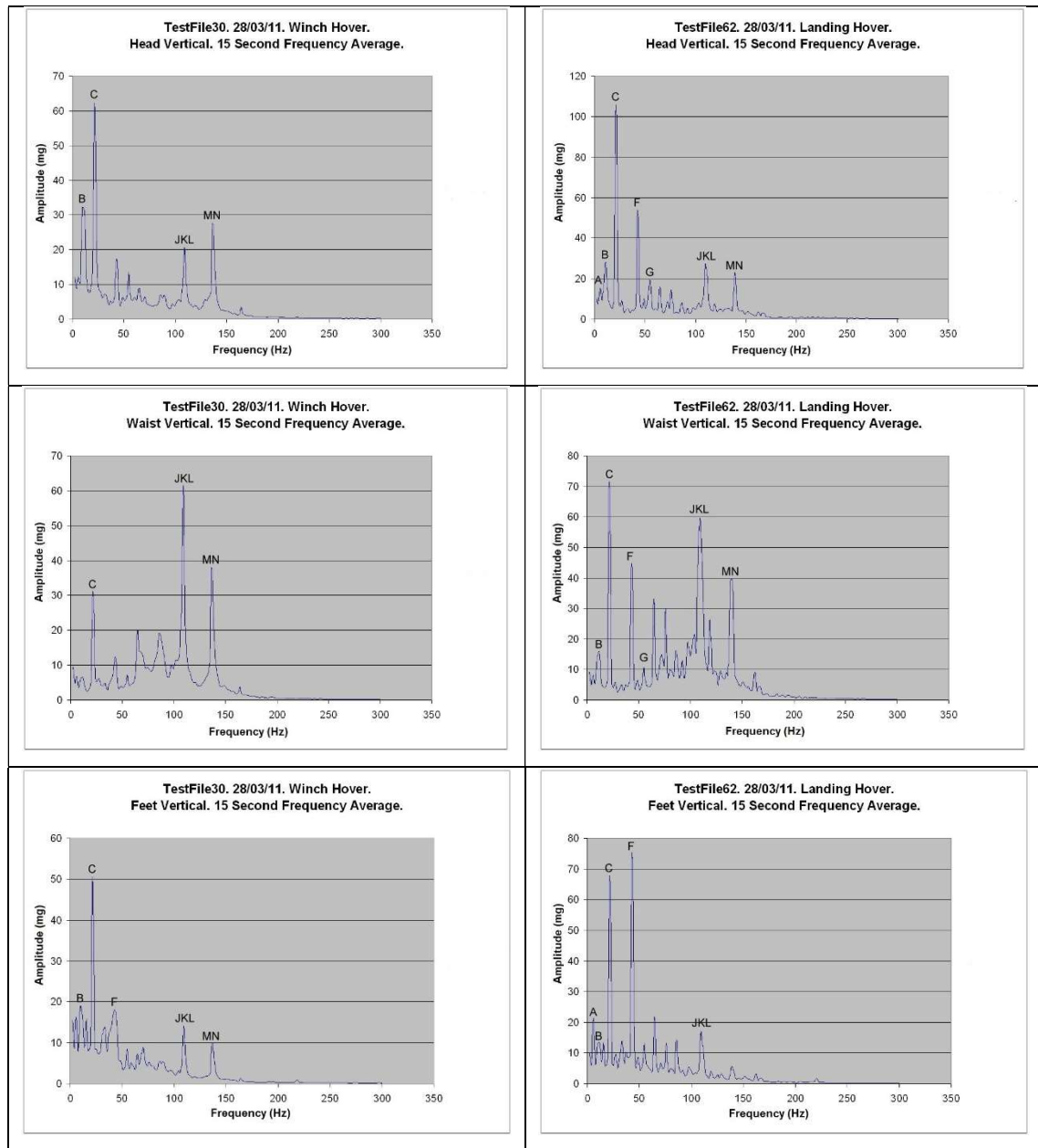


Figure 4.10: Vertical axis frequency plots for the head, waist and feet during winch hover and landing hover. Each is the average of 30 spectrums over a 15 second time period. The letters match the helicopter frequencies of Table 2.3.

The RMS and peak vibration levels and crest factors for the test flight of 28th March 2011 are summarised in Table 4.4. The data is calculated for each “Testfilenn.xlcm” which is 15 seconds or 30,000 samples of the flight. The characteristics are in agreement with what is expected from anecdotal discussions with flight crew which are that the vibrations vary constantly throughout the flight and within flight modes due to the different loads that the helicopter encounters but generally they are highest during descent and landing hover when the helicopter experiences the

added turbulence generated by changes such as the large side door being opened and the rotor down wash coming into ground effect (Kottapalli 2000). The results are however consistent for individual channels indicating that they are not random. The table is included in full to show the constantly changing vibration characteristics which would make them difficult to generate artificially and reinforces the argument made by a number of authors for using real vibration data in the type of vibration simulator being investigated in this research (Birdsong 2001). Table 4.5 compares the measured vibration levels with those reported in the literature (Section 2.5) and shows that the measured levels are in close agreement with those reported by other researchers.

Therefore given the close agreement between the measured and reported vibration levels and frequency components it is concluded that the vibration measurement system is correctly recording high quality helicopter vibration signals from all its sensor boards.

Table 4.4: RMS and Peak accelerations (mg) and Crest Factors for the nine axes of vibrations during different flight modes of the flight of 28th March 2011. The TestFiles are 15 second records. The vertical axis maximums/minimums for each flight mode have been high-lighted in yellow/orange. Legend: H-Head, W-Waist, F-Feet, Lat- Lateral, Lon-Longitudinal, V-Vertical.

Vibrations in Winch Hover

RMS Acceleration (mg)

TestFile	H.Lat	H.Lon	H.V	W.Lat	W.Lon	W.V	F.Lat	F.Lon	F.V
29	43.8	101.9	94.8	44.9	71.4	92.8	47.9	99.9	73.4
30	42.8	91.7	82.6	43.8	63.2	89.7	45.9	89.7	68.3
31	42.8	93.8	84.6	43.8	66.3	89.7	45.9	91.7	70.3
32	44.9	113.2	90.7	45.9	81.6	103.0	48.9	116.2	81.6
33	45.9	115.2	101.9	47.9	87.7	104.0	51.0	125.4	89.7

Peak Acceleration (mg)

TestFile	H.Lat	H.Lon	H.V	W.Lat	W.Lon	W.V	F.Lat	F.Lon	F.V
29	158.0	461.8	396.5	168.2	334.4	386.4	192.7	408.8	340.5
30	169.2	423.1	372.1	170.2	287.5	374.1	193.7	416.9	266.1
31	182.5	406.7	306.8	173.3	315.0	389.4	182.5	444.5	281.4
32	174.3	604.5	374.1	176.4	467.9	510.7	187.6	718.7	363.9
33	203.9	413.9	394.5	213.1	420.0	411.8	215.1	501.5	342.5

Crest Factor (Peak / RMS)

TestFile	H.Lat	H.Lon	H.V	W.Lat	W.Lon	W.V	F.Lat	F.Lon	F.V
29	3.62	4.53	4.19	3.72	4.72	4.15	4.06	4.11	4.61
30	3.97	4.61	4.52	3.86	4.57	4.17	4.22	4.62	3.90
31	4.30	4.34	3.65	3.95	4.76	4.32	3.95	4.84	4.01
32	3.89	5.35	4.12	3.83	5.73	4.97	3.87	6.17	4.49
33	4.41	3.59	3.85	4.45	4.79	3.97	4.23	4.00	3.83

Vibrations in Climb

RMS Acceleration (mg)

TestFile	H.Lat	H.Lon	H.V	W.Lat	W.Lon	W.V	F.Lat	F.Lon	F.V
35	44.9	88.7	82.6	45.9	57.1	83.6	47.9	78.5	70.3
36	42.8	59.1	71.4	43.8	37.7	75.4	44.9	52.0	59.1
37	45.9	65.2	79.5	46.9	36.7	83.6	47.9	54.0	61.2
38	52.0	77.5	107.0	54.0	59.1	106.0	55.0	93.8	89.7

Peak Acceleration (mg)

TestFile	H.Lat	H.Lon	H.V	W.Lat	W.Lon	W.V	F.Lat	F.Lon	F.V
35	162.1	314.0	320.1	165.1	228.3	336.4	165.1	371.1	267.1
36	141.7	225.3	273.2	150.9	132.5	291.5	154.9	173.3	232.4
37	142.7	241.6	308.9	140.7	125.4	325.2	144.8	181.5	293.6
38	169.2	319.1	413.9	169.2	185.5	372.1	170.2	305.8	305.8

Crest Factor (Peak / RMS)

TestFile	H.Lat	H.Lon	H.V	W.Lat	W.Lon	W.V	F.Lat	F.Lon	F.V
35	3.61	3.53	3.88	3.57	3.98	4.03	3.46	4.75	3.81
36	3.33	3.79	3.82	3.47	3.52	3.88	3.48	3.33	3.93
37	3.13	3.71	3.87	3.02	3.41	3.90	3.03	3.34	4.80
38	3.23	4.12	3.86	3.13	3.14	3.52	3.08	3.27	3.39

Vibrations in Cruise

RMS Acceleration (mg)

TestFile	H.Lat	H.Lon	H.V	W.Lat	W.Lon	W.V	F.Lat	F.Lon	F.V
39	56.1	75.4	90.7	57.1	46.9	78.5	58.1	67.3	65.2
40	59.1	73.4	93.8	60.1	47.9	95.8	62.2	73.4	77.5
41	64.2	75.4	96.8	65.2	44.9	100.9	67.3	72.4	79.5
42	67.3	79.5	100.9	68.3	45.9	106.0	69.3	74.4	88.7
43	65.2	77.5	96.8	67.3	44.9	103.0	68.3	73.4	83.6

Peak Acceleration (mg)

TestFile	H.Lat	H.Lon	H.V	W.Lat	W.Lon	W.V	F.Lat	F.Lon	F.V
39	171.3	329.3	353.7	174.3	176.4	337.4	181.5	267.1	281.4
40	189.6	277.3	447.5	187.6	172.3	378.2	190.6	250.8	309.9
41	183.5	273.2	430.2	203.9	162.1	354.8	209.0	264.0	283.4
42	212.0	300.7	458.7	218.2	172.3	401.6	225.3	286.5	363.9
43	189.6	304.8	418.0	184.5	176.4	393.5	195.7	269.1	305.8

Crest Factor (Peak / RMS)

TestFile	H.Lat	H.Lon	H.V	W.Lat	W.Lon	W.V	F.Lat	F.Lon	F.V
39	3.07	4.34	3.91	3.05	3.78	4.30	3.11	3.94	4.31
40	3.21	3.77	4.76	3.10	3.60	3.94	3.08	3.41	3.98
41	2.87	3.62	4.43	3.13	3.59	3.52	3.11	3.66	3.58
42	3.18	3.78	4.53	3.21	3.74	3.79	3.23	3.85	4.12
43	2.89	3.91	4.30	2.75	3.89	3.83	2.85	3.67	3.67

Vibrations in Approach

RMS Acceleration (mg)

TestFile	H.Lat	H.Lon	H.V	W.Lat	W.Lon	W.V	F.Lat	F.Lon	F.V
45	74.4	92.8	129.5	75.4	60.1	141.7	77.5	88.7	125.4
46	56.1	94.8	111.1	56.1	60.1	138.6	59.1	76.5	115.2
47	48.9	90.7	121.3	48.9	55.0	154.9	52.0	65.2	119.3
48	47.9	87.7	96.8	47.9	53.0	127.4	51.0	61.2	87.7
49	47.9	81.6	95.8	47.9	50.0	120.3	50.0	60.1	84.6

Peak Acceleration (mg)

TestFile	H.Lat	H.Lon	H.V	W.Lat	W.Lon	W.V	F.Lat	F.Lon	F.V
45	258.9	382.3	623.9	254.9	268.1	594.3	267.1	368.0	514.8
46	208.0	347.6	413.9	203.9	223.2	605.5	214.1	304.8	377.2
47	149.9	337.4	513.8	152.9	204.9	711.5	162.1	245.7	414.9
48	167.2	293.6	340.5	152.9	202.9	471.0	167.2	225.3	249.8
49	149.9	287.5	362.9	146.8	198.8	584.1	175.3	224.3	333.3

Crest Factor

TestFile	H.Lat	H.Lon	H.V	W.Lat	W.Lon	W.V	F.Lat	F.Lon	F.V
45	3.48	4.13	4.83	3.38	4.48	4.20	3.42	4.16	4.12
46	3.69	3.67	3.73	3.67	3.70	4.37	3.64	3.99	3.27
47	3.06	3.73	4.23	3.12	3.74	4.61	3.15	3.77	3.47
48	3.47	3.35	3.52	3.19	3.82	3.71	3.30	3.71	2.86
49	3.10	3.53	3.80	3.06	3.98	4.87	3.48	3.77	3.95

Vibrations in Landing Hover and Taxi

RMS Acceleration (mg)

TestFile	H.Lat	H.Lon	H.V	W.Lat	W.Lon	W.V	F.Lat	F.Lon	F.V
61	50.0	94.8	97.9	50.0	60.1	138.6	52.0	79.5	86.6
62	58.1	114.2	118.3	60.1	85.6	127.4	63.2	112.1	94.8
63	65.2	124.4	125.4	67.3	91.7	116.2	71.4	130.5	123.3
64	44.9	111.1	106.0	44.9	68.3	98.9	47.9	106.0	72.4
65	40.8	91.7	81.6	40.8	59.1	103.0	43.8	91.7	70.3

Peak Acceleration (mg)

TestFile	H.Lat	H.Lon	H.V	W.Lat	W.Lon	W.V	F.Lat	F.Lon	F.V
61	161.1	402.7	379.2	174.3	267.1	504.6	175.3	349.7	435.3
62	213.1	508.7	462.8	227.3	393.5	478.1	237.5	519.9	407.8
63	268.1	589.2	576.0	276.3	474.0	529.1	310.9	596.3	526.0
64	200.8	448.5	366.0	208.0	273.2	457.7	209.0	420.0	324.2
65	325.2	416.9	375.1	293.6	278.3	444.5	300.7	364.9	356.8

Crest Factor

TestFile	H.Lat	H.Lon	H.V	W.Lat	W.Lon	W.V	F.Lat	F.Lon	F.V
61	3.24	4.27	3.86	3.50	4.44	3.64	3.36	4.41	5.02
62	3.67	4.46	3.91	3.78	4.62	3.74	3.77	4.63	4.30
63	4.08	4.76	4.60	4.12	5.15	4.54	4.34	4.56	4.28
64	4.48	4.05	3.45	4.63	4.00	4.62	4.36	3.96	4.48
65	7.90	4.56	4.61	7.18	4.74	4.32	6.79	3.98	5.08

Table 4.5: Comparison of vertical vibration levels measured during the flight of 28th March 2011 (Table 4.4) with those reported in the literature (Section 2.5).

	Measured minimum	Measured maximum	Reported minimum	Reported maximum
RMS level	59.1 mg	154.9 mg	102 mg	382 mg
Peak level	232.4 mg	711.5 mg	700 mg	830 mg
Crest factor	2.86	5.08	1.8	4.38

This analysis established that the system was recording the vibrations correctly however the frequency plots such as those in the left column of Figure 4.13 include numerous unidentified vibrations which needed to be examined to ensure that they were actual vibrations and not noise generated by the measurement system. Investigations into the sources of these vibrations identified two anomalies which required further investigation.

Firstly there are substantial differences in the vibrations seen by the head, waist and feet sensors in the vertical and longitudinal helicopter axes whilst these are not present in the lateral axis vibrations. For example Figure 4.11 shows the head, waist and feet vertical (left column) and lateral (right column) vibrations averaged over the same 15 second period during winch hover. As the system samples all channels simultaneously the data refers to the same 15 second period. The vertical axis plots show the same frequencies but differing amplitudes between the head, waist and feet vibrations whereas the lateral axis shows a high correlation between the three (the longitudinal axis is similar to the vertical but not shown here) which indicates that the litter is flexing in the vertical and longitudinal axes but not in the lateral axis. Note that the orientation axes are referenced to the helicopter (Figure 2.2). This flexing is consistent with the mechanical construction of the litter which is by necessity as light as possible and therefore not rigid in the vertical and longitudinal axes but is rigid along the lateral axis as any flexing in this axis would require compression and expansion of the litter frame. Two possible reasons for this flexing were considered. Firstly, the mannequin could be moving in the litter. If this is so then it would need

to be shown that the mannequin reacts identically to a human as the mannequin must be used for winching trials. The second possibility was that the helicopter floor was flexing and the litter was flexing in sympathy with it. Both these possibilities were investigated in subsequent flights with the results showing that the helicopter floor was flexing and the litter was flexing in sympathy with it (Section 4.3.2.3).

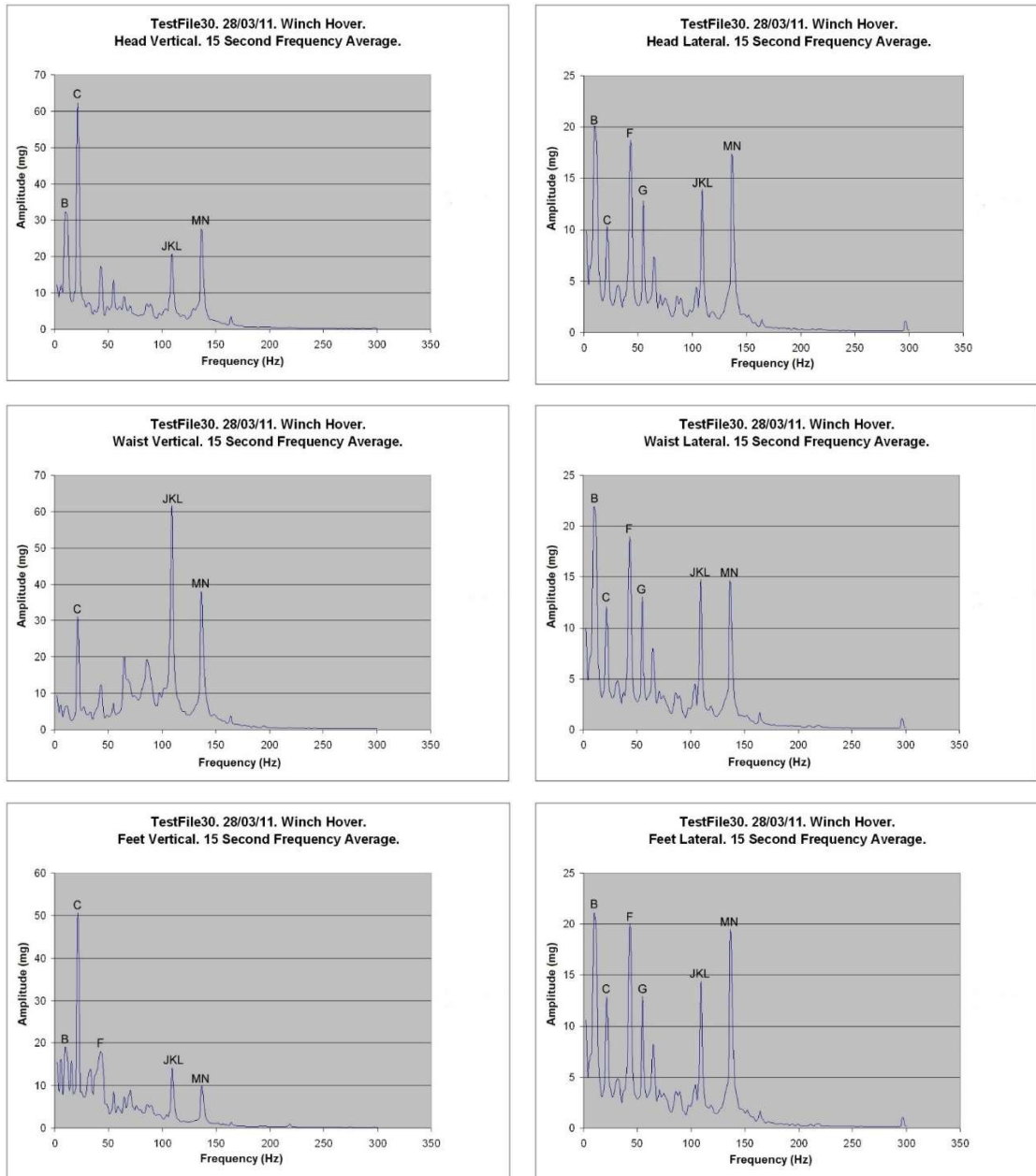


Figure 4.11: Vertical (left) and Lateral (right) axis frequency domain plots for the same 15 second period of 60 feet winch hover. The vertical axis vibrations at the head, waist and feet appear uncorrelated however there is high correlation for the lateral axis vibrations.

The second anomaly was the rapid changes in the vibrations over the short term. As an example, Figures 4.12 and 4.13 show time and frequency plots of consecutive 0.5 second periods for the waist vertical axis in winch hover. Note the considerable variation in both the frequency components present and their amplitudes even though the helicopter was in stable hover and the flight was conducted in calm conditions. This is common in helicopter machinery vibrations, see for example Tumer (Tumer 2002) who recommends that the raw vibration data be averaged using time-synchronous averaging for noise reduction and signal stabilisation. However the technique is not suitable here as it requires that the signal be periodic and a periodic trigger, such as once per revolution of the main rotor, be available. The method implemented here is that of Smith (Smith 1997) who recommends averaging of the frequency spectrum over as long a period as possible. The right column of Figures 4.13 shows three consecutive 15 second averages for the waist vertical axis during winch hover covering the same time as the left column of Figure 4.13. Note the consistent amplitudes on identified vibrations, lower levels of unidentified vibrations and lower noise levels of the averaged plots. Subsequently it was shown that the reason for the apparent short time variations was the complex three dimensional circular nature of the helicopter vibratory motions due to the helicopter being suspended from the main rotor hub at the top of the rotor mast which acts as a flexible coupling allowing the helicopter body to oscillate in multiple dimensions about the hub (Prouty 2005). There are therefore two different sources of vibrations, the regular sources such as those emanating from rotating machinery (Table 2.3) and random sources such as the small pilot control inputs needed to maintain stable hover. Frequency domain averaging stabilises the amplitudes of regular vibrations while removing the transient oscillations resulting from random sources.

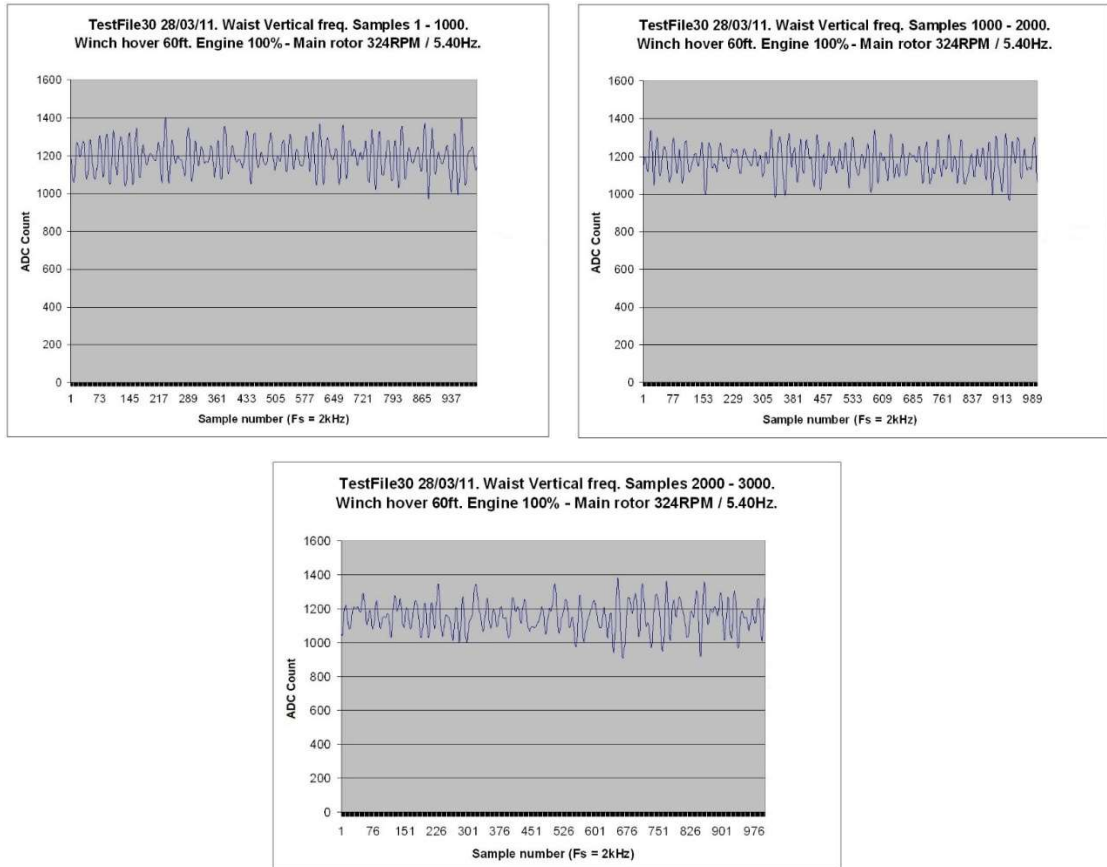


Figure 4.12: Example of short-term variations in vibration signals. Showing three consecutive 0.5 sec periods of waist vertical vibrations in the time domain.

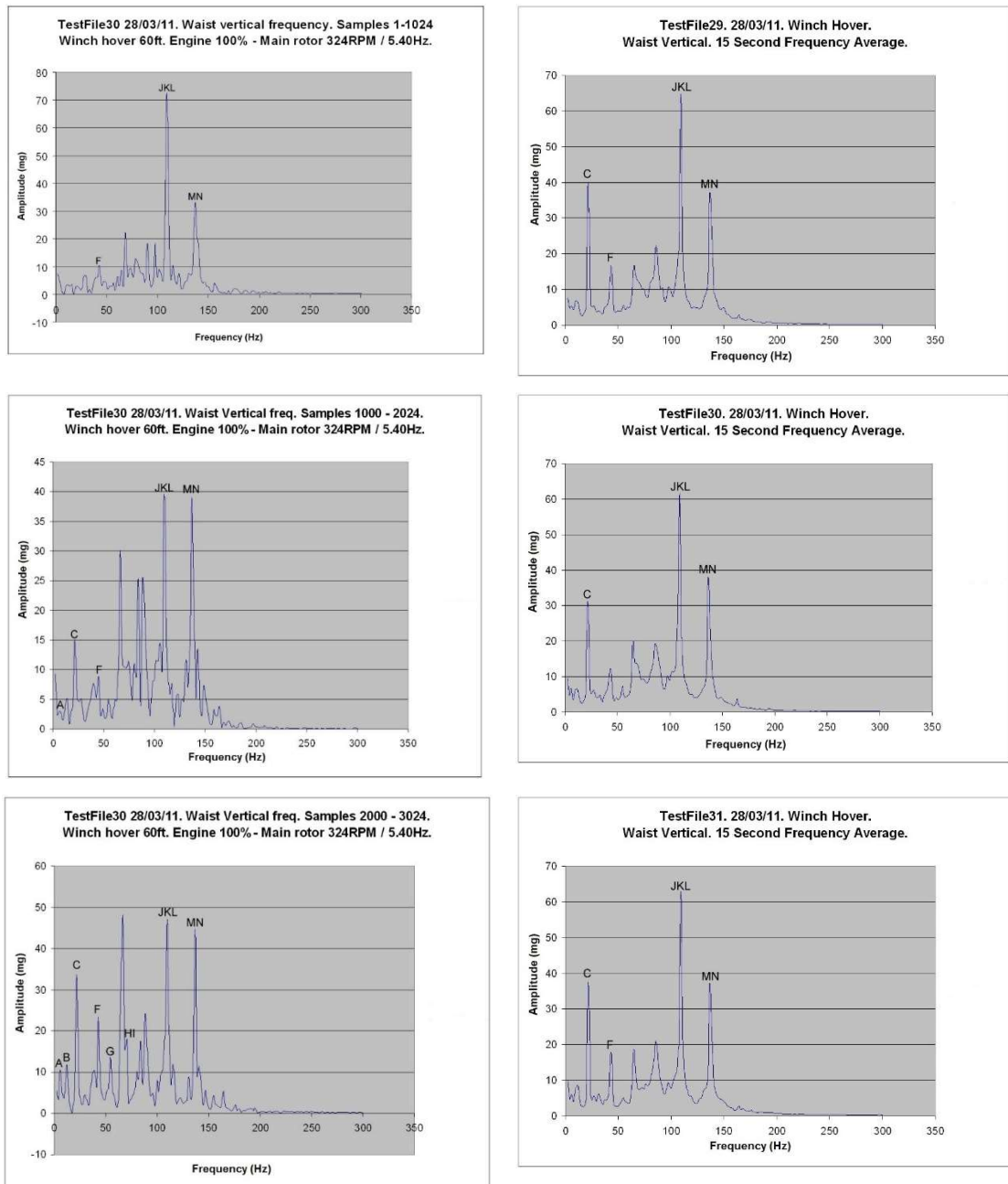


Figure 4.13: Example of short-term variations in vibration signals and the effect of averaging on the frequency plots. The left column shows three frequency plots for consecutive 0.5 sec periods of the same vibration signal. Note the variation of amplitudes for identified sources and the presence of random unidentified vibrations. The right column shows three consecutive 15 second frequency domain averaged plots for the same vibration source. Note the consistency of the identified sources, the lower level of unidentified sources and lower noise level.

Conclusions from the first flight 28th March 2011.

The purpose of the flight was to verify correct operation of the vibration measurement system:

1. The vibration measurement system has been shown to be working correctly. The data is accurate as the frequencies recorded correspond to those published by the helicopter manufacturer (Table 2.3) and the RMS and peak vibration levels and crest factors are in agreement with the levels reported in the literature (Table 4.5).
2. The vibrations experienced are complex, time varying and three dimensional. Building a simulator capable of vibrating in three dimensions is beyond the capabilities and budget for this project. We will need to limit the table to a single dimension, probably vertical, and therefore simplifications to the original specification will need to be made.
3. There are substantial differences in the vibrations seen by the head, waist and feet sensors in the helicopter vertical and longitudinal axes. The helicopter lateral axis, along which the litter is aligned (Figure 2.2), is however consistent. Two possible explanations for the differences were identified for further investigation; firstly the mannequin could be moving in the litter in which case it would need to be shown that the mannequin and a human have the same response, or secondly the helicopter floor is flexing which would be difficult to reproduce in a simulator. These issues will be investigated in future flights.
4. The vibrations vary rapidly in the short term but are stable in the long term. This would make it difficult to generate similar signals artificially and therefore the simulator should be driven with real vibration data.

4.3.2.2 FLIGHT TEST 2 – 6th April 2011

The flight on 6th April 2011 was in the same aircraft as the previous flight, a Bell 412 helicopter VH-ESB of Emergency Management Queensland and of approximately 20 minutes duration. The purpose of the flight was to collect vibration data with a human patient in the rescue litter which could then be compared with that of the rescue mannequin (Section 4.3.2.1) to confirm that the mannequin is a reasonable approximation to a human, at least as far as vibrations are concerned. It was important to show this as a human cannot be winched in the rescue litter during testing and also to determine if the significant differences in vibrations noted between the head, waist and feet in the vertical and longitudinal axes were in some way due to the construction of the mannequin. The flight profile was the same as the previous flight and included winch hover, climb, cruise, approach and landing but not actual winching. Vibration data was collected continuously from the three Sensor Boards attached to the base of the rescue litter. The atmospheric conditions were different to the first flight being turbulent with moderate winds.

A 72.5kg volunteer was restrained in the rescue basket (Figure 4.7) as normal for this type of patient retrieval. Note that while the volunteer and basket are securely restrained by safety straps this restraint is not rigid and would allow considerable movement of the basket relative to the helicopter particularly at the level of vibration signals. The plots of Figures 4.14 and 4.15 show comparisons of typical vertical axis vibrations between the first and second flights and establish that *there is no discernible difference between the vibrations measured under the rescue litter for a human patient compared to the rescue mannequin.*

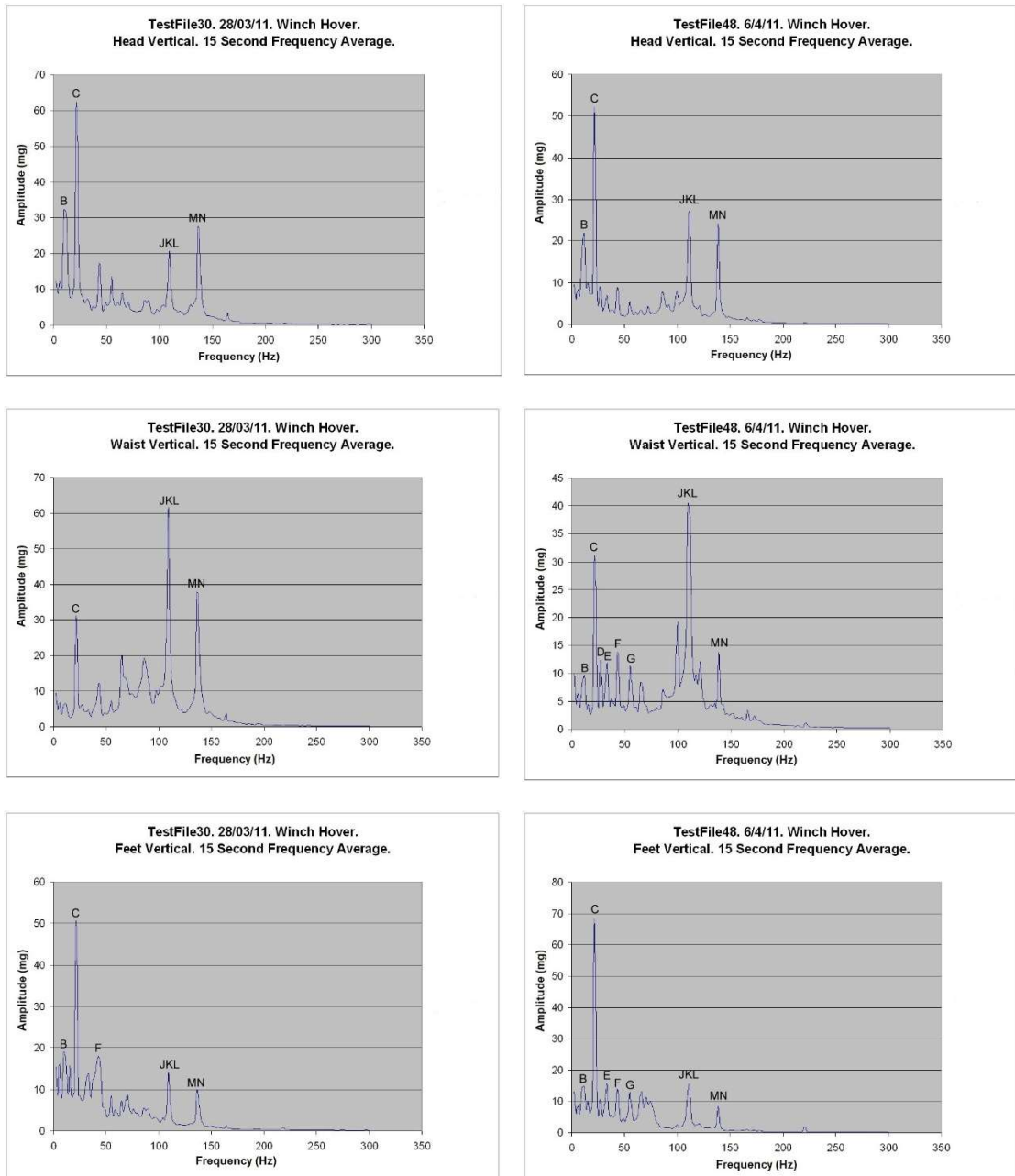


Figure 4.14: Comparison of vertical axis frequency components recorded during winch hover for a 70kg Mannequin (left column) and 72.5kg human (right column).

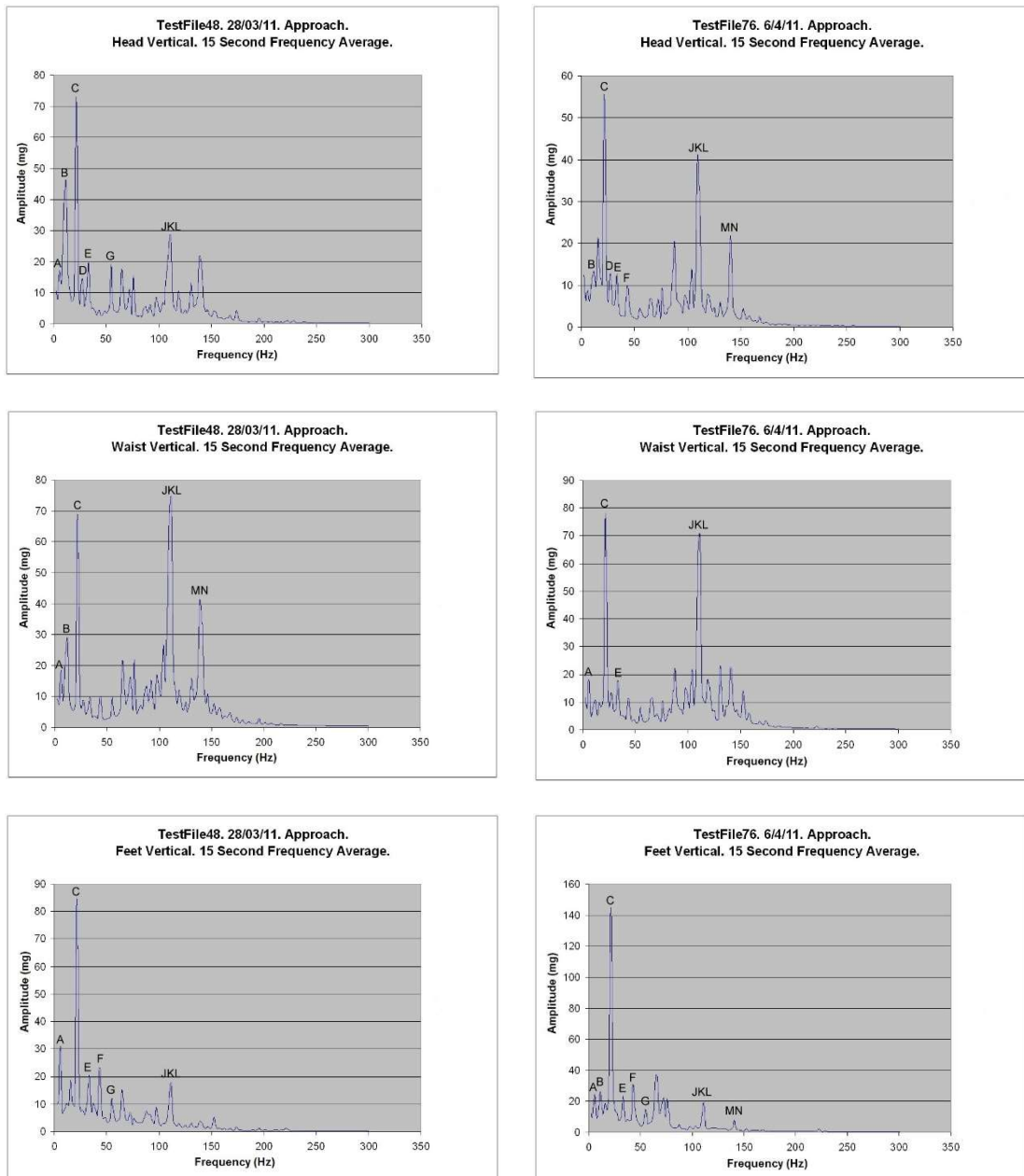


Figure 4.15: Comparison of vertical axis frequency components recorded during approach for a 70kg Mannequin (left column) and 72.5kg human (right column).

The flight results also show the marked effect that atmospheric have on the helicopter vibrations. Figure 4.16 compares the vertical axis vibrations in climb between the calm conditions experienced in the first flight and the turbulence of the second. The flight record for the second flight (Table A.1) indicates buffeting and turbulence during this period (TestFile53) due to a small

amount of wind from the port side. Notice the large increase in vibration amplitude at four times the main rotor frequency (21.6 Hz), labelled as “C” in the plots.

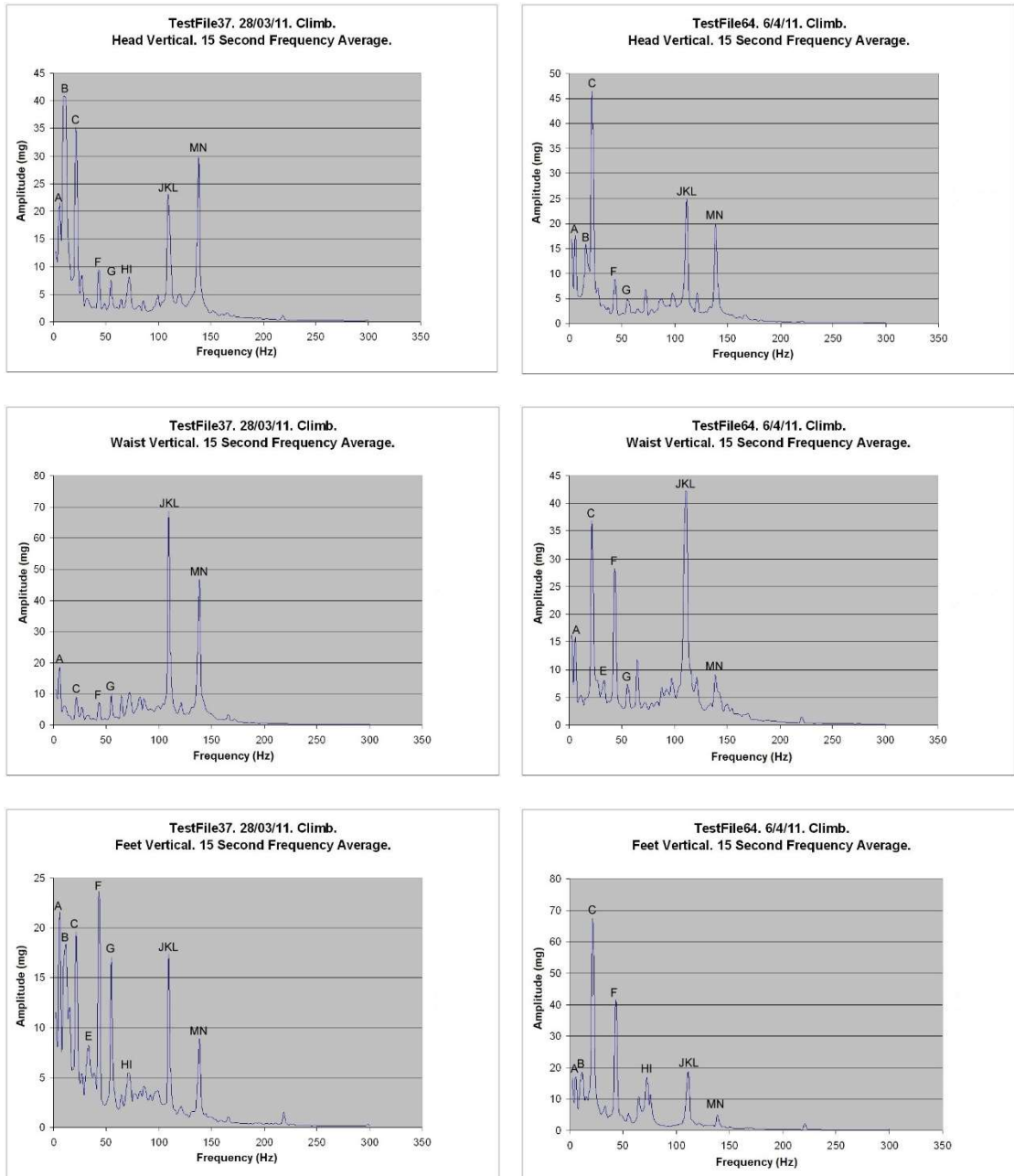


Figure 4.16: The effects of turbulence on helicopter vibrations. The left column shows vertical vibrations recorded during climb in the calm conditions of the first flight (26th March 2011). The right column shows the corresponding period during the turbulent conditions experienced in the second flight (6th April 2011). Note the increased vibration amplitude at four times the main rotor frequency (21.6 Hz) labelled as “C”.

Figure 4.17 also shows the effect that a small change in atmospheric conditions can have on the vibration spectrum but this time the comparison is between two closely separated periods during winch hover in the same flight. The left column represents calm conditions while three seconds later in the right column the helicopter is being buffeted by winds from the port side. The buffeting has resulted in a significant increase in the vibration level at 21.6 Hz or four times the main rotor frequency, labelled as "C". This can be explained by reference to helicopter aerodynamics and the physical configuration of the Bell 412 helicopter which has a four blade main rotor that rotates counter clockwise when viewed from above meaning that the main rotor blades travel port to starboard across the tail boom. Forces are applied to a helicopter via the main rotor thrust vector which acts upwards through the main rotor hub and is always perpendicular to the plane of the circular path traversed by the main rotor blade tips, called the Tip Path Plane (TPP) (Prouty 2005). The thrust vector magnitude is directly controlled by the main rotor collective pitch control which varies the pitch angle (called Feathering) and hence the thrust of all four main rotor blades by the same amount. The thrust vector direction is controlled indirectly by tilting the TPP using the main rotor cyclic pitch control which varies the individual blade pitch angle and hence its thrust within a single cycle. In the period represented by Figure 4.17 the helicopter is maintaining a stable hover against wind which is pushing on its port side. To maintain position the thrust vector is tilted to port so that it will apply a horizontal force component negating that of the wind. To do this the TPP is tilted to port by using the cyclic control to lower the blade tips when they are traversing around the front of the helicopter from starboard to port and raise them when they are traversing around the back of the helicopter from port to starboard. This up and down movement of the blades is referred to as blade Flapping. The blades are raised by increasing their pitch angle to produce more thrust and in this case this is a maximum as the blade passes directly to the rear and over the tail boom. The blade downwash hits the tail boom generating an impulsive force at four times the main rotor frequency (21.6 Hz). These impulsive forces are always present but are larger in this case due to the higher thrust being generated as each blade crosses over the tail boom. Note how a relatively small external disturbance can have a marked effect on the helicopter vibration spectrum.

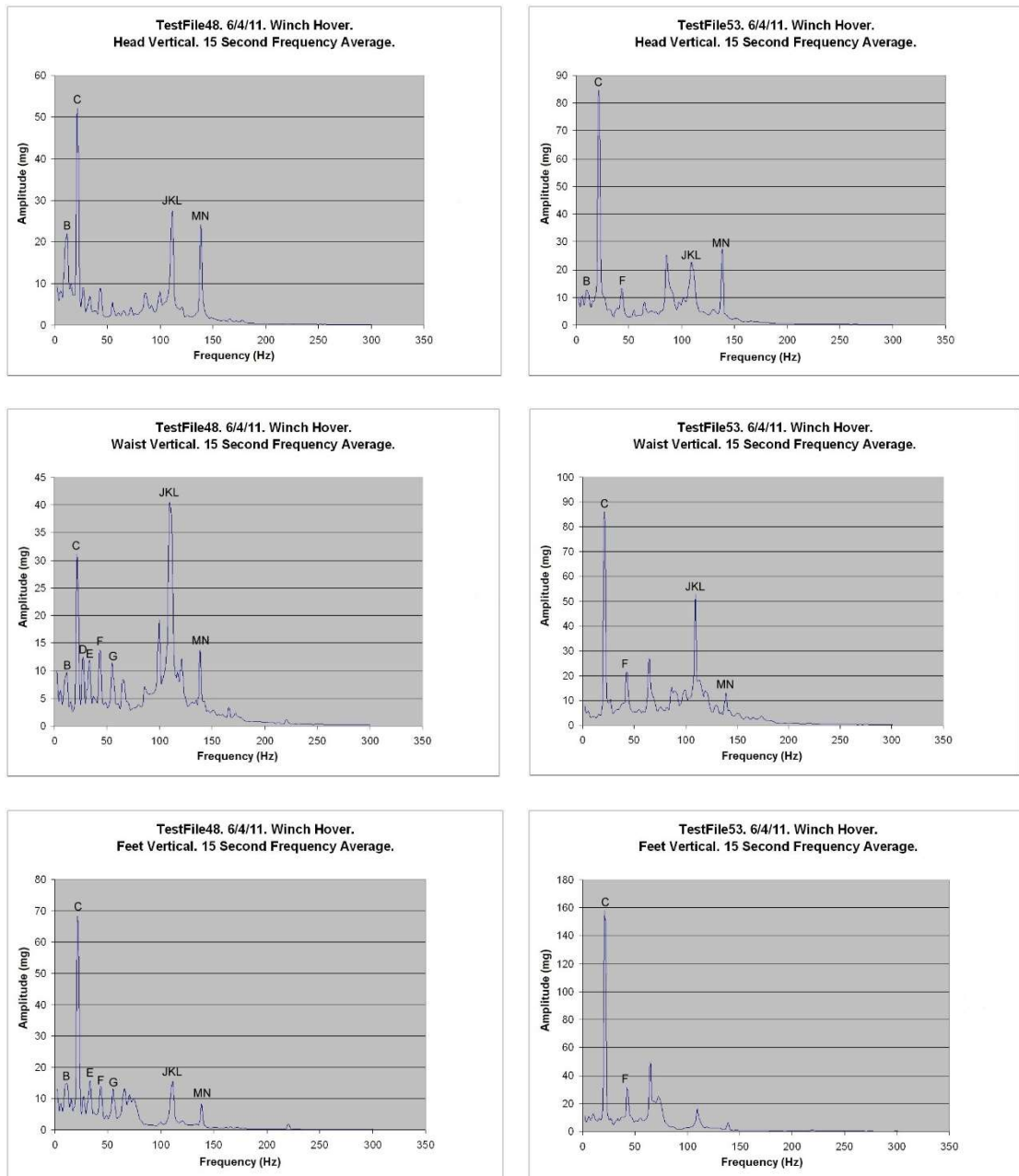


Figure 4.17: Showing the effect that a small change in atmospheric conditions can have on the helicopter vibration spectrum. The left column shows the spectrum for winch hover in calm conditions and the right column is for a small amount of wind buffeting the helicopter from the port (left) side. Note the increased vibration amplitude at four times the main rotor frequency (21.6 Hz) labelled as “C”.

Conclusions from the second flight 6th April 2011.

The purpose of the flight was to collect vibration data with a human patient which could then be compared with that of the rescue mannequin (Section 4.3.2.1) to confirm that the mannequin is a reasonable approximation to a human, at least as far as vibrations are concerned. Reference to

Figures 4.14 and 4.15 show minimal differences in the plots and therefore confirm that *the mannequin is a good approximation to a human patient*. In addition Figures 4.16 and 4.17 show that a small atmospheric disturbance can have a substantial effect on the helicopter vibration spectrum and therefore as the weather is continuously varying *there will always be differences in the vibration spectrum between and within flights*.

The significant differences noted between the head, waist and feet in the vertical and longitudinal axes for the mannequin were still present for the human patient and so it can be concluded that they are not due to the construction of the mannequin. The following two flights investigate the flexing of the helicopter floor to confirm it as the source of the significant differences noted between the head, waist and feet in the vertical and longitudinal axes.

4.3.2.3 FLIGHT TESTS 3 AND 4 – 24th April 2011

It was noted in the previous flights (Sections 4.3.2.1 and 4.3.2.2) that the rescue litter vibrations recorded at the head, waist and feet differed, in the vertical and longitudinal axes. The aim of these two flights was to show that the measurements were correct and that the underlying cause of the difference was the vibratory modes of the helicopter frame being transmitted through the floor to the litter. The experimental methodology was to apply the measurement system to:

- a. Record and analyse the unloaded helicopter floor vibrations.
- b. Record and analyse the loaded floor vibrations with the litter/mannequin in place.
- c. Investigate any correlation between the vibrations recorded on the litter (Flight 1) and on the loaded floor with the litter/mannequin present (Flight 4).

Two flight configurations were proposed;

Flight 3: recording the unloaded floor vibrations by mounting the sensors directly to the helicopter floor with no litter in place.

Flight 4: recording the loaded floor vibrations by leaving the sensors mounted to the floor with the litter/mannequin in place.

This experiment provided answers to the following questions:

1. What is the nature of the floor vibrations?
2. How does the litter/mannequin affect the floor vibrations?
3. What is the correlation between the litter and the floor vibrations, i.e. what is the correlation between the vibrations of Flight 1 and 4?

Flights 3 and 4 on 24th April 2011 were in the same Bell 412 helicopter VH-ESB of Emergency Management Queensland and of approximately 20 minutes duration each. The flight profiles were the same as previous with winch hover, climb, cruise, approach and landing but not actual winching. The weather was calm. Vibration data was collected continuously from the three Sensor Boards attached to the floor of the helicopter in the same relative positions as they had been for previous flights. i.e. under the head, waist and feet positions of the rescue litter (Figures 4.7 and 4.18). The litter was not present for the third flight but the litter with 70kg mannequin was in place for the fourth flight. The litter was held in place by safety straps as normal for this type of patient retrieval. Note that while the mannequin and litter are securely restrained by safety straps (the yellow straps in Figure 4.7) this restraint is not rigid and would allow considerable movement of the litter relative to the helicopter floor particularly at the level of vibration signals.

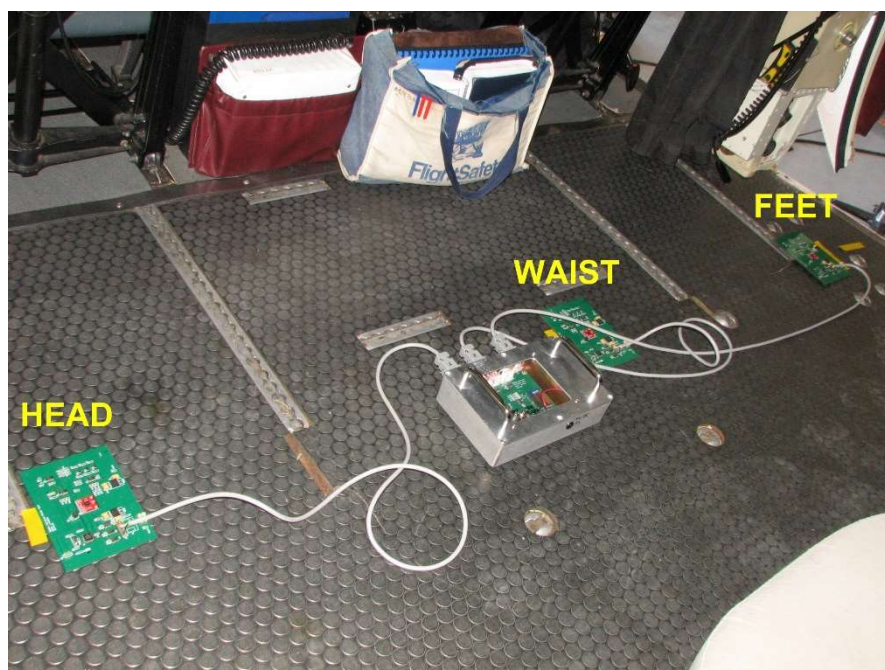


Figure 4.18: Sensors mounted on the helicopter floor for flights 3 and 4. The sensors recorded the vibrations of the helicopter floor mat as shown (Flight 3) and with the rescue litter/mannequin in place (Flight 4). The purpose was to show that the differences between vibrations seen at the head, waist and feet of the rescue litter in previous flights were emanating from the flexing of the helicopter floor and not from the litter.

Figures 4.19 to 4.21 show frequency plots of the vertical, longitudinal and lateral axis vibrations recorded in winch hover during Flight 1 (sensors mounted to the base of the rescue litter/mannequin), Flight 3 (sensors mounted to the helicopter floor with no litter present (Figure 4.18)) and Flight 4 (sensors mounted to the helicopter floor with the litter/mannequin present). These plots allow a determination of the vibration characteristics of the unloaded helicopter floor, the effect on the floor vibrations of the rescue litter/mannequin and a comparison between the floor vibrations and those measured in the rescue litter.

Detailed observations of the figures revealed the following relevant characteristics:

- Vertical axis (Figure 4.19): The head, waist and feet plots for each flight generally contain the same frequencies but with differing amplitudes. This indicates that the floor is flexing with the vibrations rather than moving as a whole in this axis which is to be expected with a mechanical structure such as the helicopter frame. A mechanical frame will exhibit resonances and nulls at different points depending on the excitation frequency. Flight 3 is a good example of this where the waist plot shows a large component JKL which is absent from the head and feet plots. The feet plot for flight 3 is not correlated to the head or waist however this is likely due to the floor matting being torn allowing it to flap freely (Figure 4.22, 4.23). Comparing the three sensor location (head, waist and feet) between flights there is a reasonable correlation between flights 3 and 4 but poor correlation between these two and flight 1. This indicated that the rescue litter is moving with respect to the floor and therefore in the simulator the sensors should be attached to the rescue litter.
- Longitudinal axis (Figure 4.20): These plots indicate that the helicopter floor is generally vibrating as a whole rather than flexing which is expected as the helicopter structure is rigid along this axis. This is shown by the high correlation between the three positions in flights 3 and 4 but less so in flight 1 indicating that the rescue litter is flexing in this axis relative to the floor.
- Lateral axis (Figure 4.21): The lateral axis plots show strong correlation both between the three sensors in individual flights and across sensors between flights 1 and 4. This indicates that the floor is not flexing in this axis and that the rescue litter is also not moving with respect to the floor.

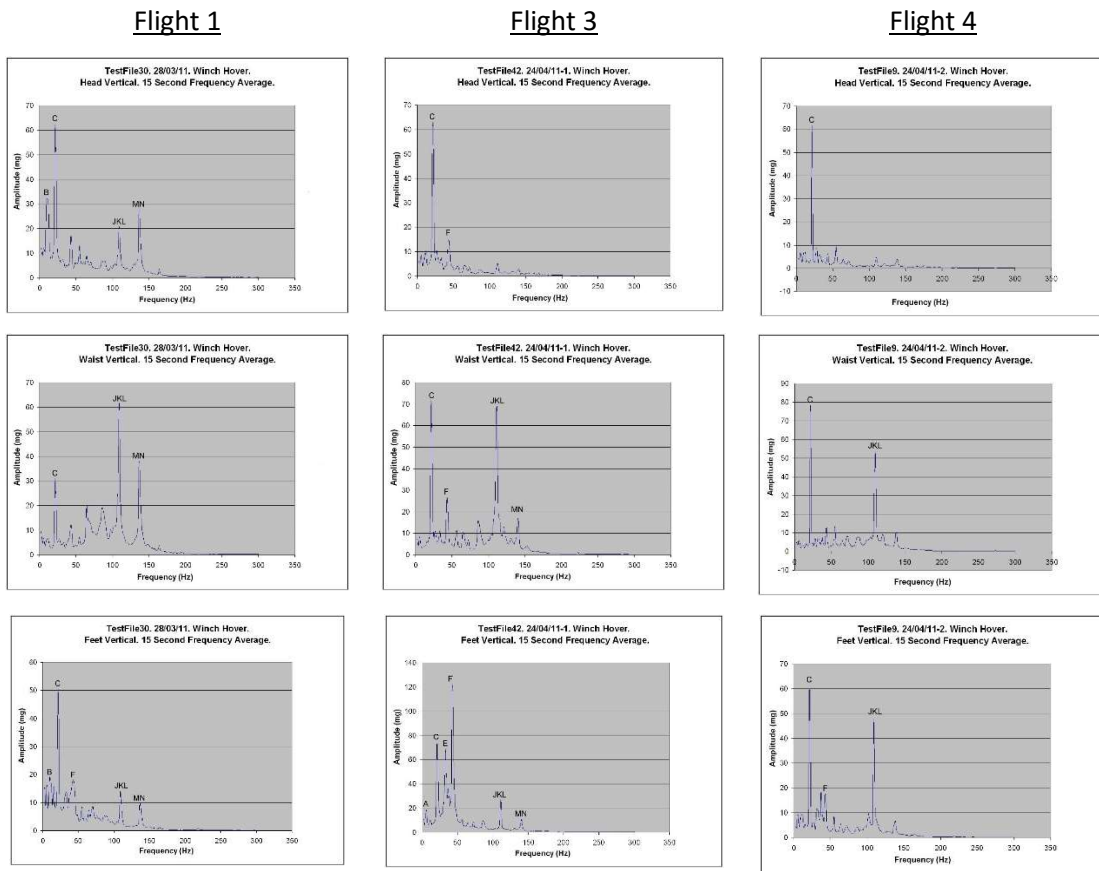


Figure 4.19: Comparison of vertical axis vibrations recorded in winch hover for three different sensor configurations. The configurations are: Flight 1 – sensors mounted to base of rescue litter; Flight 3 – sensors mounted on floor with no litter; Flight 4 – sensors mounted on floor with litter/mannequin in place. The top/middle/bottom rows show vertical vibrations at the head/waist/feet.

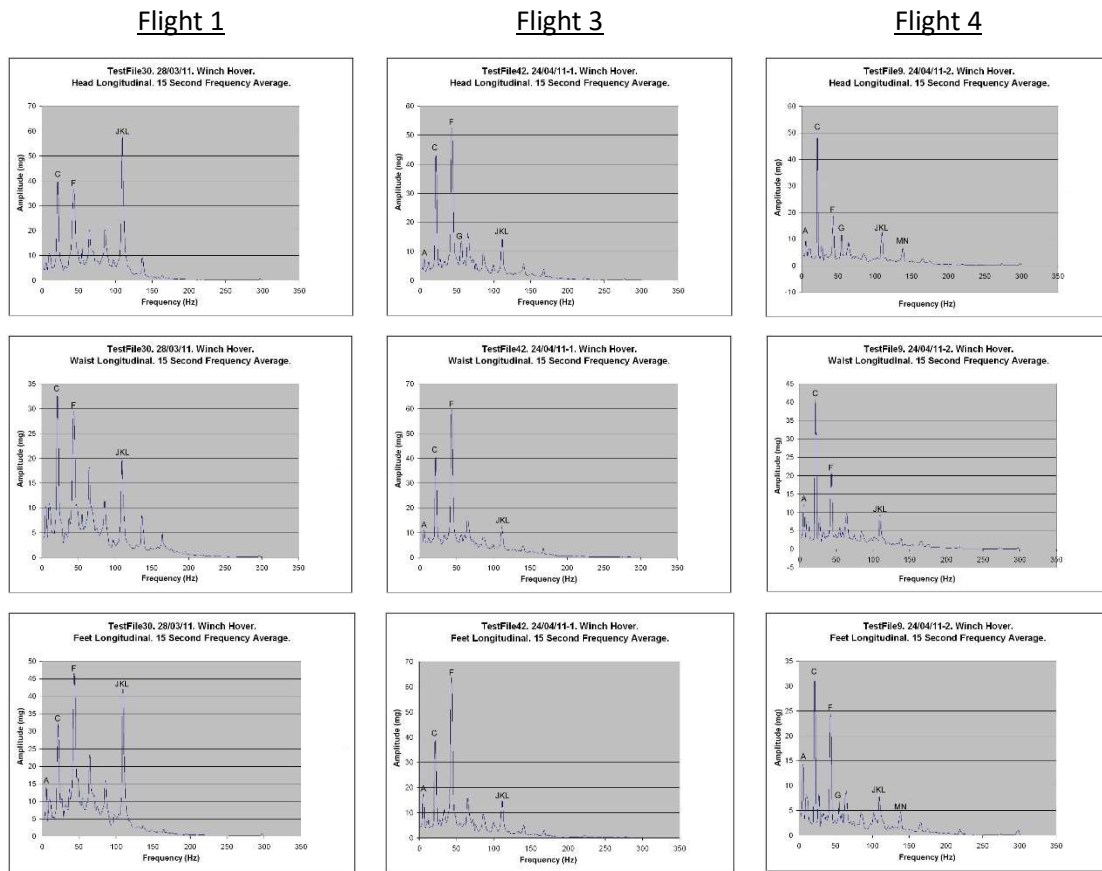


Figure 4.20: Comparison of longitudinal axis vibrations recorded in winch hover for three different sensor configurations. The configurations are: Flight 1 – sensors mounted to base of rescue litter; Flight 3 – sensors mounted on floor with no litter; Flight 4 – sensors mounted on floor with litter/mannequin in place. The top/middle/bottom rows show vertical vibrations at the head/waist/feet.

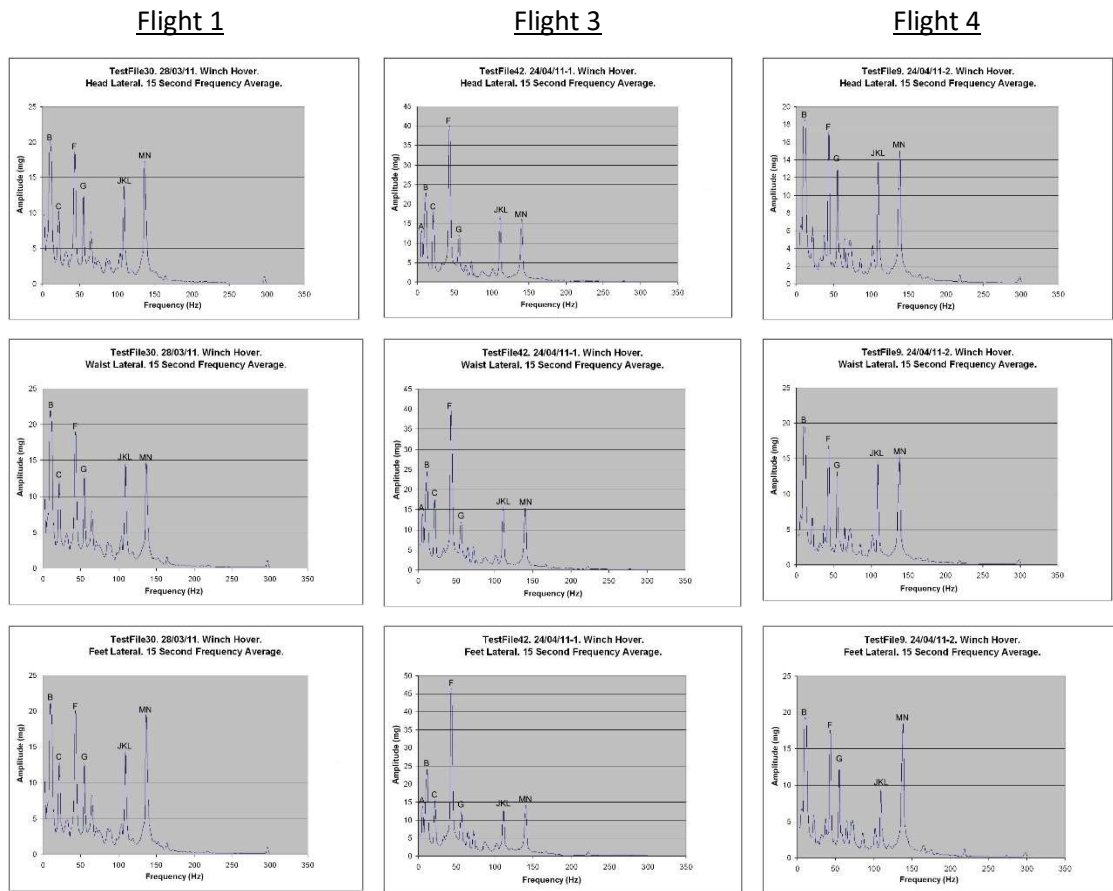


Figure 4.21: Comparison of lateral axis vibrations recorded in winch hover for three different sensor configurations. The configurations are: Flight 1 – sensors mounted to base of rescue litter; Flight 3 – sensors mounted on floor with no litter; Flight 4 – sensors mounted on floor with litter/mannequin in place. The top/middle/bottom rows show TestFile42 vibrations at the head/waist/feet.

Conclusions from the third and fourth flights 24th April 2011.

These flights have shown that the measurement system is working correctly and that the vibrations recorded underneath the rescue litter are closely matched to those of the actual helicopter floor. The vibrations of the helicopter floor are as expected for this type of structure which is quite rigid in the longitudinal and lateral axes but less so in the vertical axis. This means that the vibration amplitudes at the three measuring points can differ in the vertical axis due it flexing but are closely correlated in the longitudinal and lateral axes. Due to its small relative mass the rescue litter has very little effect on the floor vibrations however the plots do show that the rescue litter is vibrating

differently from the helicopter floor and therefore the feedback sensors for the vibration simulator should be attached to the underneath of the rescue litter as in flights 1 and 2.

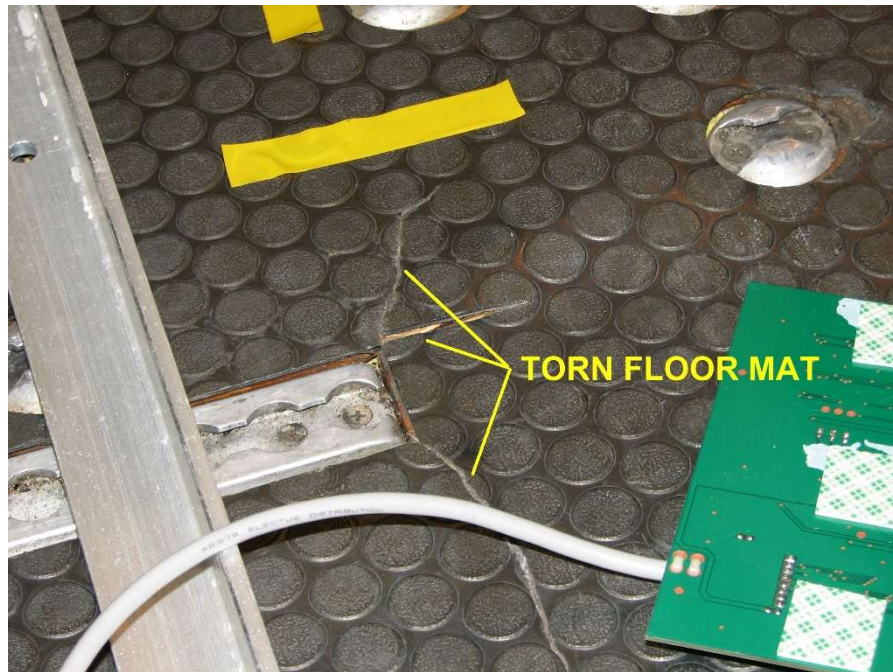


Figure 4.22: Torn and raised floor matting under feet sensor. The floor matting under the feet sensor has come away from the mat and is vibrating freely possibly giving extraneous readings.

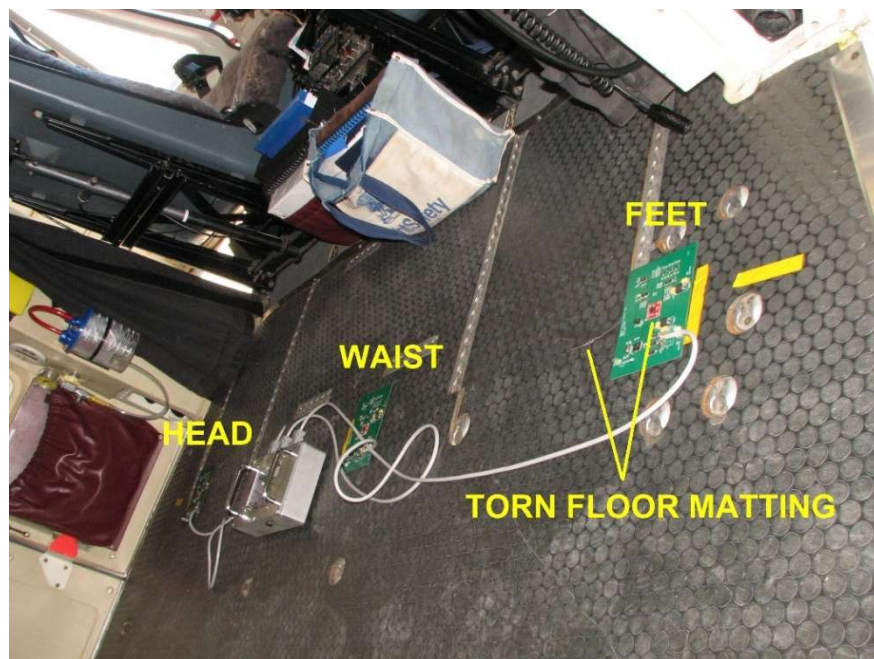


Figure 4.23: Feet sensor mounted on torn floor matting.

4.4 SUMMARY AND CONCLUSIONS

This chapter presented the testing and analysis work that was conducted to verify the operation of the vibration measurement system. This began in section 4.1 with an outline of the criteria that the system needed to meet for it to be considered a success. In constructing the criteria for success reference was made to the system operational requirements that were developed in chapter 2 and 3. Section 4.2 outlines the methodology that was employed in confirming that the system met the criteria for success. This consisted of laboratory calibration of the sensor frequency response to determine its sensitivity, bandwidth, pass/transition/stop band characteristics etc followed by flight testing to verify that the system was detecting the correct frequency tones as reported by the manufacturer (Table 2.3) and at the correct levels as reported in the literature (Table 2.2). The results and analysis of the verification are presented in section 4.3 commencing with the laboratory calibration followed by the flight testing.

Examination of the flight data has identified the nature of the helicopter floor vibrations and shown that they are similar to the vibrations of the rescue litter although there are differences indicating that the litter is moving with respect to the floor which is expected as the litter is not rigidly attached.

The contributions of this chapter are:-

- The vibration measurement system has been calibrated and its correct operation confirmed.
- The vibrations of the helicopter floor have been characterised.
- The vibrations of the rescue litter have been shown to be similar to those of the helicopter floor and the differences accounted for.

The combination of the examination of the data collected in the laboratory calibration and flight testing has verified that the vibration measurement system is working correctly and meets or exceeds the criteria for success as set out in section 4.1 therefore the first of the research questions posed in this thesis “*Is it feasible to record the vibrations experienced by patients lying supine in a rescue litter during helicopter winching and retrieval?*” has been successfully answered.

This work will be published in a paper which is currently being prepared “*The Measurement of Vibrations Experienced by Recumbent Patients During Helicopter Aeromedical Retrieval*” by Grabau, P., Blake, D., and Jacob, M. Target journal is IEEE Transactions on Information Technology in Biomedicine

CHAPTER 5

THE VIBRATION SIMULATOR

5.0 INTRODUCTION

This chapter presents the vibration simulator that was developed for simulating, in the hospital, the vibrations experienced by a patient during helicopter winching and retrieval. This is the second and final stage of the project and will answer the second research question posed in this thesis “*Is it feasible to simulate the vibrations experienced by patients lying supine in a rescue litter during helicopter winching and retrieval?*”. The simulator is required for clinical trials assessing the hypotheses that *vibrations generated by a rotary wing aircraft increase the quantity of nitrogen bubbles in the blood stream leading to more severe symptoms of Decompression Illness (DCI) in Self Contained Underwater Breathing Apparatus (SCUBA) divers* who have developed initial symptoms of DCI and are being medivaced to specialist care. The research question was examined experimentally by first undertaking a preliminary simulator design which identified a number of enabling technologies that would be key to the successful implementation of the vibration simulator and then undertaking detailed investigation, design and implementation of each technology to prove its viability.

The result of this work is a vibration simulator which vibrates in the vertical axis only, due to cost constraints, even though it has been shown that the vibrations experienced by patients are three dimensional. The simulator uses real vibration data as its input (target signal) and simulates all the flight modes experienced in a typical retrieval. The complete system consisting of the vibration measurement system and the simulator is unique and will allow clinical trials investigating the effects of vibrations in a range of scenarios. It is also versatile and will be able to simulate the vibrations of any combination of helicopter/litter, flight mode and atmospherics. Despite only reproducing vertical axis vibrations the vibration simulator is considered a successful and useful research tool.

The simulator is not complete as some work remains to be done implementing the Frequency Response Function estimation and Time Waveform Replication software. This will be finalized following the completion of the thesis write-up. However sufficient work has been completed to confidently say that it is *feasible to simulate the vibrations experienced by patients lying supine in a rescue litter during helicopter winching and retrieval* and therefore the research question has been successfully answered.

The chapter is organised as follows:

Section 5.1 presents the operational specification that was developed as part of the first stage of the design to quantify the required system performance.

Section 5.2 presents the detailed design of the vibration simulator including the choice of vibration actuator, support method for the vibrating table and computer control and communications.

Section 5.3 is a detailed description of the Time Waveform Replication strategy for controlling the reproduction of the real vibration signals as implemented in this simulator.

Section 5.4 is the summary and conclusions for this chapter.

5.1 OPERATIONAL SPECIFICATION

The operational specification was created from a range of sources including the recorded flight vibration data to ensure that the vibration simulator reproduced as closely as possible the vibrations experienced during actual flight and that the simulations were verifiable. The specification is detailed under the following criteria:

1. **Actuator:** The actuation energy will be provided by electrodynamic shakers which are rated by the force that they can generate, the actuator displacement, bandwidth and the mass that they can support.

Force: The required force is determined using Newton's second law

$$Force = mass \times acceleration \quad (1)$$

where mass is the mass of the moving parts of the simulator (test subject + rescue litter + table top + shaker armature) and acceleration is the maximum acceleration required as determined from the recorded flight data.

The following masses were used in the design and are considered to be quite conservative.

- Mass of test subject – 110 Kg. Allows for a large range of subjects.
- Mass of moving part of table – 37 Kg. Estimate from the quantity of metal used in the design.

The maximum accelerations both peak (7.49ms^{-2}) and RMS (1.79ms^{-2}) were recorded in *flight 24/04/2011-2 TestFile41 Approach* (Table 5.0). However it should be noted that the times of high acceleration were relatively short as outlined below:

- 80% of the time the acceleration is less than $2.272ms^{-2}$.
- 85% of the time the acceleration is less than $2.55ms^{-2}$.
- 90% of the time the acceleration is less than $2.914ms^{-2}$.

also

- 80% of $7.49ms^{-2} = 5.99ms^{-2}$, and this is exceeded 0.167% of the time.
- 85% of $7.49ms^{-2} = 6.37ms^{-2}$, and this is exceeded 0.0667% of the time.
- 90% of $7.49ms^{-2} = 6.74ms^{-2}$, and this is exceeded 0.043% of the time.

The maximum peak/RMS vertical accelerations recorded were 7.49/1.79 ms^{-2} during the approach phase of flight 4 (Table 5.0) and these would require forces of 1101 Nt and 263 Nt respectively.

Table 5.0: This table shows the maximum peak/rms vibration levels and crest factor recorded during the flights. These occurred in the approach phase of the fourth flight. The peak levels have been highlighted. Note that ISO-2631 defines rms vibrations in the range 1.25 to 2.5 ms^{-2} as “Very uncomfortable”

RMS Acceleration (ms^{-2})

TestFile	H.Lat	H.Lon	H.V	W.Lat	W.Lon	W.V	F.Lat	F.Lon	F.V
38	0.42	0.79	0.63	0.45	0.66	1.44	0.43	0.59	1.29
39	0.43	0.83	0.58	0.46	0.71	1.58	0.44	0.66	1.3
40	0.5	0.84	0.66	0.53	0.74	1.33	0.52	0.72	1.44
41	1.01	1.71	1.09	1	1.68	1.79	0.98	1.8	2.05
42	0.47	1.08	0.51	0.48	0.76	1.09	0.54	0.85	1.15

Peak Acceleration (ms^{-2})

TestFile	H.Lat	H.Lon	H.V	W.Lat	W.Lon	W.V	F.Lat	F.Lon	F.V
38	1.44	3	2.11	1.59	2.43	5.34	1.51	2.25	4.04
39	1.57	3.15	1.95	1.76	2.7	6.34	1.69	2.29	4.07
40	1.86	2.93	1.96	1.92	2.33	4.32	1.88	2.45	4.1
41	3.65	5.55	3.47	3.83	4.78	7.49	3.5	5.18	7.78
42	1.78	4.53	2.08	1.9	2.85	5.03	2.35	3.71	4.57

Crest Factor

TestFile	H.Lat	H.Lon	H.V	W.Lat	W.Lon	W.V	F.Lat	F.Lon	F.V
38	3.4	3.81	3.35	3.56	3.69	3.71	3.51	3.81	3.12
39	3.64	3.8	3.36	3.84	3.8	4	3.85	3.46	3.14
40	3.72	3.51	2.97	3.64	3.17	3.23	3.64	3.4	2.85
41	3.6	3.25	3.18	3.83	2.85	4.18	3.58	2.87	3.8
42	3.82	4.19	4.07	3.95	3.74	4.62	4.39	4.36	3.97

Displacement: The maximum displacement is calculated from the recorded acceleration data. The displacement, velocity and acceleration of a sinusoidal vibration are related as:

$$\text{Displacement } x(t) = A \sin 2\pi f t \quad (2)$$

$$\text{Velocity } v(t) = \dot{x}(t) = 2\pi f A \cos 2\pi f t \quad (3)$$

$$\text{Acceleration } a(t) = \ddot{x}(t) = -(2\pi f)^2 A \sin 2\pi f t \quad (4)$$

therefore

$$\text{Displacement amplitude} = A \quad (5)$$

$$\text{Velocity amplitude} = 2\pi f A \quad (6)$$

$$\text{Acceleration amplitude} = (2\pi f)^2 A \quad (7)$$

The acceleration v/s frequency plots (for example Figure A.2) show the measured acceleration components to be sinusoidal tones of the form

$$A_f(t) = X_f \sin 2\pi f t \quad (8)$$

where X_f is the amplitude of acceleration $A_f(t)$ at frequency f . Using equations 7 and 8 the displacement amplitude A can be determined from

$$A = \frac{X_f}{(2\pi f)^2} \quad (9)$$

Note that for the same acceleration amplitude the largest displacements will be at the lowest frequency which is that of the main rotor (5.4Hz). The maximum acceleration recorded at this frequency was 0.6ms^{-2} (Feet vertical 24/04/2011-2 TestFile20 Cruise). Therefore for an acceleration of 0.6ms^{-2} at a frequency of 5.4Hz the displacement amplitude would be

$$A = \frac{0.6}{(2 * \pi * 5.4)^2} = 523 \mu\text{m} = 0.523 \text{mm} \quad (10)$$

Bandwidth: The simulator must have a bandwidth of at least 150 Hz which equals that of the measurement system and includes the majority of the helicopter vibration sources.

Supported mass: Electrodynamic shakers can only support limited masses therefore the moving mass of the simulator will need to be independently supported.

2. **Input data:** The simulator will be driven with time-domain Field Data Replication vibration signals which are now available from the vibration measurement system detailed in chapter 3 and 4.
3. **Verifiable:** The vibrations generated by the simulator must be verifiable to ensure that the system is functioning correctly.

5.2 SIMULATOR DESIGN

The original intent for the simulator was to have it vibrating in three dimensions however the literature survey and design process showed that this was not feasible due to cost and time constraints. After referring to the literature and ISO-2631 the decision was made to limit the vibrations to the vertical direction only as this was considered the most important axis with the highest weighting by ISO-2631. It was also unfeasible to have the table top flexing in the same manner as the helicopter floor with different vibrations at the head, waist and feet therefore the simulator uses the *waist vertical vibrations* only. As part of this decision process a vibration actuator was selected. The standard actuator for generating high power high bandwidth vibrations is the electrodynamic shaker which is used extensively for reliability testing of equipment and instrumentation particularly in the aerospace industry. Electrodynamic shakers operate in the same manner as an acoustic speaker with a moving ferrous core surrounded by a high power coil. Shakers are however expensive particularly at the power level required for this project however two ESS-050 500Nt shakers and amplifiers were sourced from Dongling in China (Figure 5.1). The specification for the ESS-050 is given in Table 5.1. Although the combined maximum force of 1000Nt is slightly less than the design maximum of 1101Nt it is considered adequate due to the relatively short periods that such high power vibrations are experienced (Section 5.1).



Figure 5.1: Dongling ESS-050 500 Nt shaker (left) and PA1200 amplifier (right). The moving shaker core is the disk with five attachment bolts inside the rubber seal on top of the shaker.

Table 5.1: Specifications for the ESS-050 Electrodynamic Shaker

<ul style="list-style-type: none">• Maximum force – 500Nt• Maximum acceleration – 30g• Frequency range – 5-10,000Hz• Maximum displacement – 16mm• Maximum vertical load support – 20Kg• Power requirement – Single phase 220Vac• Table diameter – 120mm• Dimensions – 440 x 330 x 270mm (L x W x H)• Weight – 95Kg• Maximum input signal – 1Vrms

The maximum load (weight) that these shakers can support is 20Kg. The table will therefore require an independent vibration isolating support to carry this weight. There are a range of vibration isolating mounts available off the shelf however they are all designed to isolate a particular frequency and consequently have a nonlinear frequency response making them unsuitable for this design. It was decided to design custom mounts using linear compression springs as the vibration isolating element. The mounts are shown in Figures 5.2 and 5.3. Ten vibration mounts were located between the table base and top positioned to spread the load equally

(Figures 5.4 and 5.5). Vertical linear bearings are also installed at each end of the table to keep the table top horizontal and minimise horizontal or torsional movement of the table top.

When positioning the shakers in the table base it is important to ensure that each shaker provides approximately equivalent vibration force by ensuring that each is driving approximately equivalent masses. As body mass is not distributed uniformly along the human torso (Armstrong 1988) moments theory was used to calculate the optimum shaker locations using a mid-size male as a typical example. The shaker locations are shown in Figure 5.4.

The table base and top are constructed of heavy aluminium angle section to give maximum rigidity to the structure and reduce unwanted secondary vibrations in the moving top section.

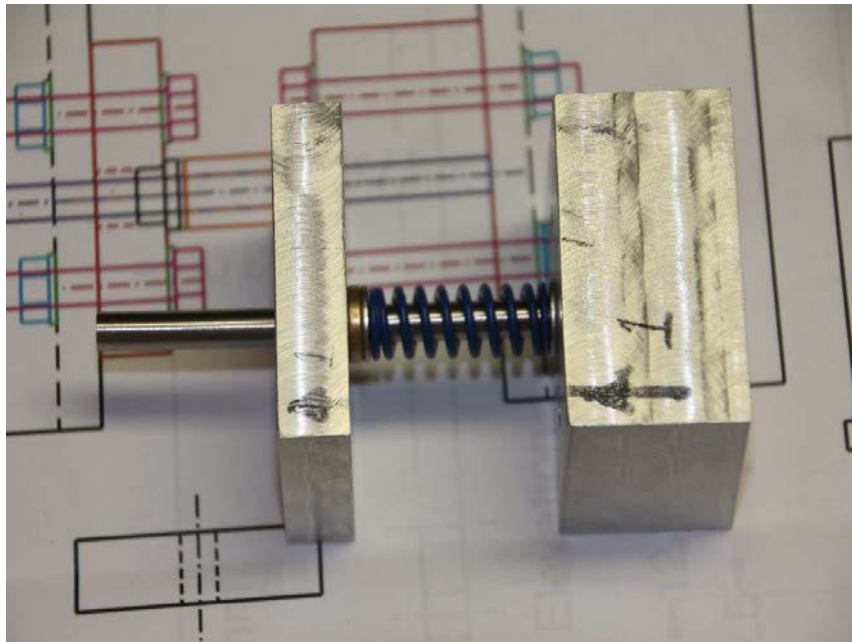


Figure 5.2: Spring based vibration isolating mount. The base is on the right and the top which attaches to the moving part of the table is on the left. The shaft serves to keep the spring from dislodging as well as assist in minimising sideways movement of the table top. The shaft is anchored to the base and slides on a brass bush in the top.

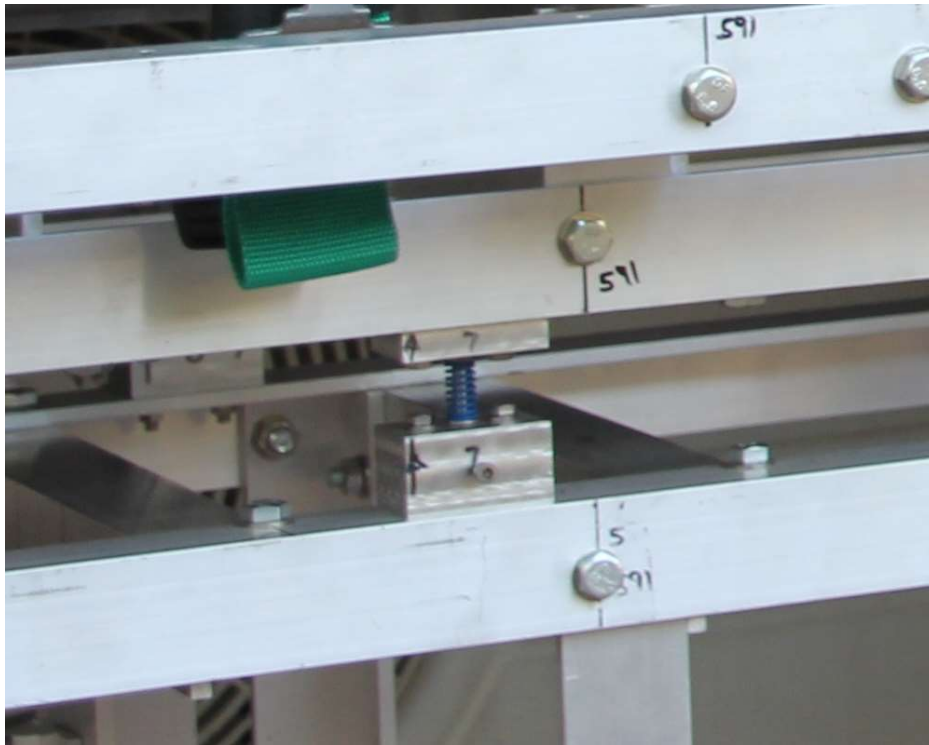


Figure 5.3: An example of the vibration isolating mount installed in the table. Ten of these mounts are used to distribute the load evenly around the table.

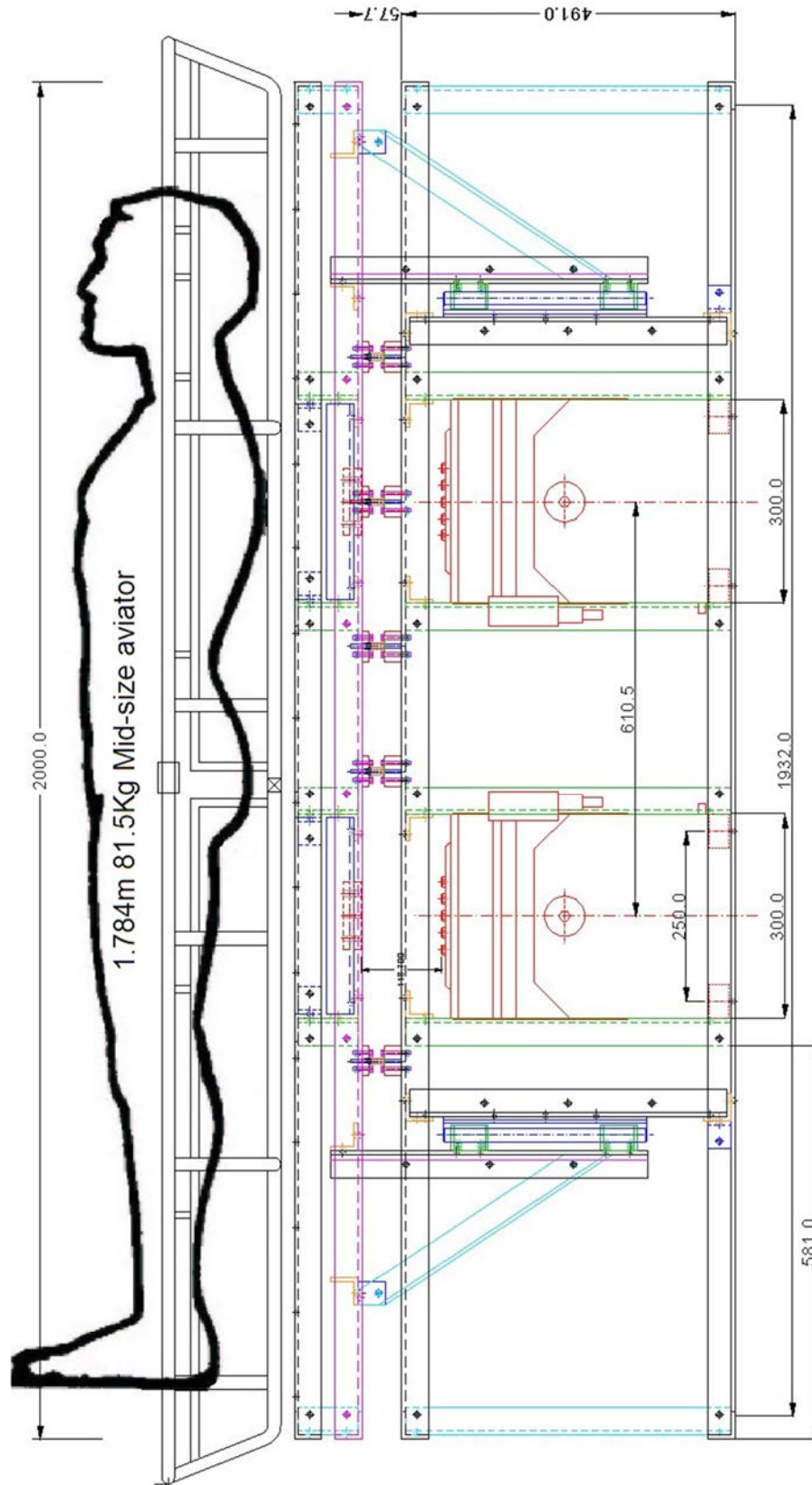


Figure 5.4: Side elevation schematic drawing of the vibration simulator.

Figure 5.6 is a block diagram showing the flow of signals in the vibration simulator. The system software and communications are designed to ensure accuracy, reliability and verifiability of the vibrations generated for the clinical trials. The PC provides the Graphical User Interface (GUI) that gives the operator control and feedback of the simulation as well as storage for the vibration data (target signal $r(t)$ (Section 1.3) and shaker systems output $y_1(t)$, $y_2(t)$) and USB host communications to the FRDM-K64F embedded microcontroller (MCU) located in the simulator table. To guarantee reliability all communications between the PC and MCU uses a fixed message structure with ASCII encoding of all characters (Figure 5.7). ASCII encoding allows for control of the communications system using ASCII control characters at the expense of higher data volumes. Message integrity is maintained by the inclusion of checksum characters to detect any data corruption within the message, while the data message sequence is maintained by the inclusion of a 16-bit data message counter at the start of each data message which indicates any missing or out of sequence data messages. All messages must be acknowledged by the recipient within 10 milli seconds or the transmitting device assumes that the message has not been received correctly and it is resent. The transmitting device will attempt to retransmit an unacknowledged message up to three times before informing the operator that communications have failed. This mechanism is in addition to the inherent quality control of USB Bulk Data Transactions. Extensive testing of the communications system has shown 100% reliability.

Two types of message are used, Commands and Data. Commands control the operation of the system therefore they have priority and are actioned immediately by the MCU. Data is stored in circular buffers until required with software data flow control exercised using XON/XOFF control characters.

The MCU USB port is set up as a Full Speed USB 2.0 Vendor Defined Class Device using USB Bulk Data transactions to ensure adequate speed and high quality communications between the PC and MCU. The vendor defined class allows the use of WinUSB for the PC device driver. The peak data transfer rate does not exceed 25 kBytes/sec which is well within the 300-500 kBytes/sec capability of Full Speed USB 2.0 using Bulk 64 byte packets.

Byte 0	Byte 1	Byte 2-5	Maximum 4101 bytes	Byte $(n-2)/(n-1)$	BYTE n
STX	MSG TYPE	BYTE COUNT	MESSAGE $(n-6)$ bytes	CHECK SUM	ETX
<p>PC-to-MCU Message Structure:</p> <ul style="list-style-type: none"> • Byte 0: STX – ASCII 0x02. • Byte 1: MESSAGE TYPE <ul style="list-style-type: none"> ○ Command – ‘0’ ASCII 0x30. ○ Data – ‘1’ ASCII 0x31. • Bytes 2 – 5: BYTE COUNT – number of bytes in message = $n-8$, 16-bit (4 ASCII characters). • Bytes 6 – $(n-3)$: MESSAGE – maximum of 4101 bytes <ul style="list-style-type: none"> ○ For COMMANDS: <ul style="list-style-type: none"> • Byte 0: COMMAND – single ASCII character (0x30 to 0x39, and ‘XON’, ‘XOFF’) <ul style="list-style-type: none"> ○ ‘0’ ASCII 0x30 – Setup ○ ‘1’ ASCII 0x31 – Start test ○ ‘2’ ASCII 0x32 – Pause test ○ ‘3’ ASCII 0x33 – Stop test ○ ‘4’ ASCII 0x34 – Communications test ○ ‘XON’ ASCII 0x11 – Continue Data Transmission ○ ‘XOFF’ ASCII 0x13 – Pause Data Transmission • Byte 1 – $(n-3)$: Optional data associated with the command. ○ For DATA: <ul style="list-style-type: none"> • Byte 0: DATA TYPE – single ASCII character (0x30 to 0x39) • Bytes 1 – 4: 16-bit data message counter (4 ASCII char) • Bytes 5 – $(n-3)$: up to 1024 16-bit data values (4 ASCII char each). • Bytes $(n-2)/(n-1)$: CHECK SUM – 8 bit unsigned sum of ASCII values for Byte 0 to Byte $(n-3)$. 2 ASCII characters. • Byte n: ETX – ASCII 0x03. 					

Figure 5.7: Message Structure used for PC-to-MCU communications. Maximum message size is 4110 bytes ($n = 4109$). Communications use USB BULK transfers.

The analog vibration signals that control the shakers are generated using two Pulse Width Modulated (PWM) ports of the MCU. The PWM signals are low pass filtered using first order passive filters to remove high frequency components and then input to the shaker amplifiers. Feedback for the system is provided by two accelerometer sensor boards (Section 3.2.2) mounted under the table top at the shaker attachment points. The accelerometer data is sampled by the MCU and used by the shaker controller as well as being sent back to the PC for storage and later analysis if system verification is required.

5.3 TIME WAVEFORM REPLICATION

The vibration simulator of figure 5.6 uses a pair of electrodynamic shaker based systems (SHAKER 1 and SHAKER 2) to supply the vibratory force. Each system is independent and consists of a Dongling ESS-050 electrodynamic shaker with its associated PA1200 power amplifier, a controller implemented in software on the FRDM-K64F MCU and an accelerometer for feedback (AC1 and AC2). The function of the controller is to ensure that the vibrations experienced by the test subject are as close as possible to those experienced in actual flight. This is achieved by having the controller implement a frequency domain *Time Waveform Replication* (TWR) algorithm which is the current state-of-the-art solution for vibration simulators (Reilly 2008, Cornelis 2014). The algorithm generates the shaker drive signal by the convolution, in the frequency domain (fast convolution), of the estimate of the Inverse Frequency Response Function (FRF) of the shaker system with the processed recorded flight data (target signal). TWR has been in use for many years, for example, in the automotive industry for road simulation and durability testing (Deckers 2009, Wang 2009). It is a multi-step process that typically involves the following steps:

1. Recording of flight data
2. Processing of flight data to produce the clinical trial vibration target signal $r[n]$
3. Determination of shaker system inverse Frequency Response Function (FRF)
4. Drive signal generation during testing

The description of each of these steps is presented in the following sections.

5.3.1 RECORDING OF FLIGHT DATA

The recording and analysis of the flight data is covered in chapters 3 and 4. The main points that need to be emphasised are:

1. The recorded flight data is used to generate the test simulation file (vibration target signal $r(t)$) to be used in the clinical trial. The test simulation file will be quite large with approximately one hour of data.
2. The vibration simulator will reproduce the vertical axis vibrations recorded at the patient's waist.
3. The recorded vibration data includes a dc offset which is present due to the accelerometers ability to measure the gravity vector. This is not constant as the vertical axis gravity component will change with the helicopter's orientation.

4. Helicopter vibrations are tonal although significant averaging of the vibration spectra is required to clearly see the tones.
5. All flight modes; winching, winch hover, climb, cruise, descent, hover in ground effect and shutdown have been recorded.

5.3.2 PROCESSING OF FLIGHT DATA READY FOR SIMULATION

The test simulation file contains the target signal $r[n]$ which is the vibration that the subject should experience during the clinical trial. Its creation involves two stages, firstly the waist vertical channel data for the different flight modes is concatenated into a single large file sufficient for the required test duration and secondly the dc offset (called velocity trend) is removed (Birdsong 2001). Note that this processing is only performed once and not each time a test is conducted. The nine channels of flight data are saved in multiple 15 second excel spreadsheet files. A C++ program was written to extract the waist vertical channel data from these files and create a binary test file. Care is taken to blend the vibration data from one source file to the next to avoid any large discontinuities. The duration of the recorded cruise mode is relatively short when compared to a typical recovery flight and it is therefore repeated multiple times to extend the test duration to a more realistic time scale.

The dc offset is removed using a high pass filter with a cut-off of 1Hz, sufficient to pass the lowest frequency of interest 5.4Hz corresponding to the main rotor frequency.

5.3.3 DETERMINATION OF THE SHAKER SYSTEM FREQUENCY RESPONSE FUNCTION (FRF)

The Time Waveform Replication (TWR) strategy uses an open-loop controller to generate the shaker drive signal $u[n]$ by the convolution of the estimate of the shaker system inverse Frequency Response Function (FRF), $\hat{G}(j\omega)^{-1}$ and the target signal $r[n]$ (Figures 5.8, 5.11). $G(j\omega)$ is the FRF of the actual shaker system and $y[n]$ is its output which are the vibrations experienced by the test subject during the clinical trial. As shown in figure 5.4 to figure 5.8 the vibration simulation system uses two identical shakers each with their own inverse FRF estimate however their operation is identical and the explanation will therefore refer only to a single instance. The shakers have been positioned in the vibration simulator so that they will each experience approximately the same load and their individual inverse FRF estimates will ensure that each is generating the same level of vibrations (Section 5.2).

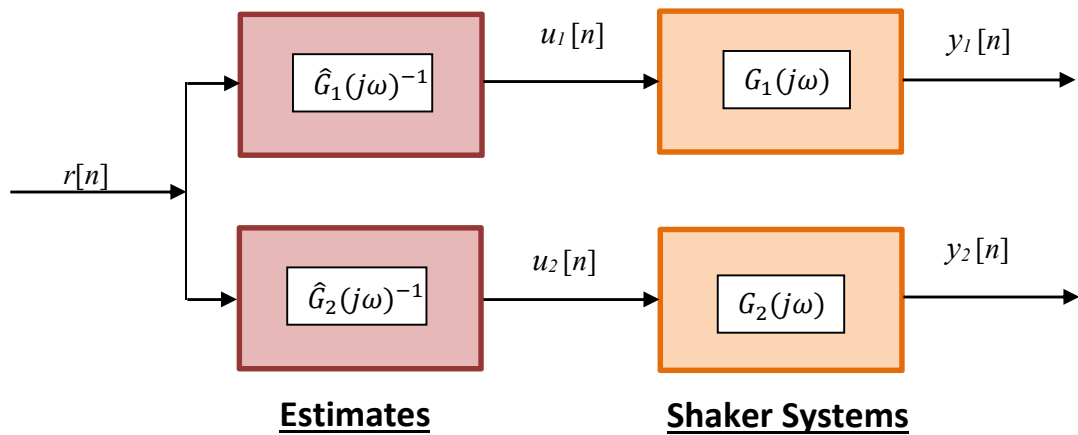


Figure 5.8: The Time Waveform Replication strategy is an open-loop control system and is identical for each of the two shakers. The target signal $r[n]$ is filtered by the estimates of the shaker system inverse FRFs $\hat{G}_1(j\omega)^{-1}$, $\hat{G}_2(j\omega)^{-1}$ to produce the shaker system drive signals $u_1[n]$, $u_2[n]$ which are then input to the actual shaker systems. The shaker systems responses $y_1[n]$, $y_2[n]$ are the vibrations experienced by the test subject. Ideally the series combination of the estimate of the inverse and the actual shaker will make the response equal to the target signal.

The strategy is based on the following assumptions:

1. The electrodynamic shaker response is non-linear in frequency but linear in amplitude (Figure 5.9).
2. The shaker system is time invariant or slowly varying over the duration of a single test.

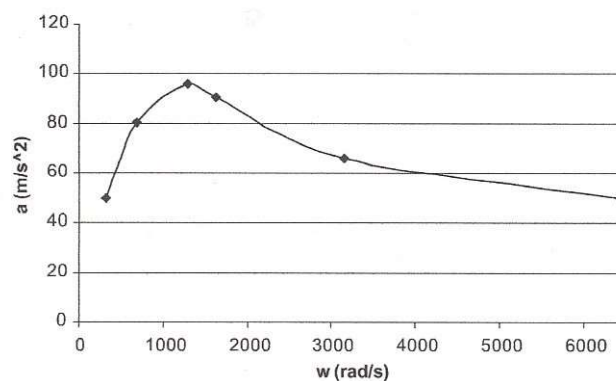


Figure 5.9: Typical Electrodynamic Shaker Frequency Response. Note that Electrodynamic Shakers produce a force proportional to the input signal and therefore as the test mass increases the acceleration curve will move downwards and tend to flatten.

The first phase of the TWR procedure involves the experimental determination of the estimate of the shaker system FRF, denoted by $\hat{G}(j\omega)$, using the H_1 estimation technique. The H_1 technique calculates the estimate of the FRF at each frequency line ω as follows:

$$\hat{G}(j\omega) = \frac{Y(j\omega)}{U(j\omega)} = \frac{\hat{S}_{yu}(j\omega)}{\hat{S}_{uu}(j\omega)} = \frac{Y(j\omega)^* \cdot U(j\omega)}{U(j\omega)^* \cdot U(j\omega)} \quad (11)$$

where $U(j\omega)$ and $Y(j\omega)$ are the Fourier transforms of the shaker drive signal $u[n]$ and measured response $y[n]$, $\hat{S}_{yu}(j\omega)$ is the estimated cross-spectrum of $y[n]$ with $u[n]$ at frequency ω , and $\hat{S}_{uu}(j\omega)$ the estimated auto-spectrum of $u[n]$ at frequency ω . The H_1 estimation technique is the best FRF estimator when there is no noise on the input but there is a possibility of having noise on the measured output signal (Dossing 1988). The shaker drive signal $u[n]$ should be an uncorrelated constant amplitude random signal to ensure that $\hat{S}_{uu}(j\omega)$ is well conditioned as well as being of a level comparable with the target signals however care must be taken to ensure that it does not affect the test subject. The determination of the FRF estimate is an iterative process where time frequency averaging is applied to a number of trials with the quality of the estimate improving as the number is increased. However this increases the overall test duration and a compromise must be reached.

The quality of the FRF estimate is checked by calculating the coherence function given by equation 12 which provides an indication of the degree of linearity between the drive and output signals. A good coherence is obtained with an input that gives a sufficient signal-to-noise ratio with minimal excitation of system non-linearities. The bounds for the Coherence function are 1 if the system is linear, and 0, for pure noise in the measurements (the two signals are totally uncorrelated). The interpretation of the Coherence Function is that for each frequency ω it is a measure of the contamination of the two signals in terms of noise and nonlinear effects.

$$\gamma(\omega) \equiv \frac{|\hat{S}_{yu}(j\omega)|^2}{\hat{S}_{uu}(j\omega) \cdot \hat{S}_{yy}(j\omega)} \quad \text{where } 0 \leq \gamma(\omega) \leq 1 \quad (12)$$

The FRF estimate can also be assessed using forward and backward prediction (De Cuyper 2006). Forward prediction assesses the FRF estimate $\hat{G}(j\omega)$ by applying the same drive signal $u[n]$ simultaneously to $\hat{G}(j\omega)$ and the actual shaker system, and then comparing the two outputs. Backward prediction assesses the inverse FRF estimate $\hat{G}(j\omega)^{-1}$ by applying a drive signal $u[n]$

to the series connection of $\hat{G}(j\omega)^{-1}$ and the actual shaker system, and then comparing the final response $y[n]$ to $u[n]$.

In an automotive durability trial the next phase is to calculate the test drive signal $u[n]$ by the convolution of the target signal $r[n]$ with the inverse FRF estimate $\hat{G}(j\omega)^{-1}$. In this type of trial the target signal is relatively short and $u[n]$ can be calculated offline before the trial begins. During the trial, referred to as Target Simulation, the drive signal will be repeated multiple times providing the opportunity to update the FRF estimate during the trial using an iterative process described as

$$u_j = u_{j-1} + \hat{G}(j\omega)^{-1} q_j (r - y_{j-1}) \quad (13)$$

where u_j is the j^{th} iteration of the drive signal, $(r - y_{j-1})$ is the error, $0 \leq q_j \leq 1$ is an iteration gain, j_1 is the first iteration and $u_0 = y_0 = 0$ (De Cuyper 2006).

It is desirable to update the FRF estimates as the trial progresses however in this trial the target signal is of approximately one hour duration and is not repeated therefore the technique of equation 13 is not suitable. Instead the FRF estimate is iteratively updated using the formula

$$\hat{G}_i(j\omega)^{-1} = \hat{G}_{i-1}(j\omega)^{-1} + q(R'(j\omega) - Y'(j\omega)) \quad (14)$$

where the error $(R'(j\omega) - Y'(j\omega))$ is the difference between the long term frequency domain averages of the target and output signals and $0 < q < 1$ is a gain term. Long term frequency domain averages are typically conducted over periods of 15 seconds (Sections 3.3.8, 4.3.2.1).

5.3.3.1 EXCITATION SIGNAL FOR FRF ESTIMATION

The system identification phase uses a pseudo-random excitation which is a special case of a multi-sine signal (Van Baren 2007, Gomes 2008, Steinwolf 2008, Cornelis 2014). For these tests the amplitude of the random signal is deterministic based on a predetermined profile specified in the frequency domain and the time domain waveform is reconstructed using the inverse Fourier transform (15). The shaker system is therefore driven by a multi-frequency signal with a large number of harmonics, N . Therefore the drive signal at time nT is given by

$$u[nT]_{n=0}^{N-1} = \sum_{k=1}^N A_k \sin(2\pi k f_0 nT + \phi_k) \quad (15)$$

where the frequency domain amplitude profile is divided into N frequency bands each of width $f_0 = F_s/N$ with centre frequency $k f_0$, amplitude A_k and phase ϕ_k . $F_s = 1/T$ is the time domain sampling frequency. The phases ϕ_k are independent random variables with a uniform distribution between 0 and 2π .

For system identification the amplitude A_k is set to a constant for all k corresponding to a white (flat) Power Spectral Density. This is combined with the random phase ϕ_k and the resultant drive signal sample is calculated using equation 15. The drive signal $u[nT]_{n=0}^{N-1}$ is termed a block which corresponds to the time domain sample size N . Identical blocks are then generated by keeping ϕ_k the same resulting in ‘delay blocks’ followed by ‘capture blocks’. The delay blocks allow any transients to die out. The drive and response for the capture blocks are averaged, in the frequency domain, to remove any noise. After a sufficient number of capture blocks are averaged a new block is realised using a new set of ϕ_k and the process is repeated. Multiple realisations allow for averaging out nonlinearities in the shaker system dynamics.

Pseudo-random excitation is periodic within a FFT block, therefore there are no spectral leakage issues and a window function is not required. Once the drive and response spectrums have been determined the FRF is evaluated using equation 11.

5.3.4 DRIVE SIGNAL GENERATION

The shaker drive signal $u[n]$ is generated by filtering the target signal $r[n]$ with the shaker system inverse FRF estimate $\hat{G}(j\omega)^{-1}$. For simplicity define $\hat{H}(\omega) = \hat{G}(j\omega)^{-1}$ to be a length L FIR filter and its impulse response $h[n]$, $0 \leq n \leq L-1$. The most efficient technique for performing this filtering is fast convolution in the frequency domain using the *overlap-add* method (Porat 1997, Birdsong 2001) (Figures 5.10, 5.11). The proper operation to filter the long sequence $r[n]$ with a length L FIR filter is to compute the linear convolution of the two sequences. i.e.

$$u[n] = \{h * r\}[n] = \sum_{l=0}^{L-1} h[l]r[n-l] \quad (16)$$

For efficiency the time-domain convolution is performed using multiplication in the frequency-domain, however it is circular convolution rather than linear (conventional or non-circular) convolution that translates to multiplication in the frequency domain. Fortunately the overlap-add method performs linear convolution by using circular convolution thus providing an efficient means of filtering the target signal.

As part of the initialisation for the overlap-add method the shaker system inverse FRF estimate $\hat{H}(\omega)$ must be transformed to $h[n]$, its impulse response, and the target signal $r[n]$ broken into more manageable size blocks. $\hat{H}(\omega)$ is not effected by spectral leakage as its frequency components are perfectly periodic within the FFT block and therefore no windowing is required (Cornelis 2014). In the overlap-add method linear convolution is performed via circular

convolution however the sequence $r[n]$ is too long for the two sequences to be zero padded to the sum of their two lengths. Therefore $r[n]$ is divided into non-overlapping blocks of length N such that

$$r[n] = \sum_i r_i[n] \quad (17)$$

where

$$r_i[n] = \begin{cases} r[n], & Ni \leq n \leq N(i+1) - 1, \\ 0, & \text{otherwise} \end{cases} \quad (18)$$

The range of the index i is not specified to indicate that it does not need to be known in advance. Each block of $r_i[n]$ (length N) will then be convolved with $h[n]$ (length L) to form the set of sequences $u_i[n]$, also of length N . However, circular convolution $\{h \circledast r_i\}[n]$, requires the two sequences to be equal length therefore $h[n]$ and $r_i[n]$ are both zero padded to a length $M \geq N + L - 1$ before convolution with the resulting sequence, denoted $u_{ia}[n]$, also being of length M . Note that $u_{ia}[n]$ will be made up of sections of non-zero and zero elements depending on the amount of zero padding that was applied to $r_i[n]$ and $h[n]$. $u_{ia}[n]$ is then split into two sequences, $v_i[n]$ made up of the first N non-zero elements of $u_{ia}[n]$ and $w_i[n]$ made up of the remaining $L - 1$ non-zero elements.

Procedure:

1. Transform the shaker system inverse FRF estimate $\hat{H}(\omega)$ into its impulse response denoted as $h[n]$.
2. Choose the target signal block size $N \geq L$.
3. Break the target signal $r[n]$ into non-overlapping blocks of length N . Denote these as $r_i[n]$.
4. Define M to be the smallest power of 2 $\geq N + L - 1$, for a radix 2 FFT.
5. Zero pad the filter impulse response sequence $h[n]$ to length M . The zero padded sequence is denoted as $h_a[n]$.
6. Compute $H_a^d[k]$, the FFT of $h_a[n]$.
7. For each i ,
 - a. Zero pad the block $r_i[n]$ to length M . The zero padded block is denoted $r_{ia}[n]$.
 - b. Compute $R_{ia}^d[k]$, the FFT of $r_{ia}[n]$. Gives an M point FFT.
 - c. Multiply the vectors $H_a^d[k]$ and $R_{ia}^d[k]$ point by point to give $U_{ia}^d[k]$.

- d. Compute $u_{ia}[n] = \text{IFFT}\{U_{ia}^d[k]\}$.
- e. $u_{ia}[n]$ is an M element sequence which is split into two sequences such that $u_{ia}[n] = v_i[n] + w_i[n]$, where:
 - f. $v_i[n]$ is nonzero in the range $Ni \leq n \leq N(i+1) - 1$. It is a partial result for the i^{th} block. Add the sequence $w_{i-1}[n]$ to its initial part. i.e.

$$u_i[n] = v_i[n] + w_{i-1}[n]$$
 - g. $w_i[n]$ is nonzero in the range $N(i+1) \leq n \leq N(i+1) + L - 2$. Called the overlap. Save it for the $(i+1)^{\text{th}}$ block.

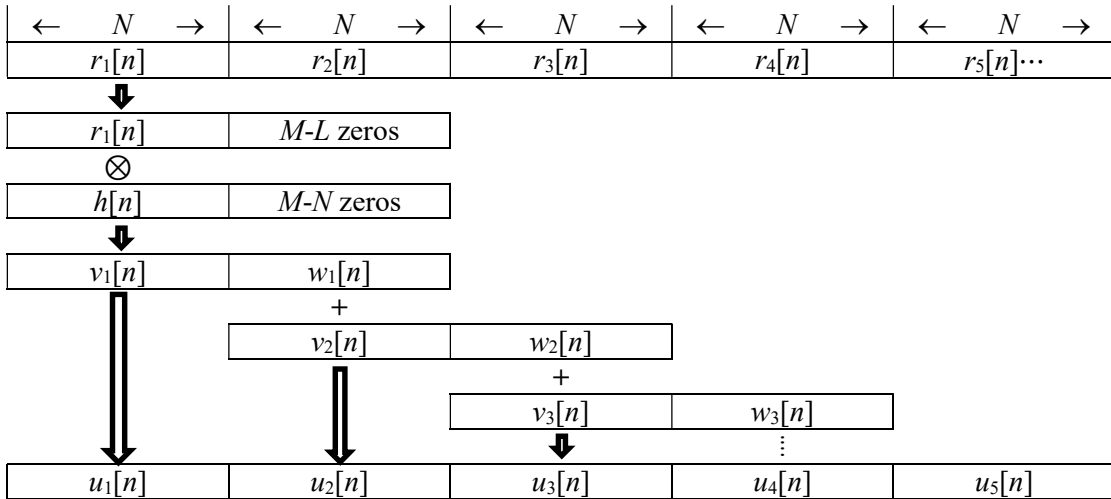


Figure 5.10: The overlap-add process for producing the shaker drive signal $u[n]$ by filtering the target signal $r[n]$ with the estimate of the shaker system inverse FRF impulse response $h[n]$. The top and bottom rows show $r[n]$ and $u[n]$ broken into non-overlapping blocks $r_i[n]$ and $u_i[n]$ of size N . In the left column $r_1[n]$ is zero padded with $M-L$ zeros before being circularly convolved with $h[n]$ which has been zero padded with $M-N$ zeros. The result is the two blocks $v_1[n] + w_1[n]$. In the second iteration $r_2[n]$ is zero padded and convolved with $h[n]$ (also zero padded) to produce $v_2[n] + w_2[n]$. $u_2[n]$ is then calculated as $v_2[n] + w_1[n]$. Subsequent iterations follow the same sequence.

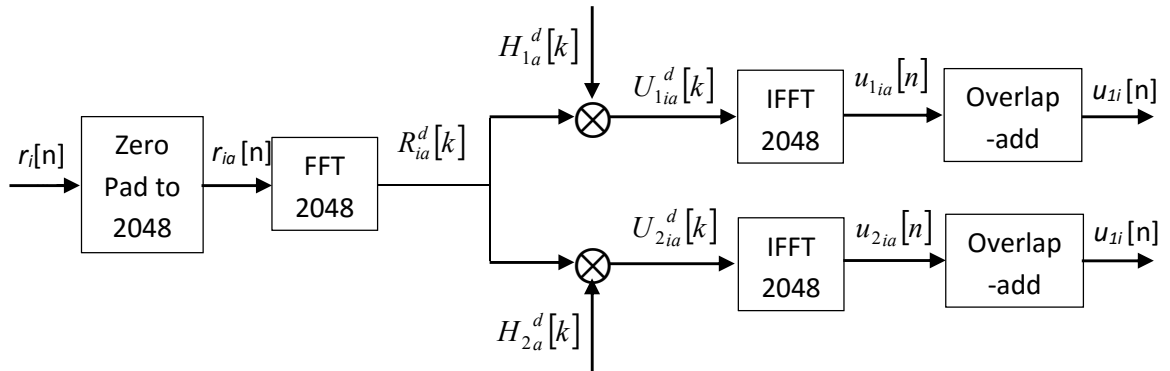


Figure 5.11: Signal flow for drive signal generation for the two shaker systems.

5.3.4.1 IMPLEMENTATION

This section discusses the practicalities of implementing the signal generation and control for the vibration simulator.

The vibration table communications, signal generation and control is implemented on a Freescale K64FN1M0VLL12 32-bit 120 MHz MCU mounted on a FRDM-K64F Freedom board. The MCU has an ARM Cortex-M4 core with added DSP and single instruction multiple data (SIMD) instructions, a single precision hardware floating point unit (FPU) and is supported by the ARM CMSIS library which provides a range of DSP functions optimised for execution in the M4 core including multiple implementations of real and complex FFTs and IFFTs up to 4096 points. It is quite capable of implementing DSP algorithms including FIR filters and FFTs for audio signals in real time (Reay 2015).

Both L , the block length of the shaker system inverse FRF estimate $\hat{H}(\omega)$, and N , the target signal $r[n]$ block size used for calculations in the system identification and drive signal generation (Sections 5.3.3 and 5.3.4) are set to 1024 which corresponds to approximately 0.5 seconds of vibration samples. Also M is set at 2048 being the smallest power of 2 greater than or equal to $N + L - 1$. This means that for the MCU to operate the vibration simulation system in real-time all calculations for a block must be completed in under this time. Section 5.3.4 and Figure 5.11 show that to generate one block of drive signal for each of the two shakers will require one 2048 point 16-bit FFT, two 2048 element complex multiplies and two 2048 point IFFTs. Benchmarks for the MCU show that it computes 2048 point 16-bit FFTs and IFFTs in under 2 milli Seconds confirming that it is more than capable of operating the vibration simulator in real time assuming that the target signal $r[n]$ is processed off-line before the test.

5.4 SUMMARY AND CONCLUSIONS

This chapter presents the results of an experimental investigation which has successfully answered the research question “*Is it feasible to simulate the vibrations experienced by patients lying supine in a rescue litter during helicopter winching and retrieval?*”. The simulations are required for clinical trials assessing the hypotheses that *vibrations generated by a rotary wing aircraft increase the quantity of nitrogen bubbles in the blood stream leading to more severe symptoms of Decompression Illness (DCI) in Self Contained Underwater Breathing Apparatus (SCUBA) divers* who have developed initial symptoms of DCI and are being medivaced to specialist care. The question was examined experimentally by first undertaking a preliminary simulator design which identified a number of enabling technologies that would be key to the successful implementation of the vibration simulator and then undertaking detailed investigation, design and implementation of each technology.

The result is a vertical axis vibration simulator capable of reproducing the vibrations experienced by a patient during helicopter winching and retrieval. The original intention was for the simulator to reproduce the vibrations in three dimensions however this proved to be beyond the capabilities of the project. The final simulator can accommodate a test subject lying supine in a rescue litter and reproduce the vertical axis vibrations experienced during a typical medivac flight covering all flight modes including winching using real flight data. The simulator is unique in that it reproduces the actual vibrations experienced in flight by using real vibration data and supporting the subject in the rescue litter as they would be in an actual retrieval flight. When combined with the vibration measurement system (Chapters 3 and 4) the simulator is able to reproduce the vibrations of any helicopter and rescue litter combination which will allow comparative studies and the development of recommendations for the safe transport of patients by helicopter. Operating in the vertical axis only is considered sufficient for the clinical trials as the results will be conservative when compared to a full three axis system however the vertical axis is considered the most important for vibration studies. The system offers substantial other benefits by enabling investigations into a range of vibration sensitive medical conditions such as the retrieval of patients suffering fractures who are transported in the same manner if they need to be winched into the helicopter or studies into the effect of vibrations on the internal body skeletal frame and organs (Hedge 2015).

The vibration simulator is not complete as time has not allowed the implementation and testing of the Frequency Response Function estimation and Time Waveform Replication algorithms before the thesis was due. However these are not substantially new unproven technologies and

have been applied to numerous previous projects. It is therefore not anticipated that their implementation will pose major difficulties and should proceed without interruption.

This work will be published in a paper which is currently being prepared “*The simulation of vibrations experienced by DCI patients during helicopter aeromedical retrieval*” by Grabau, P., Blake, D., and Jacob, M. Target journal is The Journal of Sound and Vibration.

CHAPTER 6

CONCLUSIONS AND FUTURE WORK

6.0 INTRODUCTION

There is no existing policy or recommendation for the safe transport of patients with respect to the levels of vibration experienced in helicopter transport nor is there any evidence of clinical studies into the effects of these vibrations. This is despite the facts that helicopter aeromedical retrieval including winching is very common, the high levels of vibration experienced in helicopters is well known, vibrations have a marked effect on the human body and many authors have recommended that clinical trials need to be conducted. The reasons for clinical trials not being conducted previously are the lack of real helicopter vibration data and a suitable simulator with the capability of reproducing, in the laboratory or hospital, the vibrations experienced by patients during helicopter aeromedical retrieval.

In 2010 a group, comprising staff from The Townsville Hospital and James Cook University, was formed to initiate a clinical study assessing the hypotheses that *vibrations generated by a rotary wing aircraft increase the quantity of nitrogen bubbles in the blood stream leading to more severe symptoms of Decompression Illness (DCI) in Self Contained Underwater Breathing Apparatus (SCUBA) divers* who have developed initial symptoms of DCI and are being medivaced by helicopter to specialist care. As part of this study a system for recording the actual vibrations experienced by a patient during all stages of retrieval and then reproducing them in a laboratory simulator has been developed. This system and its development are presented in this thesis.

Real vibration data from a Bell 412 helicopter of Emergency Management Queensland have been recorded and clinical trials using the simulator are due to begin in 2016. The trials will involve simulating dives and helicopter retrievals by first compressing subjects in a hyperbaric chamber during a routine hyperbaric treatment following a current T14 (241.3 kPa) dive table and then vibrating a selection of subjects in a rescue litter on a simulated helicopter platform. Following the treatment and subsequent simulated retrieval the level of nitrogen bubbles in the blood stream will be assessed using Doppler ultrasound.

Initial investigations at the start of the study identified the need for a vibration recording system to provide real vibration data and a simulator to vibrate subjects in the clinical trial. The investigations also showed that suitable instruments were not available and that there were

significant technical issues to be overcome in the development of a custom system. As it was unclear if the systems were practical they were divided into separate research projects each addressing its own research question.

6.1 VIBRATION MEASUREMENT SYSTEM

Investigations into measuring the vibrations experienced by patients during aeromedical retrieval explored the research question

Is it feasible to record the vibrations experienced by patients lying supine in a rescue litter during helicopter winching and retrieval?

This investigation was successfully concluded and resulted in a system which records the real vibration data needed for the vibration simulator. The contributions of this work were:

- A non-invasive portable system that records the vibrations experienced by patients during helicopter flight modes including winching
 - The system records vibrations in the lateral, longitudinal and vertical axes at the patient head, waist and feet
 - All channels are sampled simultaneously
 - The system is suitable for use with a large range of helicopters and rescue litters
- An algorithm for high speed data streaming to an SD card with a low-power microcontroller
- The use of low cost, low power, low profile Micro Electromechanical Systems (MEMS) accelerometers as vibration sensors.

As the investigation was successfully concluded the answer to the research question is that *it **is** feasible to record the vibrations experienced by patients lying supine in a rescue litter during helicopter winching and retrieval.*

6.2 VIBRATION SIMULATOR

Investigations into simulating the vibrations experienced by patients during aeromedical retrieval explored the research question

Is it feasible to simulate the vibrations experienced by patients lying supine in a rescue litter during helicopter winching and retrieval?

This investigation concluded that the vertical axis vibrations were the most important and that it was feasible to simulate the vibrations in this axis. It also concluded that three axis vibration simulation would require substantially more resources than those available and therefore was

unfeasible in this project. A vertical axis vibration simulator was developed and will be installed in the hospital adjacent to the hyperbaric chamber. Clinical trials using this simulator will commence in 2016. The simulator is not complete as some work remains to be done implementing the Frequency Response Function estimation and Time Waveform Replication software. This will be finalized following the completion of the thesis write up. However sufficient work has been completed to confidently say that *it is feasible to simulate the vibrations experienced by patients lying supine in a rescue litter during helicopter winching and retrieval* and therefore the research question has been successfully answered.

The contributions of this work were:

- A vibration simulator capable of reproducing the vertical axis vibrations experienced by a patient during helicopter aeromedical retrieval
 - The simulator can be installed in a hospital adjacent to a hyperbaric chamber
 - The simulator uses real vibration data and therefore can simulate different helicopters
 - The patient is accommodated in a rescue litter in the same manner as in an actual retrieval
 - The simulator is capable of reproducing real vibrations recorded in any type of vehicle
- The vibration simulator offers substantial other benefits by enabling investigations into a range of vibration sensitive medical conditions such as the retrieval of patients suffering fractures who are transported in the same manner if they need to be winched into the helicopter or studies into the effect of vibrations on the internal body skeletal frame and organs.

6.3 FUTURE WORK

The vibration simulator is not complete as time has not allowed the implementation and testing of the Frequency Response Function estimation and Time Waveform Replication algorithms before the thesis was due. However these are not substantially new unproven technologies and have been applied to numerous previous projects. It is therefore not anticipated that their implementation will pose major difficulties and should proceed smoothly.

APPENDIX A

EXAMPLE FLIGHT RECORD

Table A.1: Flight Record for the second flight of 6th April 2011

File	Interrupt count start/end	Comments
TestFile1		Recording system start. No engines running.
TestFile2		
TestFile3		
TestFile4		
TestFile5		
TestFile6		
TestFile7		
TestFile8		
TestFile9		
TestFile10		
TestFile11		
TestFile12		
TestFile13		
TestFile14		
TestFile15		
TestFile16		
TestFile17		
TestFile18		Time: 4:15-4:30. Start engine 1. Blades start turning
TestFile19		Time: 4:30-4:45.
TestFile20		Time: 4:45-5:00.
TestFile21		Time: 5:00-5:15. Blades turning on trolley.
TestFile22		Time: 5:15-5:30. Blades turning on trolley.
TestFile23		Time: 5:30-5:45. Blades turning on trolley.
TestFile24		Time: 5:45-6:00.
TestFile25		Time: 6:00-6:15.
TestFile26		Time: 6:15-6:30.
TestFile27		Time: 6:30-6:45.
TestFile28		Time: 6:45-7:00.

TestFile29		Time: 7:00-7:15.
TestFile30		Time: 7:15-7:30.
TestFile31		Time: 7:30-7:45.
TestFile32		Time: 7:45-8:00.
TestFile33		Time: 8:00-8:15.
TestFile34		Time: 8:15-8:30.
TestFile35		Time: 8:30-8:45.
TestFile36		Time: 8:45-9:00. 8:50 – RPM 76%
TestFile37		Time: 9:00-9:15.
TestFile38		Time: 9:15-9:30.
TestFile39		Time: 9:30-9:45.
TestFile40		Time: 9:45-10:00. 9:50 – RPM 100%
TestFile41		Time: 10:00-10:15.
TestFile42		Time: 10:15-10:30.
TestFile43		Time: 10:30-10:45. 10:42 – Lift off.
TestFile44		Time: 10:45-11:00.
TestFile45		Time: 11:00-11:15.
TestFile46		Time: 11:15-11:30. 11:16 – Start winch hover.
TestFile47		Time: 11:30-11:45. Winch hover.
TestFile48		Time: 11:45-12:00. Winch hover.
TestFile49		Time: 12:00-12:15. Winch hover.
TestFile50		Time: 12:15-12:30. 12:24 – Buffeting.
TestFile51		Time: 12:30-12:45. Winch hover.
TestFile52		Time: 12:45-13:00. Winch hover.
TestFile53		Time: 13:00-13:15.

		13:00 – Buffeting & turbulence. Port side down into wind.
TestFile54		Time: 13:15-13:30. Winch hover.
TestFile55		Time: 13:30-13:45. Winch hover.
TestFile56		Time: 13:45-14:00. 13:59 – To lower hover.
TestFile57		Time: 14:00-14:15.
TestFile58		Time: 14:15-14:30.
TestFile59		Time: 14:30-14:45.
TestFile60		Time: 14:45-15:00.
TestFile61		Time: 15:00-15:15.
TestFile62		Time: 15:15-15:30.
TestFile63		Time: 15:30-15:45. 15:44 – Climb 70Kts 500ft/min.
TestFile64		Time: 15:45-16:00. Climb – Buffeting & turbulence. Port side down into wind.
TestFile65		Time: 16:00-16:15. 16:03 – Right turn. 16:14 – Stop climb.
TestFile66		Time: 16:15-16:30.
TestFile67		Time: 16:30-16:45. 16:38 – Start cruise 600ft 120kts.
TestFile68		Time: 16:45-17:00. Cruise.
TestFile69		Time: 17:00-17:15. Cruise.
TestFile70		Time: 17:15-17:30. Cruise.
TestFile71		Time: 17:30-17:45. Cruise.
TestFile72		Time: 17:45-18:00. 17:50 – Stop cruise.
TestFile73		Time: 18:00-18:15. 18:13 – 18:26 Right turn.
TestFile74		Time: 18:15-18:30.
TestFile75		Time: 18:30-18:45. 18:34 – Start approach 70kts 500ft/min.
TestFile76		Time: 18:45-19:00. Approach
TestFile77		Time: 19:00-19:15.

		Approach.
TestFile78		Time: 19:15-19:30. 19:16 – Stop approach.
TestFile79		Time: 19:30-19:45.
TestFile80		Time: 19:45-20:00.
TestFile81		Time: 20:00-20:15. 20:10 – Cruise 100kts 450ft.
TestFile82		Time: 20:15-20:30.
TestFile83		Time: 20:30-20:45.
TestFile84		Time: 20:45-21:00.
TestFile85		Time: 21:00-21:15.
TestFile86		Time: 21:15-21:30.
TestFile87		Time: 21:30-21:45. 21:31 – Left turn.
TestFile88		Time: 21:45-22:00. 21:51 – Approach vibrations.
TestFile89		Time: 22:00-22:15. 22:08 – Door open. High vibrations.
TestFile90		Time: 22:15-22:30. 22:24 – Start ground hover
TestFile91		Time: 22:30-22:45.
TestFile92		Time: 22:45-23:00. 22:50 - Taxi
TestFile93		Time: 23:00-23:15. 23:03 – 23:40 Vibrations.
TestFile94		Time: 23:15-23:30.
TestFile95		Time: 23:30-23:45. 23:40 – Left turn.
TestFile96		Time: 23:45-24:00.
TestFile97		Time: 24:00-24:15.
TestFile98		Time: 24:15-24:30. 24:25 – Above cart.
TestFile99		Time: 24:30-24:45. 24:36 – Touch down.
TestFile100		Time: 24:45-25:00. 24:50 – Switch off.

BIBLIOGRAPHY

International Organization for Standardization, ISO2631-1 Mechanical vibration and shock - Evaluation of human exposure to whole-body vibration - Part 1: General requirements, 1997.

Albarbar, A., Badri, A., Sinha, J. K. and Starr, A. (2009). "Performance Evaluation of MEMS Accelerometers." Measurement **Vol. 42**(Issue 5): pp. 790-795.

Albarbar, A., Mekid, S., Starr, A. (2008). "Suitability of MEMS Accelerometers for Condition Monitoring: An experimental study." Sensors **Vol, 8**(Issue 2): pp 784-799.

Alberti, E., Chiappa, D., Moschioni, G., Saggini, B. and Tarabini, M (2006). "Whole Body Vibrations in Mountain-rescue Operations." Journal of Sound and Vibrations **298**: pp. 580-593.

Alonso, A., Ramirez, J.L., Fernandez, J. (2010). Advanced Seismic Testing Techniques. 14th European Conference on Earthquake Engineering, Ohrid, Macedonia.

Amirsadri, A., Jonghyuk Kim, Peterson, L., Trumpf, J., (2012). Practical considerations in precise calibration of a low-cost MEMS IMU for road-mapping applications. American Control Conference (ACC). Montreal, QC, IEEE: 881-888.

Anderson, G. C., Finnie, B. W., and Roberts, G. T. (1967). "New Noise Generator Syntheseses Pseudo-Random Gaussian Noise." Hewlett-Packard Journal **19, No. 1**: 2-17.

Anderson, G. C., Finnie, B. W., and Roberts, G. T. (1967). "Testing with Pseudo-Random and Random Noise." Hewlett-Packard Journal **19, No. 1**: 18-20.

Armstrong, H. G. (1988). Anthropometry and Mass Distribution for Human Analogues. Bethesda, MD 20889-5044, Naval Biodynamics Laboratory: pp-74.

Artese, G., Trecroci, A. (2008). Calibration of a low cost MEMS INS sensor for an integrated navigation system. The International Archives of the Photogrammetry, Remote Sensing and Spatial Information Sciences. Beijing. **Vol. XXXVII. Part B5**: 877-882.

Badri, A. E., Sinha, J.K. and Albarbar, A. (2010). "A typical filter design to improve the measured signals from MEMS accelerometer." Measurement **Vol. 43**: pp 1425-1430.

Bennett, M. (1995). "The retrieval of diving injuries in new south wales a retrospective review of two years of practice." SPUMS **25**(3): 142-147.

- Bennett, M. (1998). "Evacuation methods in diving injuries." SPUMS **28**(3): 10-14.
- Birdsong, C. (2001). An Integrated Measurement to Road Vibration Simulation System, Dactron Inc., .
- Bouchut, J.-C., Lancher, E.V., Chritin, V. and Gueugniaud, P-Y (2011). "Physical Stressors during Neonatal Transport: Helicopter Compared with Ground Ambulance." Air medical Journal **Vol.30**.(No. 3.).
- Chen, P.-C., Lai, C-T. (2015). Alternative Acceleration Performance Assessment Method for Seismic Shaking Tables. 6th International Conference on Advances in Experimental Structural Engineering. University of Illinois, Urbana-Champaign, United States.
- Cornelis, B., Toso, A., Verpoest, W., and Peeters, B. (2014). Improved MIMO FRF estimation and model updating for robust Time Waveform Replication on durability test rigs. Proceedings of the 26th International Conference on Noise and Vibration Engineering (ISMA 2014), Leuven, Belgium.
- Cunha, A., and Caetano, E. (2006). Experimental Modal Analysis of Civil Engineering Structures. Sound and Vibration: pp 12- 20.
- De Cuyper, J. (2006). Linear feedback control for durability test rigs in the automotive industry. PhD, Katholieke Universiteit Leuven.
- Deckers, K., Guillaume, P., Lefeber, D., De Baere, D. (2009). Turning Point Based Fatigue Testing Using Amplitude Adapted Time Waveform Replication. Proceedings of the SEM Annual Conference, Albuquerque, New Mexico USA,.
- Dossing, O. (1988). BR0458 Structural Testing – Part 1: Mechanical Mobility Measurements, Bruel & Kjae Technical Note.
- Freescale (Q4/2005). MMA7260Q 1.5g - 6g Three Axis Low-g Micromachined Accelerometer, Freescale Semiconductor Technical Data.
- Germonpré, P., Pontier, J., Gempp, E., et al (2009). "Pre-dive vibration effect on bubble formation after a 30 m dive requiring a decompression stop." Aviation, Space and Environmental Medicine **80**(12): 1044-1048.
- Gomes, H. M., Ferreira, F.S., Thomas, C.A.K., and Gaspareto, D.S. (2007). "An Automatic System for Electrodynamical Shaker Control by Acceleration Power Spectral Density." Mecanica Computacional **Vol XXVI**: pp. 2959-2970.

Gomes, H. M., Gaspareto, D.S., de Souza Ferreira, F., and Thomas C.A.K. (2008). "A Simple Closed-Loop Active Control of Electrodynamic Shakers by Acceleration Power Spectral Density for Environmental Vibration Tests." Experimental Mechanics **48**: pp. 683-692.

Goud, D. R., Gupta, H.O., Agarwal, P. (2009). "Design of Random Vibration Controller using Adaptive Filtering." International Journal of Recent Trends in Engineering **2(5)**: pp. 75-79.

Hedge, A. (2015). DEA 3500 - Human Factors: The Ambient Environment - Course Notes, Cornell University.

Ifassiouen, H., Guisser, M., and Medromi, H. (2008). "Robust Nonlinear Control of a Miniature Autonomous Helicopter using Sliding Mode Control Structure." International Journal of Applied mathematics and Computer Sciences **4(1)**: 12-17.

Keller, T. (2002). On the use of Tracking Filters During Sine Vibration Testing. Sound and Vibration Magazine. **Vol. 36, No. 1**: pp. 82-85.

Kian, S. T., Awad, M., Dehghani, A., Moser, D., Zahedi, S. (2011). Triaxial Accelerometer Static Calibration. World Congress on Engineering 2011, London, U.K.

Kjær, B. (2014). "Calibration of Accelerometers." Retrieved 05/01/2014, 2014, from <http://www.bksv.com/ServiceCalibration/Services/Calibration/Accelerometers>.

Kok, R. a. F., C. (2005). "Development and Characterization of a Wireless MEMS Inertial System for Health Monitoring of Structures. Part 1 and Part 2: ." Experimental Techniques **Volume 29**(Issue 6): pp 46-53.

Kottapalli, S. (2000). Neural-Network-Based Modeling of Rotorcraft Vibrations for Real-Time Applications. AIAA Modeling and Simulation Technologies Conference and Exhibit, Denver, CO.

Lang, G. F. (1997). Electrodynamic Shaker Fundamentals. Sound and Vibration. **Vol. 31, No. 4**: pp. 14-23.

Lang, G. F., Snyder, D., (2001). Understanding the Physics of Electrodynamic Shaker Performance. Sound and Vibration. **Vol. 35, No. 10**: pp. 24-33.

Lepine, J., Champoux, Y., and Drouet, J. M. (2013). "A Laboratory Excitation Technique to Test Road Bike Vibration Transmission." Experimental Techniques(DOI: 10.1111/ext. 12058).

Li, S., Ren, D., Gao, Y., Liu, X. (2014). "Methodologies of Electrodynamic Shaking Table Seismic Test on Reduced Scale Specimen of Building Structures." Sensors & Transducers **182**(11): 194-202.

Luan, Q., Chen, Z., Chen, Y. (2014). The Application of Adaptive Inverse Control Algorithm in Shaking Tables. The 21st International Congress on Sound and Vibration, Beijing, China.

Lythgo, N., Eser, P., de Groot, P., Galea, M. (2009). "Whole-body vibration dosage alters leg blood flow." Clinical Physiology Funct Imaging **Vol 29**(1): pp 53-59.

Martino, J., Harri, k. (2012). Random Vibration Testing Using a Pseudo-Random Method with Crest-Factor Limiting. 9th National Congress on Theoretical and Applied Mechanics, Brussels.

MEI, S., Toshiba, (2000). SD Memory Card Specifications, Part 2, FILE SYSTEM SPECIFICATION, SD Group.

Otsuki, T., Takanami, Y., Aoi, W., et al. (2008). "Arterial stiffness acutely decreases after whole-body vibrations in humans." Acta Physiologica. **194**(3): pp 189-194.

Pedley, M. (2013). "AN3461: Tilt Sensing Using a Three-Axis Accelerometer." Freescale application notes.

Pedley, M. (2013). AN4399: High Precision Calibration of a Three-Axis Accelerometer. Freescale Application Notes.

Plett, G. L. (1998). Adaptive Inverse Control of Plants with Disturbances. PhD thesis, Stanford University.

Pollock, N. W. (2007). Annual diving report-2007 edition (based on 2005 data), Divers Alert Network, Durham, NC,.

Porat, B. (1997). A Course In Digital Signal Processing, John Wiley & Sons, Inc.

Prouty, R. W. (2005). Helicopter Performance, Stability, and Control. Malabar, Florida, Krieger Publishing Company.

Randall, R. B. (1977). Application of B & K Equipment to Frequency Analysis, Bruel & Kjaer.

Reay, D. S. (2015). Digital Signal Processing Using the ARM Cortex M4, Wiley.

Reilly, T. (2008). Time Domain and Frequency Domain Techniques for Multi Shaker Time Waveform Replication. Proceedings of the 78th Shock and Vibration Symposium, Philadelphia, PA,.

Scott, R. J. (2006). Ernsting's Aviation Medicine.

Severn, R. T., Stoten, D. P., Tagawa, Y. (2012). The Contribution of Shaking Tables To Earthquake Engineering. 15th World Conference on Earthquake Engineering, Lisbon.

Shakernia, O., Y. Ma, T. J. Koo and S. S. Sastry (1999). "Landing an Unmanned Air Vehicle: Vision Based Motion Estimation and Nonlinear Control." Asian Journal of Control **1**(3): 128-145.

Silbergleit, R., Dedrick, D.K., Pape, J. and Burney, R.E. (1991). "Forces Acting During Air and Ground Transport on Patients Stabilized by Standard Immobilization Techniques." Annals of Emergency Medicine **Vol. 20**.(Issue 8.): pp. 875-877.

Smith, S. W. (1997). The Scientist & Engineer's Guide to Digital Signal Processing. San Diego, California, California Technical Publishing.

Steinwolf, A. (2008). Two Methods for Random Shaker Testing with Low Kurtosis. Sound and Vibration: pp. 18-22.

Stephenson, J. (2009). "Pathophysiology, treatment and aeromedical Retrieval of SCUBA related DCI." Journal of Military Veterans Health **Vol. 17**(3).

Thanagasundram, S. a. S., F. S. (2006). "Comparison of integrated micro-electrical-mechanical system and piezoelectric accelerometers for machine condition monitoring." Proc. IMechE Col. 220 Part C: J. Mechanical Engineering Science: pp. 1135-1146.

Tumer, I. Y., and Huff, E. M. (2002). Principal Components Analysis of Triaxial Vibration Data from Helicopter Transmissions. 56th Meeting of the Society for Machinery Failure Prevention Technology, Virginia Beach, VA.

Uchiyama, Y., Fujita, M. (2003). Application of Two-Degree-of-Freedom Control to Electrodynamic Shaker using Adaptive Filter Based on H-infinity Filter. European Control Conference, Cambridge, UK.

Uchiyama, Y., Fujita, M. (2006). Robust Acceleration and Displacement Control of Electrodynamic Shaker. IEEE International Conference on Control Applications, Munich.

Uchiyama, Y., Hatanaka, T., Fujita, M. (2011). Preview Control of an Electrodynamic Shaker using Explicit Receding Horizon Control. 18th IFAC World Congress, Milano, Italy.

Uchiyama, Y., Mukai, M., Fujita, M. (2005). Robust Acceleration Control of Electrodynamic Shaker Using u -Synthesis. 44th IEEE Conference on Decision and Control, Seville, Spain.

Van Baren, J., and Van Baren, P. (2007). The Third Dimension of Random Vibration Control. SAE Noise and Vibration Conference and Exhibition. St. Charles, IL.

Walker, D., Lippmann, J., Lawrence, C., Houston, J & Fock A. (2009). "Provisional report on diving-related fatalities in Australian water 2004." Diving and Hyperbaric Medicine **39**(3): pp 138-161.

Wang, Y., Gao, F., Doyle, F. J. (2009). "Survey on iterative learning control, repetitive control, and run-to-run control." Journal of Process Control **19**: 1589-1600.

Wellman, P., Barlow, B.C., Murray, A. S. (1985). Report 261: Gravity base-station network values, Australia. Canberra, Bureau of Mineral Resources, Geology & Geophysics.

Widrow, B., Walach, E. (2014). Adaptive Inverse Control: A Signal Processing Approach, Wiley-IEEE Press.

Wu, J., Zhang, R.R., Wu, Q. and Stevens, K.K. (2003). "Environmental vibration assessment and its applications in accelerated tests for medical devices." Journal of Sound and Vibration **Vol. 267**(2): pp 371-383.